arXiv:2505.02429v1 [hep-ex] 5 May 2025

Search for emerging jets in pp collisions at $\sqrt{s}$ = 13.6 TeV with the ATLAS experiment

The ATLAS Collaboration

A search for emerging jets is presented using 51.8 fb^{-1} of proton–proton collision data at $\sqrt{s}$ = 13.6 TeV, collected by the ATLAS experiment during 2022 and 2023. The search explores a hypothetical dark sector featuring "dark quarks" that are charged under a confining gauge group and couple to the Standard Model via a new mediator particle. These dark quarks undergo showering and hadronisation within the dark sector, forming long-lived dark mesons that decay back into Standard Model particles. This results in jets that contain multiple displaced vertices known as emerging jets. The analysis targets events with pairs of emerging jets, produced either through a vector mediator, Z', in the s-channel, or a scalar mediator, Φ, in the t-channel. No significant excess over the Standard Model background is observed. Assuming a dark pion proper decay length between 5 mm and 50 mm, Z' mediator masses between 600 GeV and 2550 GeV are excluded for quark and dark quark coupling values of 0.01 and 0.1, respectively. For a quark dark-quark coupling of 0.1, Φ mediator masses between 600 GeV and 1375 GeV are excluded. These results represent the first direct search targeting emerging jet pair production via a Z' mediator, as well as the first study of emerging jet production mediated by a scalar particle exchanged in the t-channel.

Contents

1   Introduction

Dark Matter (DM) remains one of the most significant mysteries in physics. Despite overwhelming evidence for the existence of DM [1–3], its particle nature and interactions with Standard Model (SM) fields have yet to be determined. Various extensions to the SM have proposed new stable, weakly interacting massive particles (WIMPs) as DM candidates, motivated by their natural production mechanism in the early universe through thermal freeze-out [4, 5]. However, decades of experimental searches, including direct detection [6–14], indirect detection [15, 16], and collider experiments [17, 18], have increasingly constrained the parameter space for WIMPs, prompting the exploration of alternative theoretical frameworks that can address the DM puzzle.

One particularly compelling alternative to the WIMP paradigm is the existence of a "dark sector" (DS), consisting of particles that are neutral under the SM gauge group but charged under a new symmetry group within the DS [19–21]. In these models, interactions between DS states and SM particles occur via mediator particles that couple to both sectors. Among the various possibilities, dark sectors with a gauge structure and particle content resembling quantum chromodynamics (QCD) have attracted significant theoretical interest due to their rich phenomenology and their potential to naturally explain the observed relic abundance of DM [22–24]. In these "dark QCD" models, the SM is extended with N_f flavours of dark quarks that are charged under a new non-Abelian gauge symmetry, $SU(N_c)$, which confines at a scale Λ_D, where N_c is the number of dark colours. As in QCD, these dark quarks undergo parton showering and subsequently hadronise, forming bound dark hadron states. While some dark hadrons may be stable,

2

providing viable DM candidates, others can be unstable and decay back into SM particles via an off-shell exchange of the mediator particle.

The lifetimes of unstable dark mesons depend on the strength of their effective couplings to the SM. For large couplings, dark mesons will decay promptly, producing "dark jets" with distinctive substructure features or, in cases where some dark states remain invisible, giving rise to "semi-visible jets" with significant missing transverse momentum aligned with the jet direction [25]. However, for weaker couplings, unstable dark mesons naturally acquire longer lifetimes, leading to the distinctive topology of an "emerging jet" (EJ) [26]. These jets are characterised by multiple secondary vertices within the jet cone, with potentially macroscopic displacements from the primary pp interaction point, resulting from the gradual emergence of SM particles as the dark mesons decay in flight.

The ATLAS and CMS collaborations have carried out multiple searches for signatures predicted by dark QCD scenarios, focusing on a variety of production mechanisms and jet topologies. ATLAS has investigated the resonant production of dark jets, where all dark mesons decay promptly into SM particles [27]. Semi-visible jet scenarios have been studied by both ATLAS and CMS in the s-channel [28, 29] and t-channel [27]. A Run 1 ATLAS search explored scenarios with long-lived dark pions decaying within the tracker volume, giving rise to signatures resembling emerging jets [30]. Additionally, CMS has conducted two dedicated searches for emerging jets, both considering the pair production of a bi-fundamental mediator that is charged under both the dark and SM gauge groups, which placed limits on mediator masses up to 1.9 TeV, assuming a dark pion proper decay length of approximately 100 mm [31, 32]. However, these searches have exclusively focused on the pair production of a bi-fundamental mediator, leaving alternative production mechanisms, such as s-channel exchange of a vector mediator, largely unexplored.

The search presented in this paper considers emerging jet production from two different mediator scenarios. The first scenario involves s-channel production through a new vector boson Z' that couples both to SM quarks and to a dark sector containing dark quarks. As illustrated in Figure 1, the Z' is produced in proton–proton (pp) collisions via quark–antiquark annihilation, $q\bar{q} \rightarrow Z'$, and subsequently decays into a pair of dark quarks, $Z' \rightarrow q_D\bar{q}_D$. These dark quarks then undergo showering and hadronisation within the dark sector, leading to the formation of emerging jets.
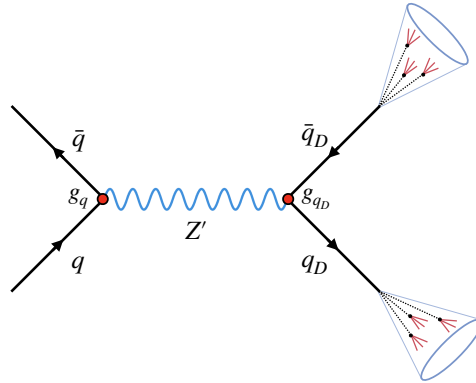

Figure 1: A diagram illustrating the production of emerging jets via an s-channel mediator, Z'. Filled circles represent the Z' couplings. Emerging jets are depicted as cones, with the trajectories of long-lived dark pions shown as dashed lines and solid lines indicating their Standard Model decay products.

The interactions of the Z' mediator with both the SM and DS are governed by two distinct couplings. The coupling between the Z' and the SM quarks is denoted by g_q, which determines the production

cross-section of the mediator. The coupling between the Z' and the dark quarks is denoted by g_{q_D}, which, along with g_q controls the branching fraction of the mediator's decay into the dark sector.

In the second scenario, emerging jets are produced via a t-channel process, where Φ, a bi-fundamental scalar mediator, serves as a portal between the SM and the DS. In this model, Φ couples to both down-type SM quarks and dark quarks via a coupling matrix κ, as described in Ref. [33]. As illustrated in Figure 2, the final state consists of two dark quarks and up to two SM quarks, resulting in a signature similar to the s-channel case, characterised by the presence of two emerging jets.
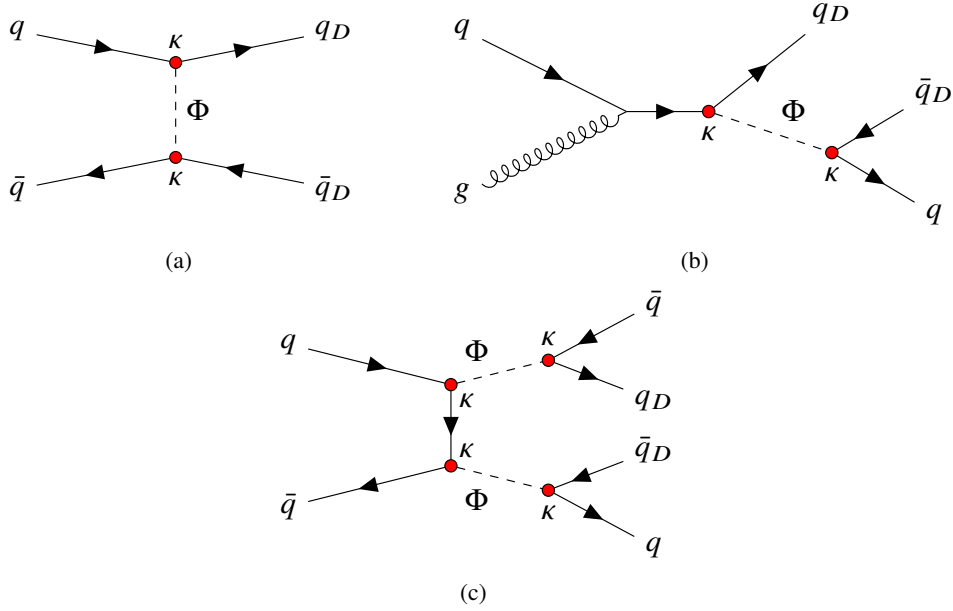
Figure 2: Feynman diagrams for $q_D \bar{q}_D$ production with up to two additional SM jets via a scalar Φ.

This analysis uses two complementary strategies to identify emerging jet signatures: one using selections on high-level jet observables and another using machine learning (ML) techniques to improve signal identification. To maximize sensitivity across different mediator mass ranges, the search is divided into two regions based on the invariant mass of the two leading jets (m_{jj}), each with distinct trigger strategies. The low-m_{jj} region ($m_{jj} < 1$ TeV) utilises a dedicated jet trigger, introduced for Run 3, specifically designed to select emerging jets. The high-m_{jj} region ($m_{jj} > 1$ TeV) relies on a standard single-jet trigger. Combining these two regions provides sensitivity for mediator masses between 600 GeV and 3500 GeV. The dominant background comes from QCD multijet events, which are modelled using a data-driven approach.

This paper is structured as follows: Section 2 provides a description of the ATLAS detector, followed by an overview of the dataset and simulated samples used in the analysis in Section 3. The definitions of the reconstructed objects are outlined in Section 4. Section 5 details the analysis strategies and event selection criteria for each signal region. Background estimation strategies are described in Section 6, while systematic uncertainties are discussed in Section 7. Finally, the statistical analysis and results are presented in Section 8, with conclusions provided in Section 9.

4

2 ATLAS detector

The ATLAS detector [34, 35] at the LHC covers nearly the entire solid angle around the collision point.[1] It consists of an inner tracking detector surrounded by a thin superconducting solenoid, electromagnetic and hadronic calorimeters, and a muon spectrometer incorporating three large superconducting air-core toroidal magnets.

The inner-detector system (ID) is immersed in a 2 T axial magnetic field and provides charged-particle tracking in the range $|\eta| < 2.5$. The high-granularity silicon pixel detector covers the vertex region and typically provides four measurements per track, the first hit normally being in the insertable B-layer installed before Run 2 [36, 37]. The geometry of the pixel detector consists of concentric barrel layers with r = 33, 50.5, 88.5, and 122.5 mm in the central region, and three disks in each of the endcaps at $|z|$ = 495, 580, and 650 mm. It is followed by the silicon microstrip tracker (SCT), consisting of barrel layers at r = 299, 371, 443, and 514 mm, spanning $|z| < 746$ mm, and nine wheels in each of the endcaps with $854 < |z| < 2720$ mm. The SCT usually provides eight measurements per track. These silicon detectors are complemented by the transition radiation tracker (TRT), which enables radially extended track reconstruction up to $|\eta| = 2.0$. The TRT also provides electron identification information based on the fraction of hits (typically 30 in total) above a higher energy-deposit threshold corresponding to transition radiation.

The calorimeter system covers the pseudorapidity range $|\eta| < 4.9$. Within the region $|\eta| < 3.2$, electromagnetic calorimetry is provided by barrel and endcap high-granularity lead/liquid-argon (LAr) calorimeters, with an additional thin LAr presampler covering $|\eta| < 1.8$ to correct for energy loss in material upstream of the calorimeters. Hadronic calorimetry is provided by the steel/scintillator-tile calorimeter, segmented into three barrel structures within $|\eta| < 1.7$, and two copper/LAr hadronic endcap calorimeters. The solid angle coverage is completed with forward copper/LAr and tungsten/LAr calorimeter modules optimised for electromagnetic and hadronic energy measurements, respectively.

The muon spectrometer comprises separate trigger and high-precision tracking chambers measuring the deflection of muons in a magnetic field generated by the superconducting air-core toroidal magnets. The field integral of the toroids ranges between 2.0 and 6.0 T m across most of the detector. Three layers of precision chambers, each consisting of layers of monitored drift tubes, cover the region $|\eta| < 2.7$, except in the innermost layer of the endcap region, where layers of small-strip thin-gap chambers and Micromegas chambers both provide precision tracking in the region $1.3 < |\eta| < 2.7$. The muon trigger system covers the range $|\eta| < 2.4$ with resistive-plate chambers in the barrel, thin-gap chambers in the endcap regions, and the aforementioned small-strip thin-gap chambers and Micromegas chambers in the innermost layer of the endcap.

The luminosity is measured mainly by the LUCID–2 detector that records Cherenkov light produced in the quartz windows of photomultipliers located close to the beampipe [38].

Events are selected by the first-level trigger system implemented in custom hardware, followed by selections made by algorithms implemented in software in the high-level trigger [39]. The first-level trigger accepts

---

[1] ATLAS uses a right-handed coordinate system with its origin at the nominal interaction point (IP) in the centre of the detector and the z-axis along the beam pipe. The x-axis points from the IP to the centre of the LHC ring, and the y-axis points upwards. Polar coordinates (r, ϕ) are used in the transverse plane, ϕ being the azimuthal angle around the z-axis. The pseudorapidity is defined in terms of the polar angle θ as $\eta = -\ln\tan(\theta/2)$ and is equal to the rapidity $y = \frac{1}{2}\ln\left(\frac{E+p_z}{E-p_z}\right)$ in the relativistic limit. Angular distance is measured in units of $\Delta R \equiv \sqrt{(\Delta y)^2 + (\Delta\phi)^2}$.

events from the 40 MHz bunch crossings at a rate below 100 kHz, which the high-level trigger further reduces in order to record complete events to disk at an average rate of about 3 kHz.

The Run 3 detector configuration benefits from several upgrades compared with that of Run 2 to maintain high detector performance at the higher pile-up levels of Run 3. The improvements include a new innermost layer of the muon spectrometer in the endcap region, which provides higher redundancy and a large reduction in fake muon triggers. The trigger system also benefits from new LAr digital electronics with significantly increased granularity. Other updates and further details are provided in Ref. [35].

A software suite [40] is used in data simulation, in the reconstruction and analysis of real and simulated data, in detector operations, and in the trigger and data acquisition systems of the experiment.

3 Data and simulated events

This analysis uses 51.8 fb^{-1} of $\sqrt{s}$ = 13.6 TeV pp collision data collected by the ATLAS experiment from 2022 to 2023 during Run 3 of the LHC. Only data recorded under stable beam conditions with all detector subsystems fully operational are included, and standard data quality requirements are applied to ensure reliable event reconstruction [41].

Monte Carlo (MC) events are used to evaluate the signal acceptance, optimise the analysis methodology, and validate the performance of the background estimation methods. The effect of multiple interactions in the same and neighbouring bunch crossings (pile-up) is modelled by overlaying [42] the simulated hard-scattering event with inelastic pp events generated from a mix of Epos 2.0.1.4 [43] and Pythia 8.308 [44]. The MC events are then weighted to reproduce the distribution of the average number of interactions per bunch crossing ($\langle \mu \rangle$) observed in the data. All simulated events are processed through a detailed simulation of the ATLAS detector using Geant4 [45] to model the detector response [46], and are reconstructed using the same algorithms applied to the data.

3.1 Signal simulation

Samples of $pp \rightarrow Z' \rightarrow q_D \bar{q}_D$ are simulated using Pythia 8.309 [44] with Z' masses ranging from 600 GeV to 3.5 TeV. The production cross-section is a free parameter that depends on the coupling of the Z' to SM quarks, g_q. For benchmark values of $g_q = 0.01$ and $g_{q_D} = 0.1$, the production cross-section computed at leading-order (LO) ranges from 220 fb at $m_{Z'}$ = 600 GeV to 0.035 fb at $m_{Z'}$ = 3500 GeV, with branching ratios to dark quarks of approximately 85%. For the cross-section values explored, varying g_q does not affect the dijet mass distribution because the true Z' width remains much smaller than the reconstructed width, which is dominated by resolution and reconstruction effects. When calculating the theoretical cross-sections it is assumed that the Z' mediator has axial-vector couplings [47].

Signal samples for t-channel production are generated using the MadGraph5_aMC@NLO v3.4.2 event generator [48], with the `darkqcd_fv_down` model from Ref. [33] used to calculate matrix elements (ME) at LO, including up to two additional partons. The coupling between the mediator Φ, dark quarks, and SM

quarks is described by a matrix κ_{ij}. In this study, Φ is assumed to couple only to down-type SM quarks [2] and to the first-generation dark quark. As a result, only the matrix elements κ_{ij} with $i = 1$ (corresponding to the dark quark flavour) and $j = 1, 2, 3$ (corresponding to the SM down-type quark flavours) are considered. For $\kappa_{1j} = 0.1$, the cross-section computed at LO ranges from 10 fb at $m_\Phi = 600$ GeV to 0.0082 fb at $m_\Phi = 2000$ GeV. Jet matching is performed using the MLM [49] scheme, with a matching parameter of 20 GeV. For both mediator scenarios, the NNPDF2.3LO [50] parton distribution function (PDF) set and the A14 tuned parameter set [51] are used.

In all samples, the dark sector showers are produced in PYTHIA 8.309 using the Hidden Valley module [52, 53]. Following Ref. [26], the number of dark colours is set to $N_c = 3$, the number of dark quark flavours is set to $N_f = 7$, and the confinement scale, Λ_D, the dark quark masses, q_D, the dark pion masses, m_{π_D}, and the dark vector meson masses, m_{ρ_D} are set with the following hierarchy: $m_{\rho_D} = 2\Lambda_D = 2m_{q_D} = 4m_{\pi_D}$. The dark rho mesons are set to decay via $\rho_D \to \pi_D \pi_D$, with the resulting dark pions forced to decay into down quarks. The proper decay length of the dark pions is fixed per generated sample with values ranging from 1 mm to 1000 mm, ensuring that the majority of decays occur prior to reaching the calorimeter. Dark baryon production, which is suppressed by a factor of $1/N_c^2$ [25], is not considered. Three different sets of model parameters are considered, corresponding to m_{π_D} values of 5, 10, and 20 GeV, respectively. A summary of the signal benchmarks is provided in Table 1.

Table 1: Benchmark models used in the analysis. In the headings, Λ_D corresponds to the dark confinement scale and the masses m_{π_D} and m_{ρ_D} correspond to the masses of the dark pion and dark rho mesons, respectively. For each mediator mass—either $m_{Z'}$ or m_Φ—and each set of dark sector parameters ($m_{\pi_D}, \Lambda_D, m_{\rho_D}$), samples are generated with dark pion proper decay lengths of 5 mm, 50 mm, and 500 mm, indicated in bold in the table. For mediator masses $m_{Z'}$ and m_Φ equal to 0.6, 1.5, or 3.0 TeV, an extended grid of dark pion lifetimes is generated, spanning proper decay lengths from 1 mm to 1000 mm.

$(m_{\pi_D}, \Lambda_D, m_{\rho_D})$ [GeV]	(5, 10, 20), (10, 20, 40), (20, 40, 80)
$m_{Z'}$ [TeV]	0.6, 0.8, 1.0, 1.2, 1.5, 1.8, 2.2, 2.6, 3.0, 3.5
m_Φ [TeV]	0.6, 1.0, 1.5, 2.0
$c\tau_{\pi_D}$ [mm]	1, **5**, 10, **50**, 100, **500**, 1000

3.2 Background simulation

While the background modelling strategy used in this analysis is fully data driven, samples of simulated background events are used to optimise the analysis selections and validate the background estimation methods.

Multijet production was generated using PYTHIA 8.230 [54] with ME at LO for dijet production which were matched to the parton shower. The NNPDF2.3LO PDF set was used in the matrix element generation, the parton shower, and the simulation of the multi-parton interactions. The A14 [51] set of tuned parameters was used.

---

[2] The choice of coupling to down-type quarks corresponds to the scenario where Φ is an $SU(2)_L$ singlet with hypercharge $Y = 1/3$. Alternative quantum number assignments could instead lead to couplings to up-type quarks. For the values of κ considered in this analysis, this choice has a negligible impact on both the final-state signature and the theoretical production cross-section [33].

The production of $t\bar{t}$ events was modelled using the Powheg Box v2 [55–58] generator at next-to-leading-order (NLO) with the NNPDF3.0NLO [59] PDF set and the h_{damp} parameter[3] set to $1.5\,m_{\text{top}}$ [60]. The events were interfaced to Pythia 8.230 [54] to model the parton shower, hadronisation, and underlying event, with parameters set according to the A14 tune [51] and using the NNPDF2.3LO set of PDFs. The decays of bottom and charm hadrons were performed by EvtGen 1.6.0 [61].

The production of V+jets was simulated with the Sherpa 2.2.14 [62] generator using ME at NLO for up to two partons, and LO for up to five partons calculated with the Comix [63] and OpenLoops [64–66] libraries. They were matched with the Sherpa parton shower [67] using the MEPS@NLO prescription [68–71] using the set of tuned parameters developed by the Sherpa authors. The NNPDF3.0NNLO set of PDFs was used and the samples were normalised to a next-to-next-to-leading-order (NNLO) prediction [72].

4 Event reconstruction and selections

Tracks are reconstructed from collections of energy deposits (hits) in the ID using a combinatorial Kalman filter [73] in two passes. The primary pass is optimised for reconstructing tracks originating near the primary interaction point (IP) and is designed to efficiently reconstruct prompt charged particles with $p_{\text{T}} > 500$ MeV. This algorithm primarily selects tracks with transverse impact parameters of $|d_0| < 5$ mm relative to the IP, making it largely insensitive to displaced tracks from decays of long-lived particles. To extend tracking acceptance to displaced signatures, a secondary large-impact parameter track reconstruction pass is performed using hits not associated with tracks in the primary pass. This secondary pass relaxes the impact parameter requirements, enabling the reconstruction of tracks with $p_{\text{T}} > 1$ GeV and transverse impact parameters up to $|d_0| < 300$ mm [74].

The jet reconstruction strategy employed in this analysis is tailored to the distinct characteristics of jets originating from dark sector quarks. Unlike conventional QCD jets, these jets undergo a two-stage showering process—first within the dark sector and then in the SM—resulting in a broader radiation pattern. To fully capture the resulting hadronic shower, jets are reconstructed using the anti-k_t algorithm [75, 76] with a radius parameter of $R = 1.0$. Additionally, the displaced nature of the jet constituents poses challenges for track-based jet reconstruction. In particular, the ATLAS particle flow algorithm [77], which associates jet constituents with the primary hard-scatter vertex (PV), may reject displaced tracks that fail this association, thereby reducing sensitivity to the emerging jet topology. To mitigate these effects, a calorimeter-based jet reconstruction strategy is adopted, where uncalibrated topological clusters [78, 79] are first clustered into $R = 0.4$ jets using the anti-k_t algorithm. The subset of these small-R jets with transverse momentum $p_{\text{T}} > 15$ GeV are subsequently reclustered into large-R ($R = 1.0$) jets. This reclustering approach allows for the calibration and uncertainty assessment of the small-R jets using standard ATLAS techniques, which can then be propagated to the large-R jets. Additionally, the transverse momentum requirement on the small-R jets acts as an effective grooming mechanism, reducing soft contamination without requiring additional grooming procedures. To facilitate the data-driven background estimation strategy outlined in Section 6, small-R jets are identified as b-jets if they satisfy the 77% efficiency working point of the DL1r algorithm [80]. As part of the reconstruction of reclustered $R = 1.0$ jets, a track-to-jet association is performed for both standard and large-impact parameter tracks using the ghost-association technique [81] that defines which tracks are later used to calculate discriminants for emerging jets identification. All large-R jets considered in this analysis are required to have $p_{\text{T}} > 200$ GeV

---

[3] The h_{damp} parameter is a resummation damping factor and one of the parameters that controls the matching of Powheg ME to the parton shower and thus effectively regulates the high-p_{T} radiation against which the $t\bar{t}$ system recoils.

and $|\eta| < 1.5$. Unless otherwise stated, the term "jet" in this paper refers to a large-R jet that satisfies these selection criteria.

Photons can mimic the signature of emerging jets due to their low associated track activity, and are therefore treated as a potential background. Photon candidates are reconstructed from clustered energy deposits in the electromagnetic calorimeter, either without a matching ID track or with an associated photon conversion vertex in the ID material. The *Loose* identification and *Tight* isolation criterion are applied [82]. To mitigate this background, an overlap removal procedure is implemented where large-R jets are discarded if a photon with $p_T > 10$ GeV is found within $\Delta R = 1.0$ of the jet axis.

Events are required to have a reconstructed primary vertex with at least two associated tracks [83]. The hard scatter (HS) primary vertex is selected as the one with the largest Σp_T^2, where the sum is over all primary tracks with transverse momentum $p_T > 0.5$ GeV that are associated with the vertex.

Events are selected using one of two unprescaled single jet triggers [39], both with the same Level 1 requirement that at least 100 GeV of transverse energy, at the EM scale, is deposited in a region of the calorimeters of size 0.8×0.8 in $\eta - \phi$ space [39, 84, 85]. The first trigger, henceforth referred to as the *high-p_T trigger*, selects events containing a large-R jet and $p_T > 460$ GeV. This trigger is fully efficient offline for jets with $p_T > 520$ GeV. The second, henceforth referred to as the *emerging jet trigger*, selects events containing at least one large-R jet with $p_T > 200$ GeV, $|\eta| < 1.8$ and a prompt track fraction (PTF) smaller than 0.08. The PTF is defined as the ratio of the transverse momentum sum of tracks within $\Delta R = 1.2$ of the jet to the jet's transverse momentum,

$$\text{PTF} = \frac{\sum_{\text{trk} \subseteq \Delta R < 1.2} p_T^{\text{trk}}}{p_T^{\text{jet}}} \tag{1}$$

calculated using the standard track finding algorithm only. The tracks entering into the PTF calculation are required to have $p_T > 1$ GeV, $|d_0|/\sigma(d_0) < 2.5$, and $\Delta z = |z_{\text{PV}} - z_0| < 10$ mm, where $\sigma(d_0)$ is the uncertainty on the d_0 measurement and z_{PV} is the position of the HS PV along the z-axis. These selections are applied to suppress contributions from pile-up interactions.

A displaced vertex reconstruction algorithm is applied to the combined collection of tracks from both the primary and large-impact parameter tracking passes [86]. To suppress backgrounds from photon conversions and long-lived SM hadrons, vertices are required to have at least three associated tracks. Additionally, to reduce contamination from neutral kaons, a vertex mass requirement of $m_{\text{vtx}} > 0.6$ GeV is imposed, where the vertex mass is computed as the invariant mass of the sum of the four-momenta of the associated tracks, assuming a pion mass hypothesis. A material veto is then applied to remove vertices whose positions coincide with the location of known detector material. The mapping of the ID material was performed using Run 2 data [87] and validated with 2022 collision data. These selection criteria enhance sensitivity to displaced vertices from LLP decays while effectively suppressing backgrounds from detector interactions and SM processes. For a given jet, N_{vtx} is defined as the number of displaced vertices that satisfy the above criteria and fall within $\Delta R < 1.0$ of the jet axis.

5 Analysis strategy

This analysis employs two complementary analysis strategies. The first approach, referred to as the "cut-based strategy", identifies candidate EJs based on selections applied to high-level jet observables,

including track-based, vertex-based, and jet substructure-based selections. The second approach, referred to as the "ML-based strategy", uses a per-jet transformer-based ML algorithm trained to differentiate emerging jets from SM jets. While the cut-based method facilitates reinterpretation of the results for alternative theoretical models beyond those considered in this study, the ML-based strategy maximizes sensitivity for the specific models considered by this analysis.

For each strategy, two orthogonal event selections are defined based on the dijet invariant mass. The low-m_{jj} selection targets lower mediator masses, specifically selecting events with $m_{jj} < 1$ TeV. This region makes use of the emerging jet trigger that has sensitivity to final states with lower p_T jets. The high-m_{jj} selection targets higher mediator masses, requiring $m_{jj} > 1$ TeV. This region is probed using the high-p_T trigger, which is fully efficient after the offline selections. All events considered in this analysis are required to have at least two large-R jets satisfying the definitions given in Section 4.

5.1 Cut-based strategy

The cut-based strategy uses jet-level properties to exploit both the displaced nature and multi-pronged structure of emerging jets, enabling effective rejection of SM backgrounds. An initial set of selections, referred to as preselections, is applied based on these observables. The signal region (SR) is then defined by applying two additional selections on top of the preselections. These two variables also define a two-dimensional space referred to as the *ABCD plane* in which control regions (CRs) are identified. The CRs are used to estimate the background through a data-driven method known as the *ABCD method*, described in detail in Section 6.

In both high-m_{jj} and low-m_{jj} selections, the leading and subleading jets are each required to have at least one associated secondary vertex ($N_{vtx} \geq 1$). The distributions of N_{vtx} are shown in Figure 3. In
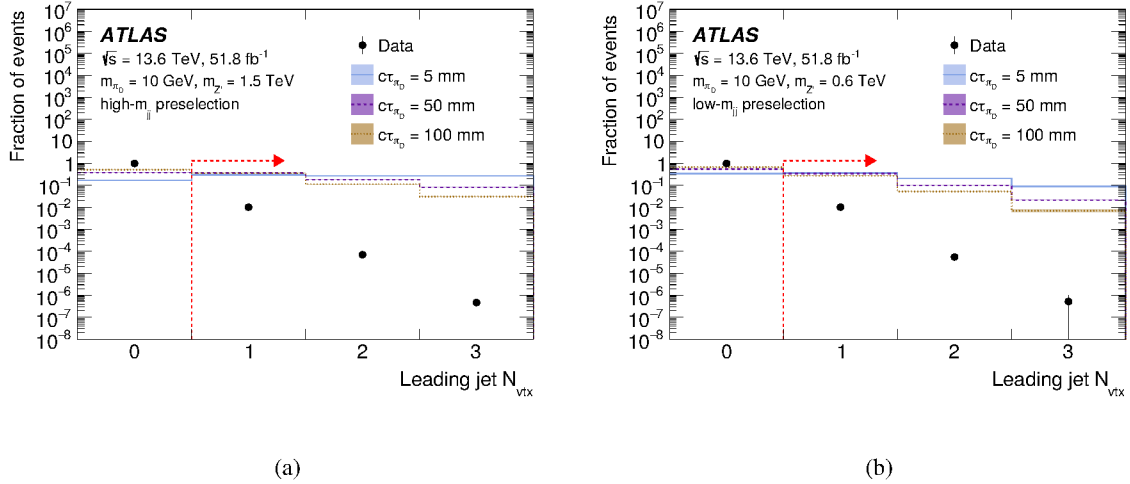
Figure 3: Normalised distributions of N_{vtx} for the leading jet in (a) the high-m_{jj} preselection and (b) the low-m_{jj} preselection for signal events (lines) and data (circles). The selection placed on the observable in the analysis is indicated with a dashed arrow. The rightmost bins include contributions from overflow events.

both regions, PTF is used to suppress background from SM jets using the same definition as in the trigger (Eq. 1). A key challenge in defining the PTF variable is the potential misassignment of the primary vertex in high-pile-up events. If a pile-up vertex is incorrectly identified as the HS PV, prompt tracks in the

leading jets may have a large Δz relative to the misidentified PV, resulting in artificially low PTF values and populating the SRs with background events. To mitigate this, the difference between the PTF values with and without the Δz requirement is computed:

$$\Delta\text{PTF} = |\text{PTF} - \text{PTF}_{\text{no } \Delta z \text{ cut}}| \tag{2}$$

In both high-m_{jj} and low-m_{jj} selections, the leading and subleading jets are required to have $\Delta\text{PTF} < 0.4$ to help reduce background contamination from PV misassignment. This criterion has minimal impact on signal efficiency, rejecting fewer than 1% of events.

5.1.1 High-m_{jj} region

In the high-m_{jj} region, events are required to pass the high-p_T trigger. To ensure full trigger efficiency, the leading jet is required to have $p_T > 520$ GeV, while the subleading jet must satisfy $p_T > 300$ GeV to reduce background. Both jets are further required to have PTF < 1.0. To further suppress background contributions, a selection is applied based on the 2-point energy correlation function (ECF2) [88], defined as:

$$\text{ECF2} = \sum_{i<j\in\text{trk}} p_T^i p_T^j \Delta R_{ij} \tag{3}$$

where the sum runs over all pairs of tracks associated with the jet. ECF2 quantifies the angular energy dispersion of a jet by measuring pairwise correlations between the transverse momenta of tracks and their angular separation. It is particularly sensitive to jets with multi-pronged substructure, such as those arising from dark quarks. In such cases, the presence of multiple hard prongs leads to larger ECF2 values compared to jets from standard QCD processes, which typically exhibit a more collimated, single-prong structure. To exploit this feature, a requirement of $\text{ECF2}/p_T > 40$ GeV is imposed on both the leading and subleading jets. This selection rejects approximately 40% of background jets while retaining over 90% signal efficiency across the benchmark models considered.

As discussed above, the surviving events are mapped onto an ABCD plane defined by two independent variables, allowing a data-driven background estimation, as described in Section 6. In the high-m_{jj} region, the ABCD variables are the PTF of the leading and subleading jets. The SR is defined by requiring both the leading and subleading jet PTF to be less than 0.2. Distributions of the leading jet PTF are shown in Figure 4(a). The corresponding subleading jet distributions exhibit similar behaviour and are therefore omitted. The full set of selections applied in the high-m_{jj} cut-based region is provided in Table 2. For signal samples with a mediator mass of 1500 GeV and $m_{\pi_D} = 10$ GeV, the total signal selection efficiency varies from 0.070% (0.078%) in the s-channel (t-channel) at a lifetime of $c\tau_{\pi_D} = 1000$ mm to a maximum of 29% (15%) at $c\tau_{\pi_D} = 5$ mm.

5.1.2 Low-m_{jj} region

In the low-m_{jj} region, events are required to pass the emerging jet trigger. The jets matched to the trigger-level objects are required to have $p_T > 250$ GeV and PTF < 0.04. Since this p_T threshold is below the trigger efficiency plateau [39], a p_T-dependent trigger efficiency scale factor is applied to each simulated event. This scale factor is derived by comparing the emerging jet trigger efficiency in data and samples of simulated V+jets events in a dedicated event selection requiring a single-muon trigger [39]. The efficiency curves for both data and simulation are fitted using an error function, and the ratio of the

11

two fitted curves is taken as the trigger scale factor. The scale factor ranges from 0.72 at $p_T = 250$ GeV to 0.96 at $p_T = 500$ GeV.

Due to the preselection requirement on the PTF of the trigger-matched jet, jets in the low-m_{jj} region are biased toward lower PTF values, rendering this variable unsuitable for defining an ABCD plane. Instead, the low-m_{jj} ABCD plane is defined using the number of subjets (N_{subjet}) in the leading and subleading jets, where "subjets" refer to the small-R jets that serve as constituents of the large-R jets. Emerging jets typically exhibit a higher number of subjets compared to standard SM jets due to their two-stage parton shower and hadronisation process. To exploit this property, a minimum of three subjets per large-R jet is required in the SR selection. The leading jet N_{subjet} distributions for signal events and data are shown in Figure 4(b). Table 2 lists the complete set of selections used in the low-m_{jj} cut-based region. For signal samples with a mediator mass of 600 GeV and $m_{\pi_D} = 10$ GeV, the total signal selection efficiency varies from 0.011% (0.017%) in the s-channel (t-channel) at a lifetime of $c\tau_{\pi_D} = 1000$ mm to a maximum of 8.9% (3.7%) at $c\tau_{\pi_D} = 10$ mm.
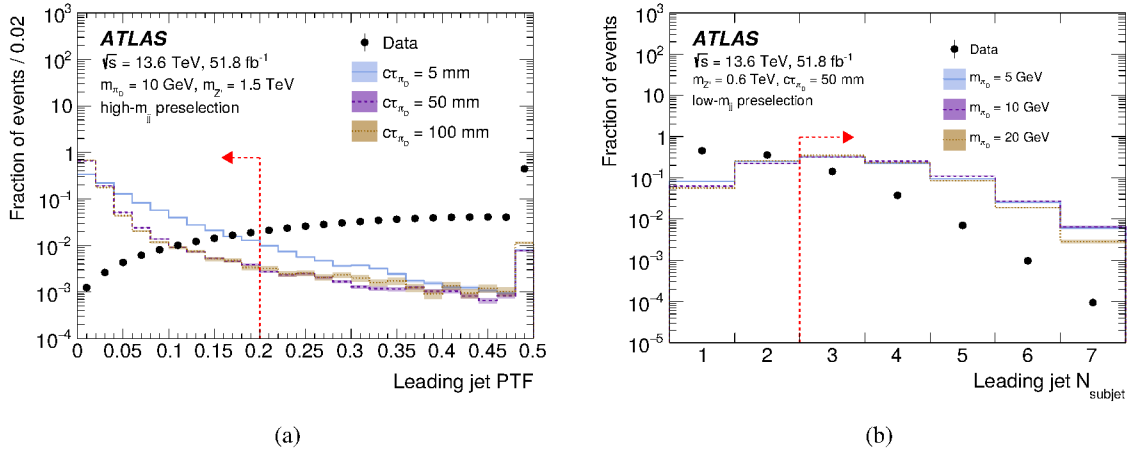
Figure 4: Normalised distributions of (a) the leading jet PTF in the high-m_{jj} preselection and (b) the leading jet number of subjets in the low-m_{jj} preselection in signal events (lines) and data (circles). The selection applied to the observable to define the signal region is indicated by a dashed arrow. The rightmost bins include contributions from overflow events.

5.2 ML-based strategy

The ML-based strategy uses a transformer jet tagging algorithm based on the ATLAS GN2 flavour tagging algorithm [89]. The input to the model consists of jet features concatenated with the feature vectors of up to 200 associated tracks. These feature vectors are processed by a per-track initialization network, which includes a hidden layer and an output layer of size 256, increasing each tracks' embedding dimension. The embedded track representations are then passed through a five-layer transformer encoder with eight attention heads to produce conditional track representations based on the other tracks in the jet. The resulting track embeddings are projected to a dimension of 128, and a global jet representation is computed using attention pooling [90].

The complete list of jet and track features is provided in Table 3. The only jet feature included is pseudorapidity, which helps to account for tracking efficiency effects related to detector acceptance. Jet p_T,

Table 2: Selection criteria for the low-m_{jj} and high-m_{jj} regions including the preselections and signal regions for the cut-based strategy. Common criteria are merged across both columns.

Preselection	Low-m_{jj}	High-m_{jj}
leading jet p_T	–	> 520 GeV
subleading jet p_T	–	> 300 GeV
trigger-matched jet	p_T > 250 GeV, PTF < 0.04	–
leading and subleading jet PTF	< 1.0	
leading and subleading jet ΔPTF	< 0.4	
leading and subleading jet N_{vtx}	≥ 1	
leading and subleading jet ECF2/p_T	–	> 40 GeV
m_{jj}	< 1 TeV	> 1 TeV
number of jets	≥ 2	
Signal Region		
leading and subleading jet N_{subjet}	≥ 3	–
leading and subleading jet PTF	–	< 0.2

an input in the GN2 algorithm, is excluded as it was found to provide no improvement in classification performance while increasing the tagger's dependence on jet momentum.

Table 3: List of the track and jet variables used in the transformer-based emerging jet tagging algorithm. Each track in the jet has its own input feature vector with this information. The first entry is a jet level input, which is common to all of the tracks. "Shared hits" refer to hits that are common between multiple reconstructed tracks.

Input	Description
Jet η	Jet pseudorapidity
d_0	Track closest distance to PV in transverse plane
$z_0\sin(\theta)$	Track closest distance to PV in longitudinal plane
$\Delta\phi$	Azimuthal angle of the track, relative to the jet ϕ
$\Delta\eta$	Track pseudorapidity, relative to jet η
q/p	Track charge over momentum
$\sigma(\phi)$	Uncertainty in track ϕ
$\sigma(\theta)$	Uncertainty in track θ
$\sigma(q/p)$	Uncertainty in track q/p
$d_0/\sigma(d_0)$	signed d_0 significance
$z_0/\sigma(z_0)$	signed z_0 significance
$N_{PIX\ hits}$	Number of Pixel hits per track
$N_{SCT\ hits}$	Number of SCT hits per track
$N_{IBL\ hits}$	Number of innermost pixel layer hits
$N_{PIX\ shared}$	Number of Pixel shared hits
$N_{SCT\ shared}$	Number of SCT shared hits

The algorithm optimises three tasks simultaneously: jet classification, track origin classification, and track-pair compatibility. The primary jet classification network, which operates on the pooled jet representation, outputs the probability that a given jet is an emerging jet, p_{EJ}, which is referred to as the jet classification score. The track origin classification network assigns each track to one of four categories based on its associated truth-matched particle [74]: prompt (originating from the hard-scatter event but not from a dark pion decay), pile-up (originating from a pile-up vertex), fake (no valid truth match), and displaced (originating from a dark pion decay). The track-pair compatibility network predicts whether two tracks originate from the same vertex using a binary classifier. Each task-specific network consists of three hidden layers with sizes 128, 64, and 32, using Rectified Linear Unit (ReLU) activation functions throughout [91]. A combined cross-entropy loss function with tunable weights ensures simultaneous optimisation of all three tasks. The output of the auxiliary tasks is not directly used in the selection of emerging jet candidates in the analysis, but it plays a crucial role in improving the convergence of the jet classification task by contributing to the overall loss function.

The model is trained on 12 million jets, equally sampled from simulated SM multijet events and $pp \rightarrow Z' \rightarrow q_D \bar{q}_D$ events taken from samples with $m_{Z'} \in \{600, 1500, 3000\}$ GeV and $c\tau_{\pi_D} \in \{5, 50\}$ mm. To prevent evaluation bias, the dataset is split into two disjoint folds (f_0, f_1), each containing six million jets. Two separate instances of the tagger are trained, one per fold, with 5.5 million jets for training and 500,000 for validation. During evaluation, jets used to train f_0 are tested with f_1, and vice versa. The two folds yield statistically consistent performance.

Figure 5 shows a matrix representation comparing the true and predicted classifications of tracks and vertex groupings for an example signal jet with a classification score of $p_{EJ} = 1.000$. The tracks are displayed along the diagonal and are distinguished by marker style according to their origin: pile-up/fake, prompt, or displaced. Vertex groupings are marked by black areas and are formed using the track pair-wise compatibility scores via a union-find algorithm [92]. The auxiliary tasks exhibit high performance on this example jet, with 85% of tracks correctly labeled and 79% successfully assigned to their respective vertices. Across the full test dataset, displaced tracks are correctly labeled with an average accuracy of 91%, and 80% are successfully grouped into their corresponding vertices.

Similar to the cut-based strategy, events are categorised into high-m_{jj} ($m_{jj} > 1$ TeV) and low-m_{jj} ($m_{jj} < 1$ TeV) regions. In the high-m_{jj} region, events are required to pass the high-p_T trigger, with the leading jet satisfying $p_T > 520$ GeV and the subleading jet having $p_T > 300$ GeV. In the low-m_{jj} region, events must pass the emerging jet trigger, and the jet that is matched to the trigger-level object is required to have $p_T > 300$ GeV and PTF < 0.04. The p_T threshold in the ML-based strategy is higher than in the cut-based approach, as the background rejection of the jet classification task is observed to degrade at low p_T, as discussed in Section 6. These requirements define the preselection for the ML-based strategy. No selection is applied on N_{vtx} or ΔPTF.

The distribution of the jet classification score is shown in Figure 6. The probability p_{EJ} is used to tag emerging jet candidates with a threshold of 0.98. Jets with $0.90 < p_{EJ} < 0.98$ are used to define a validation region (VR) tag, as described in Section 6. For both low-m_{jj} and high-m_{jj} regions, a SR is defined by requiring $n_{tag} \geq 2$, where n_{tag} is the number of tagged jets in the event, and a CR is defined by requiring $n_{tag} < 2$. The threshold of 0.98 was chosen to optimise background rejection while ensuring that the level of signal contamination in the control region remained below 10%, assuming signal cross sections to which the analysis is expected to be sensitive. This threshold yields a 97.5% EJ tagging efficiency and a background rejection factor of 2600 on the testing dataset.
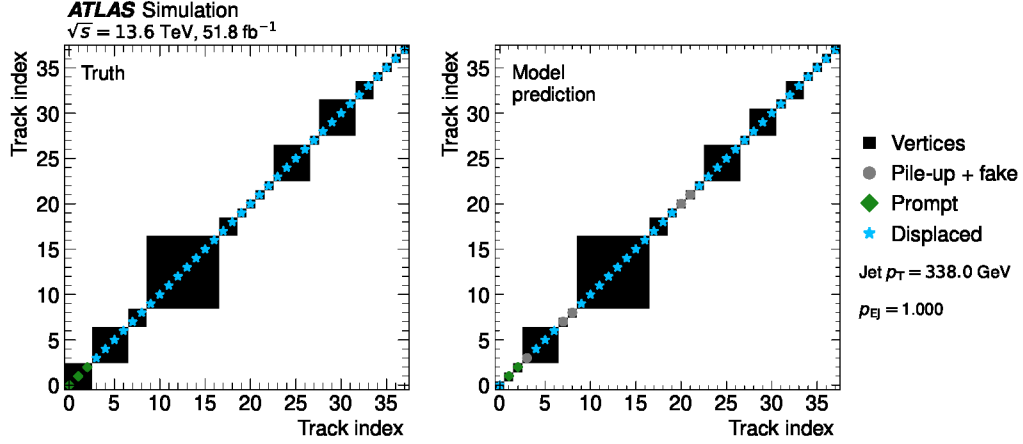
Figure 5: Example of the auxiliary task performance on a single jet with $p_{\mathrm{EJ}} = 1.000$ from a sample of simulated signal events with $m_{Z'} = 1500$ GeV, $m_{\pi_D} = 10$ GeV, and $c\tau_{\pi_D} = 50$ mm. The reconstructed tracks in the jet are shown along the diagonal and are displayed using different markers based on their origin, with displaced tracks shown as stars, prompt tracks shown as diamonds, and both pile-up and fake tracks shown as circles. Groups of tracks that form a common vertex are shown as filled squares. The left diagram shows the true track and vertex labels, and the right diagram shows the model predictions. Track indices are ordered such that tracks originating from the same truth vertex appear consecutively.
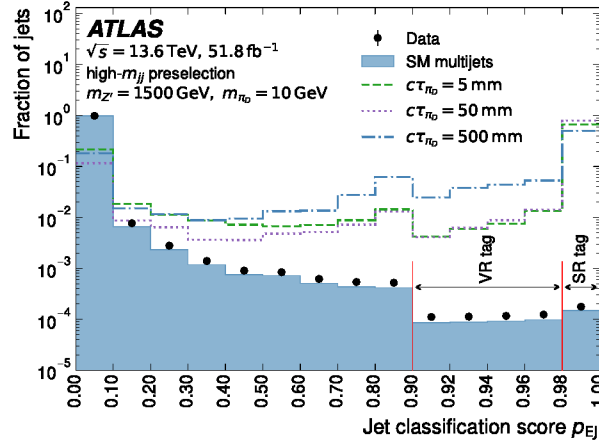
Figure 6: Normalised distribution of the jet classification score for all jets in data, simulated SM multijets background, and selected signal samples with $m_{Z'} = 1500$ GeV and $m_{\pi_D} = 10$ GeV passing the ML-based high-m_{jj} preselection. Vertical lines indicate the selections placed on the classification score used to define a validation tag and a signal tag. No uncertainties are shown on the background MC, which is intended for qualitative comparison only.

The complete set of selections for the ML-based analysis are listed in Table 4. For samples with $m_{Z'} = 1500$ GeV and $m_{\pi_D} = 10$ GeV, the total signal selection efficiency considering both low-m_{jj} and high-m_{jj} regions ranges from 28% at $c\tau_{\pi_D} = 1$ mm to 0.8% at $c\tau_{\pi_D} = 1000$ mm, reaching a maximum of 35% at $c\tau_{\pi_D} = 50$ mm. In the case of the t-channel scalar mediator scenario with $m_\Phi = 1500$ GeV, the efficiency spans from 53% to 2.5% over the same lifetime range, with a maximum of 65% observed at $c\tau_{\pi_D} = 10$ mm.

Table 4: Selection criteria for low-m_{jj} and high-m_{jj} regions. Common criteria are merged across both columns.

Variable	Low-m_{jj}	High-m_{jj}
leading jet p_{T}	> 300 GeV	> 520 GeV
trigger-matched jet	p_{T} > 300 GeV & PTF < 0.04	-
sub-leading jet p_{T}	> 200 GeV	> 300 GeV
m_{jj}	< 1 TeV	> 1 TeV
number of jets	≥ 2	
number of tagged jets (p_{EJ} > 0.98)	CR: 0, 1; SR: ≥ 2	

6 Background estimation

In both the cut-based and ML-based analyses, the dominant background arises from SM multijet production. Due to the difficulties in accurately modelling this background with simulation, data-driven techniques are used for background estimation in both strategies.

6.1 Cut-based strategy

In the cut-based strategy, the data-driven ABCD method is employed to estimate the contribution from SM background in each of the two selections. The method employs a 2D parameter space divided into four regions—A, B, C, and D—by applying selection criteria on each of the two variables. If the background distributions of these variables are independent, the expected background yield in one region is mathematically related to those in the three other regions. Specifically, when the background primarily populates regions B, C, and D, while the signal is concentrated in region A, the background yield in A is estimated as:

$$N_A = \frac{N_B \times N_C}{N_D} \qquad (4)$$

This formula is thus employed in both low-m_{jj} and high-m_{jj} selections to predict the background in their respective SRs, A. When performing the final statistical analysis, any signal contamination in the background regions is accounted for using a simultaneous fit, as described in Section 8.

As described in Section 5.1, the ABCD plane is constructed with the N_{subjet} variable for the leading and subleading jets in the low-m_{jj} selection and the PTF variable in the high-m_{jj} selection. The distribution of events in the ABCD planes as well as the SR and CR are shown in Figure 7 for both the high-m_{jj} and low-m_{jj} selections.

To validate the background estimation method, control regions from the standard ABCD plane are used in both the low-m_{jj} and high-m_{jj} event selections. In the high-m_{jj} case, three modified ABCD planes are defined to probe regions closer to the SR while still being dominated by background. These planes are constructed within merged ABCD control regions—specifically, regions BD, CD, and D—and are used to define new signal-like regions, denoted as A'_{BD}, A'_{CD}, and A'_D. The region A'_{CD} is defined by requiring a subleading jet PTF below 0.2 and a leading jet PTF in the range $0.2 < \mathrm{PTF}_{\mathrm{lead}} < 0.4$. In A'_{BD} events are selected with subleading jet PTF in the range $0.2 < \mathrm{PTF}_{\mathrm{sublead}} < 0.4$, while the leading jet PTF remains below 0.2. Finally, A'_D is defined by selecting events where both the leading and subleading jet PTFs lie within $0.2 < \mathrm{PTF} < 0.4$. A sketch of the signal-like A' regions is shown in Figure 8.

(a)

(b)

(c)

(d)
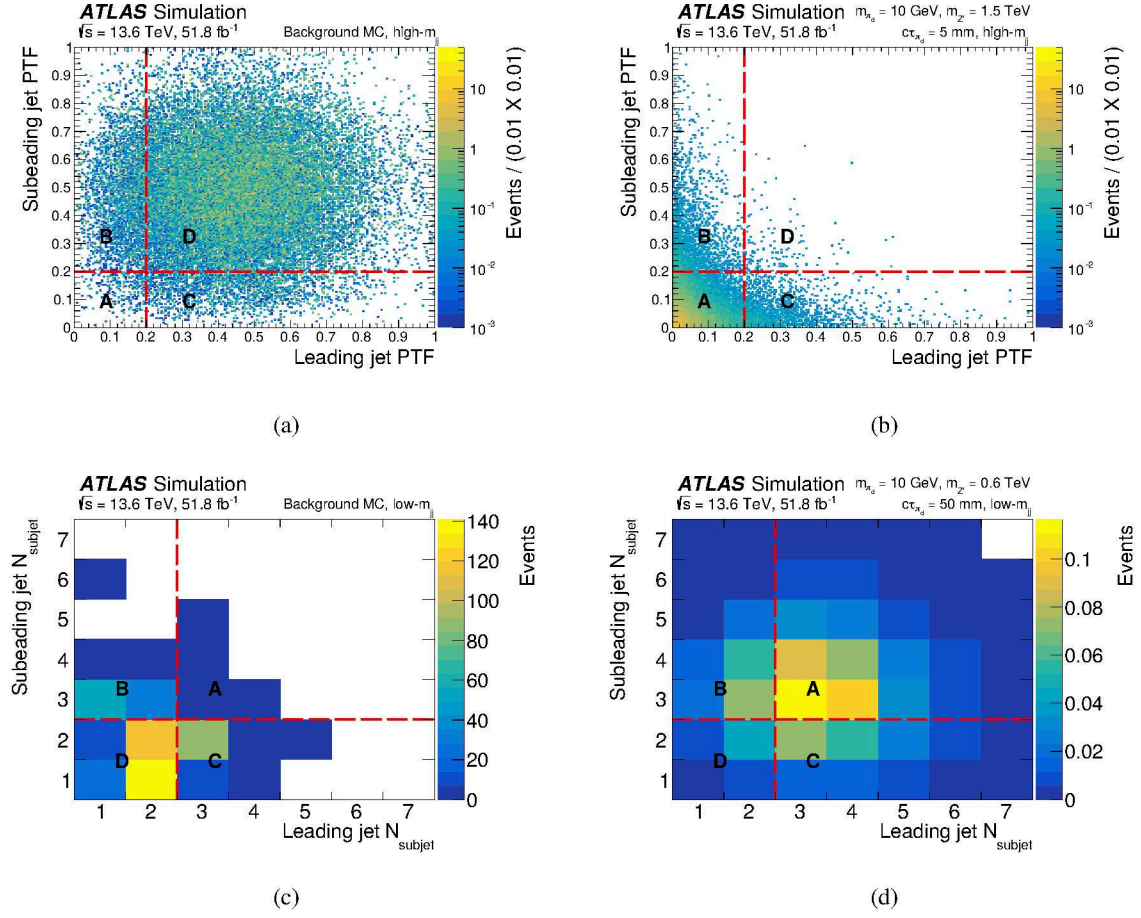
Figure 7: The distributions of (a,c) simulated background events (b,d) and signal events in the (a,b) high-m_{jj} region and (c,d) low-m_{jj} region (bottom). The parameters of the simulated signal shown in (b) corresponds to $m_{Z'} = 1.5$ TeV, $m_{\pi_D} = 10$ GeV, $c\tau_{\pi_D} = 5$ mm and the signal shown in (d) corresponds to $m_{Z'} = 0.6$ TeV, $m_{\pi_D} = 10$ GeV and $c\tau_{\pi_D} = 50$ mm.
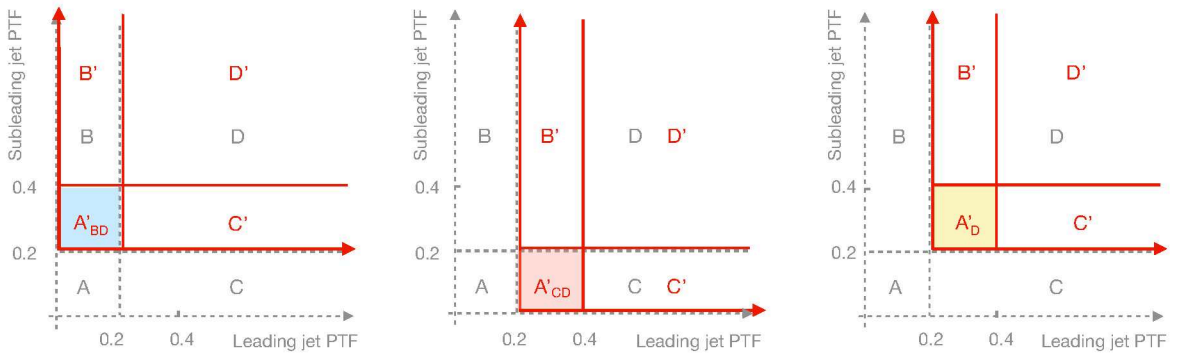
Figure 8: Schematic definitions of the A' control regions within the nominal ABCD plane of the high-m_{jj} selection.

These regions are designed to be the closest approximations to the nominal SR within their respective

Table 5: Predicted and observed yields in the A'_{BD}, A'_{CD}, and A'_D regions of the high-m_{jj} selection, which are closest to the nominal signal region. The predictions are obtained from the ABCD relation in Equation 4.

	A'_{BD}	A'_{CD}	A'_D
Predicted	43 ± 5	26 ± 4	160 ± 14
Observed	49	34	182

modified ABCD planes, thus serving as critical areas for validating the background estimation. The ABCD method is applied in each modified plane to estimate the event yield in the corresponding A' regions. The predicted and observed yields are summarised in Table 5. In each CR, the significance of the deviation is quantified by the absolute difference between the predicted and observed yields, normalised by the quadrature sum of the statistical uncertainty on the prediction and the Poisson uncertainty on the observed yield. To estimate a representative potential nonclosure significance for the SR, the average of these normalised absolute differences across the three A' regions is computed, yielding a value of 1.0. An additional systematic uncertainty is therefore assigned to the SR background prediction, taken as $1.0 \times \sigma_{\text{stat}}(N_{\text{pred},A})$.

Similarly, in the low-m_{jj} region, control regions are merged to define a BD and CD portion of the nominal ABCD plane to test the background estimation strategy. However, due to the discontinuity of the ABCD plane and the limited statistics, constructing a statistically robust test with A' regions closer to the nominal SR is challenging. To mitigate this, the ensemble of A' regions is rather defined by systematically varying the selection thresholds on N_{subjet}, resulting in eight different A' regions and reducing the impact of individual fluctuations on the nonclosure uncertainty. Averaging over these eight tests, the mean absolute discrepancy is found to be 1.0 times the statistical uncertainty of the difference in prediction. Consequently, a nonclosure uncertainty of $1.0 \times \sigma_{\text{stat}}(N_{\text{pred},A})$ is assigned to the background estimate in the low-m_{jj} SR.

Finally, in both the high-m_{jj} and low-m_{jj} regions, additional validations are performed using an ML-inverted VR, where the jet classification scores of the leading and subleading jets in the ABCD plane are required to be less than 0.95. It is verified in simulation that inverting this requirement removes the vast majority signal events while leaving the background nearly unchanged. Consequently, this defines a signal-free plane with a background composition closely matching that of the nominal region, enabling a robust validation of the ABCD method on this background-enriched sample, including in a region A' that closely resembles region A. In both the high-m_{jj} and low-m_{jj} regions, the observed yields in the ML-inverted A' region are found to be in agreement with the ABCD predictions within uncertainties, as shown in Table 6. The ABCD background estimates were further validated using simulated background samples and were found to be consistent within statistical uncertainties.

Table 6: Predicted and observed yields in the A' region of the ML-inverted VR in the high-m_{jj} and low-m_{jj} selections. The predictions are obtained from the ABCD relation in Equation 4 and the systematic uncertainties are the nonclosure uncertainties described in the text.

	low-m_{jj} VR	high-m_{jj} VR
Predicted	$12.7 \pm 3.9(\text{stat.}) \pm 3.9(\text{syst.})$	$7.5 \pm 1.1(\text{stat.}) \pm 1.1(\text{syst.})$
Observed	8	8

6.2 ML-based strategy

In the ML-based strategy, the jet classification score is correlated with several jet-level features, including the p_T and PTF of the jet, as well as the jet flavour. These correlations therefore lead to correlations between the tagger scores of individual jets in each background event. Hence, the ABCD method is not well-suited for predicting the expected background in the GNN-based SRs. Instead, a different data-driven background estimation strategy is used, which relies on the determination of the probability that a given background jet will be misclassified as signal, a quantity henceforth referred to as the *mistag rate*. The mistag rate is measured directly in data using the $n_{tag} < 2$ CR by computing the ratio of tagged jets to all jets in this region.

After calculating the mistag rate, the probability of tagging exactly one or exactly zero jets in an event can be calculated from

$$P(1 \text{ tag}|\text{event}) = \sum_{i=1}^{n_{jet}} P(\text{tag}|j_i) \times \prod_{k \neq i}^{n_{jet}} (1 - P(\text{tag}|j_k)) \tag{5}$$

$$P(0 \text{ tag}|\text{event}) = \prod_{i=1}^{n_{jet}} (1 - P(\text{tag}|j_i)) \tag{6}$$

where n_{jet} is the number of jets in the event and $P(\text{tag}|j_i)$ is the mistag rate of jet i in an event ($i = 1, \ldots, n_{jet}$). The probability of obtaining two or more tags is given by the complement of $P(1 \text{ tag}|\text{event})$ and $P(0 \text{ tag}|\text{event})$:

$$P(\geq 2 \text{ tag}|\text{event}) = 1 - P(1 \text{ tag}|\text{event}) - P(0 \text{ tag}|\text{event}) \tag{7}$$

To get a prediction on the number of events in the one and two tag regions, the probabilities $P(1 \text{ tag}|\text{event})$ and $P(\geq 2 \text{ tag}|\text{event})$ calculated from each preselected event are used as per-event weights, with the sum of weights comprising the final background prediction.

Mistag rates are calculated differentially based on jet-level observables. As previously mentioned, the tagger score is correlated with several jet observables, which can also be correlated between individual jets in an event. The dominant correlations include jet p_T, jet PTF, the number of heavy-flavour decays, the number of reconstructed secondary vertices, and the total number of tracks associated with the jet. For example, at high p_T, SM jets have a large number of high-momentum tracks with low $|d_0|$, making it easier to distinguish between signal and background jets. As the jet p_T decreases, the number of prompt tracks decreases, leading to an increased mistag rate. Conversely, if a background jet contains more heavy-flavour hadrons, the displaced vertices that mimic dark pion decays make it harder to discriminate between signal and background, thereby increasing the mistag rate.

To capture these correlations and address the dominant sources of jet–jet correlations, the mistag rates used for both the low-m_{jj} and high-m_{jj} regions are parameterised based on the observables with the strongest correlations: jet p_T and jet PTF. Figure 9 shows the mistag rate as a function of jet p_T and jet PTF, both of which exhibit clear correlations with the mistag rate. The mistag rate is therefore calculated in 2-dimensional bins of jet p_T and PTF.

Two sources of uncertainty on the background prediction are considered. The first is the statistical uncertainty arising from the finite number of events in the control region used to derive the mistag rates. This is estimated by generating an ensemble of background predictions using a set of 100 statistically
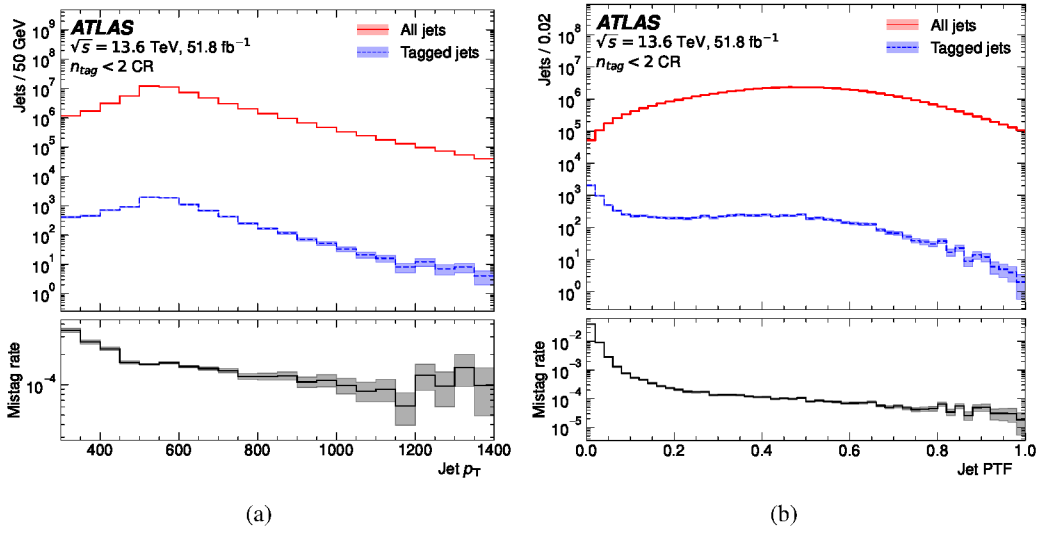
Figure 9: Distributions of (a) p_T and (b) PTF for all jets (solid lines) and jets with a classification score greater than 0.98 (dashed lines) in the high-m_{jj} selection for data events with $n_{\text{tag}} < 2$. The bottom panel shows the mistag rate as a function of each observable.

varied per-jet mistag rates, where each bin is randomly shifted according to a Gaussian distribution with a width set by its statistical uncertainty. The standard deviation of the resulting 100 background estimates defines the statistical uncertainty on the nominal prediction. The statistical uncertainty computed from this toy method is 6.2% and 2.6% for the high-m_{jj} and low-m_{jj} regions, respectively.

The second source of uncertainty is a systematic effect related to the choice of mistag rate parameterisation. The nominal mistag rate is parameterised using jet p_T and PTF, as these observables are strongly correlated with the transformer jet classification score and account for potential correlations between jets in an event. However, alternative jet-level observables exhibiting similar correlations could also be used. To assess the impact of this choice, three additional parameterisations are considered: the number of b-tagged subjets, the number of tracks associated to the jet, and the number of reconstructed secondary vertices associated with the jet using the independent vertex reconstruction algorithm described in Section 4.

To ensure that the dominant p_T and PTF correlations remain accounted for, all alternative mistag rates include p_T as a parameter and are separated into low-PTF (< 0.04) and high-PTF (> 0.04) categories, resulting in 16 possible parameterisation permutations. The impact of these variations is evaluated by computing background estimates for each SR using the different parameterisations. The largest observed variation in the predicted background is taken as the systematic uncertainty due to the choice of mistag rate parameterisation. This approach quantifies the effect of potential residual correlations not captured by the nominal parameterisation in p_T and PTF. The resulting systematic uncertainty is 61% in the high-m_{jj} region and 23% in the low-m_{jj} region.

To validate the background estimation strategy, a *validation region tag* is used that defines a "tag" as a jet having a jet classification score between 0.9 and 0.98. This provides a tag definition which captures jets that are adjacent to the signal tag definition, while removing signal jets, thereby offering a region to further study the ability of the mistag rate method to predict yields in a $n_{\text{tag}} \geq 2$ selection. The level of signal contamination in the $n_{\text{tag}} \geq 2$ selection using this VR tag definition was checked in simulation and found to be below 10%.

20

The background estimation strategy described above is applied using the VR tag definition. Mistag rates are computed following the same procedure as in the nominal SR, and systematic uncertainties are derived using the same methodology. The statistical uncertainties are found to be negligible compared to the systematic uncertainties and are not considered. The predicted and observed yields are summarised in Table 7. The observed yields in the $n_{\text{VR tag}} \geq 2$ region are found to be in agreement with the prediction within uncertainties, demonstrating the robustness of the background estimation in a signal-adjacent region and indicating that no additional nonclosure systematic uncertainties are required. The background estimation strategy was further validated by deriving predictions from simulated SM multijet events and confirming their agreement with the observed event yields within uncertainties.

Table 7: Predicted and observed yields using the validation tag definition in the high-m_{jj} and low-m_{jj} selection. The predictions are obtained by summing the event tagging probabilities from Equation 7 and 6.

	Low-m_{jj} VR tag	High-m_{jj} VR tag
Pred.	174 ± 42 (syst.)	29 ± 16 (syst.)
Obs	185	31

7 Signal systematic uncertainties

Instrumental and theoretical uncertainties are assigned to the modelling of the simulated signal samples. The experimental uncertainties include contributions from jets, tracks, and luminosity. The uncertainties associated with large-R jets arise from the jet energy scale (JES) and jet energy resolution (JER) [79]. The constituent small-R jets are varied within their respective uncertainties, and these variations are propagated to the large-R jets to quantify their impact on the final signal yields. The resulting uncertainty on the signal expectations depend mostly on the mass of the mediator and range between 1% and 10% in the cut-based analysis and between 1% and 50% in the ML-based analysis. The larger uncertainties in the ML-based analysis are driven by samples with a mediator mass of 600 GeV, where the 300 GeV jet p_{T} requirement lies near the kinematic threshold, making the acceptance more sensitive to downward fluctuations in the jet energy scale.

Uncertainties in track reconstruction are considered for both the primary and large-impact parameter track reconstruction passes. The uncertainty on the efficiency of large-impact parameter track reconstruction is derived from comparisons between data and MC simulation in K_S^0 events [74]. For primary tracks, uncertainties are estimated by evaluating the reconstruction efficiency in alternative simulated samples where the amount of passive material in the detector is varied [93]. These uncertainties affect track-based observables in the analysis, including the PTF, ECF2, vertex reconstruction, and the transformer jet classification score. To assess their impact, each observable is recomputed using a varied track collection, and the signal yields are rederived. In particular, secondary vertex reconstruction is repeated on the modified track collection to propagate tracking uncertainties to vertex-based observables. The total impact of tracking uncertainties on the final signal yield is estimated to be below 10%.

To ensure accurate modelling of pile-up conditions, simulated events are reweighted so that the average number of interactions per bunch crossing matches that observed in data. Since this number depends on the inelastic pp cross-section, differences between the predicted and measured values [94] are propagated

Table 8: The predicted number of background events and the observed event yields, including statistical and systematic uncertainties in the background estimation. The cut-based predictions are computed from the background-only fit.

Strategy	Region	Prediction (± stat ± syst)			Observed yield
Cut-based	High-m_{jj}	7.5	±1.1	±1.1	8
	Low-m_{jj}	17.4	±5.1	±5.1	10
ML-based	High-m_{jj}	4.5	±0.3	±2.8	3
	Low-m_{jj}	31.8	±0.8	±7.5	24

as a systematic variation of the reweighted distribution, resulting in an uncertainty of the order of 1% on the signal yield, except in samples with high dark pion lifetime where this uncertainty is as large as 5%.

In the cut-based low-m_{jj} selection, an uncertainty on the trigger scale factor is evaluated by varying the functional form and the parameters of the function modelling the efficiency of the trigger. The envelope of these variations around the nominal scale factor is chosen as the uncertainty. Its impact on the final signal yield is found to be below 10%.

Finally, the expected number of signal events is subject to an uncertainty in the total integrated luminosity of the dataset. The combined integrated luminosity for the 2022–2023 dataset has an uncertainty of 2%, determined using the LUCID-2 detector [38], which provides the primary luminosity measurement.

The MC generator uncertainties applied to the signal include uncertainties in the PDFs [95], renormalisation and factorisation scales, and the strong coupling constant. Additionally, uncertainties related to the parton shower tuning parameters in initial- and final-state radiation—such as variations of the renormalisation scale for QCD emission and the inclusion of non-singular terms—are considered [96]. The combined impact of these theoretical uncertainties on the signal acceptance is estimated to be between 2% and 10%.

The leading source of uncertainty varies across the signal parameter space, with jet-related uncertainties dominating in s-channel scenarios with $m_{Z'}$ = 600 GeV, and theoretical modelling uncertainties dominating at higher mediator masses.

8 Results

The predicted event yields (as obtained from the background-only ABCD fit or the mistag rate methods discussed in sections 6.1 and 6.2) and the corresponding observed yields for both analysis strategies are summarised in Table 8. No significant excess above the expected background is observed.

Two separate statistical treatments are performed, one for the cut-based analysis and another for the ML-based analysis. Within each approach, a simultaneous likelihood fit is performed, combining the low-m_{jj} and high-m_{jj} signal regions. Systematic uncertainties on the signal and background predictions are incorporated as nuisance parameters in both likelihood functions.

In the cut-based analysis, the background estimation follows the ABCD method separately in the low-m_{jj} and high-m_{jj} regions. An overall profile likelihood function is constructed from the product of the

Poisson probabilities of observing the number of events $N_{\mathrm{obs},X}$, given an expectation $N_{\mathrm{exp},X}$, in each region $X \in \{A, B, C, D\}$. The expected yield in each region is expressed as $N_{\mathrm{pred},X} = \mu N_{\mathrm{sig},X} + N_{\mathrm{bkg},X}$ where $N_{\mathrm{sig},X}$, is the number of expected signal events entering region X, μ is the signal strength and $N_{\mathrm{bkg},X}$ the expected background yield in this region. The background yields in each ABCD plane are expressed using three free parameters, m, τ_B and τ_C, as :

$$N_{\mathrm{bkg},A} = m$$
$$N_{\mathrm{bkg},B} = m\tau_B$$
$$N_{\mathrm{bkg},C} = m\tau_C$$
$$N_{\mathrm{bkg},D} = m\tau_B\tau_C$$

therefore automatically imposing the ABCD relation of Equation 4. The combined fit to both low-m_{jj} and high-m_{jj} regions thus involves seven free parameters, including μ which is common to both regions.

For the cut-based search, the combined likelihood function is

$$\mathcal{L}(\mu,\theta) = \prod_{r \in \{\text{low-}m_{jj}, \text{high-}m_{jj}\}} \prod_{X \in \{A,B,C,D\}} P(N_{\mathrm{obs},X}^{(r)} \mid N_{\mathrm{exp},X}^{(r)}(\mu,\theta)) \times \prod_i G(\theta_i \mid 0, 1), \qquad (8)$$

where $P(N_{\mathrm{obs},X}^{(r)} \mid N_{\mathrm{exp},X}^{(r)}(\mu,\theta))$ represents the Poisson probability of observing $N_{\mathrm{obs},X}^{(r)}$ events given the expected yield $N_{\mathrm{exp},X}^{(r)}$, which includes both background and signal contributions, and $G(\theta_i \mid 0, 1)$ denotes Gaussian constraints on nuisance parameters θ_i.

Under the background-only hypothesis, the expected background yields are initially set to their observed values, defining the *a priori* background estimate. When the observed yields in the signal regions are included, the fit allows the expected background to adjust, resulting in the *a posteriori* background estimate. The *a posteriori* estimates differ by less than 1% from the *a priori* values and lie well within the statistical uncertainties of the fit. In the presence of a signal, the expected background contribution is modified dynamically, enabling an excess to be interpreted as a nonzero signal strength.

In the ML-based search, the likelihood function follows the same structure as in the cut-based analysis, but includes only two Poisson terms: one for the observed event yield in each of the low-m_{jj} and high-m_{jj} signal regions.

Upper limits at the 95% confidence level (CL) are set on the production cross-section times branching fraction for each signal hypothesis using the CL$_{\mathrm{s}}$ method [97]. The profile likelihood ratio is used as the test statistic, with its distribution approximated using asymptotic formulae [98]. The validity of this approximation is confirmed by comparison with a full frequentist pseudo-experiment-based method across a range of signal samples, yielding consistent results. The likelihood function is implemented using the `pyhf` framework [99, 100].

The expected and observed limits on $\sigma(pp \to Z') \times \mathrm{Br}(Z' \to q_D\bar{q}_D)$ are shown in Figure 10 as functions of $m_{Z'}$ and $c\tau_{\pi_D}$ for both the ML-based and cut-based strategies. The ML-based strategy sets the most stringent limits across the benchmark models studied. Assuming coupling values of $g_q = 0.01$ and $g_{q_D} = 0.1$, the ML-based analysis excludes Z' masses up to 2550 GeV for $c\tau_{\pi_D} = 10$ mm. Under the same assumptions, the cut-based analysis excludes Z' masses up to 2150 GeV. For $m_{Z'} = 1000$ GeV, the ML-based strategy excludes dark pion lifetimes in the range 1–500 mm, while the cut-based strategy excludes lifetimes between 1.5 mm and 200 mm. The impact of systematic uncertainties on the observed limits is typically at the percent level, with the exception of signal samples with $m_{Z'} = 600$ GeV where

larger jet-related uncertainties in the ML-based analysis lead to a degradation in sensitivity of approximately 20%.

For $m_{Z'} = 1500$ GeV and $c\tau_{\pi_D} = 50$ mm, the ML-based analysis excludes values of $g_q > 0.003$ assuming $g_{q_D} > 0.03$. This coupling strength is more than 20 times smaller than the limits set by dijet resonance searches[101, 102], demonstrating the power of the targeted emerging jet analysis strategy to probe previously inaccessible regions of parameter space.

(a)   (b)
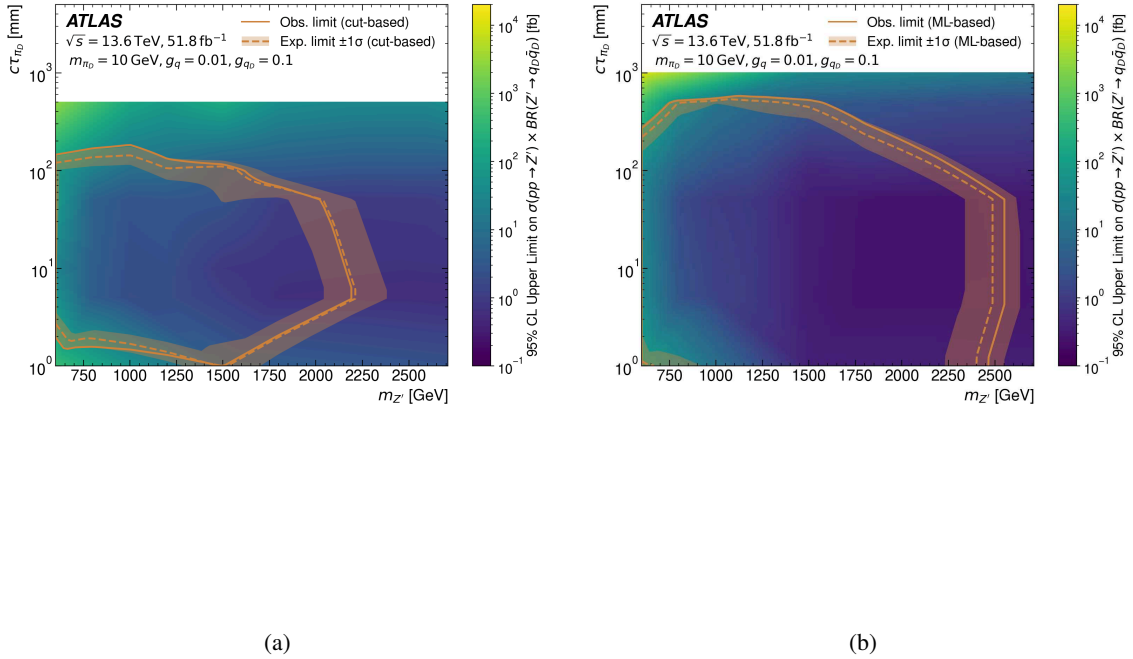
Figure 10: The 95% CL exclusion limits on $\sigma(pp \rightarrow Z') \times \mathrm{Br}(Z' \rightarrow q_D \bar{q}_D)$ as a function of $m_{Z'}$ and $c\tau_{\pi_D}$ for (a) the cut-based analysis and (b) the ML-based analysis. The excluded region computed from the observed limits for $g_q = 0.01$ and $g_{q_D} = 0.1$ is shown as a solid line.

Figure 11 shows the 95% CL upper limits as a function of either $m_{Z',\Phi}$ or $c\tau_{\pi_D}$ assuming $m_{\pi_D} = 10$ GeV. In the s-channel scenario, the limits are strongest for $m_{Z'} > 1200$ GeV, where the high-m_{jj} region becomes the dominant contribution to the signal acceptance. In the t-channel scenario, there is a reduced dependence on the mediator mass due to the weaker correlation between m_Φ and m_{jj}. In the ML-based strategy, the limits for both benchmark scenarios remain largely constant for 1 mm $< c\tau_{\pi_D} <$ 100 mm, but weaken for $c\tau_{\pi_D} > 100$ mm due to reduced track reconstruction efficiency at larger radial decay positions. In contrast, the limits obtained from the cut-based analysis weaken at lower dark pion lifetimes due to the explicit requirements placed on PTF and N_{vtx}. For the t-channel models, the limits set by the ML-based analysis are more than an order of magnitude stronger than those set by the cut-based analysis for $c\tau_{\pi_D} = 50$ mm, highlighting the ability of the transformer-based tagger to generalise to physics processes that were not considered in the network training.
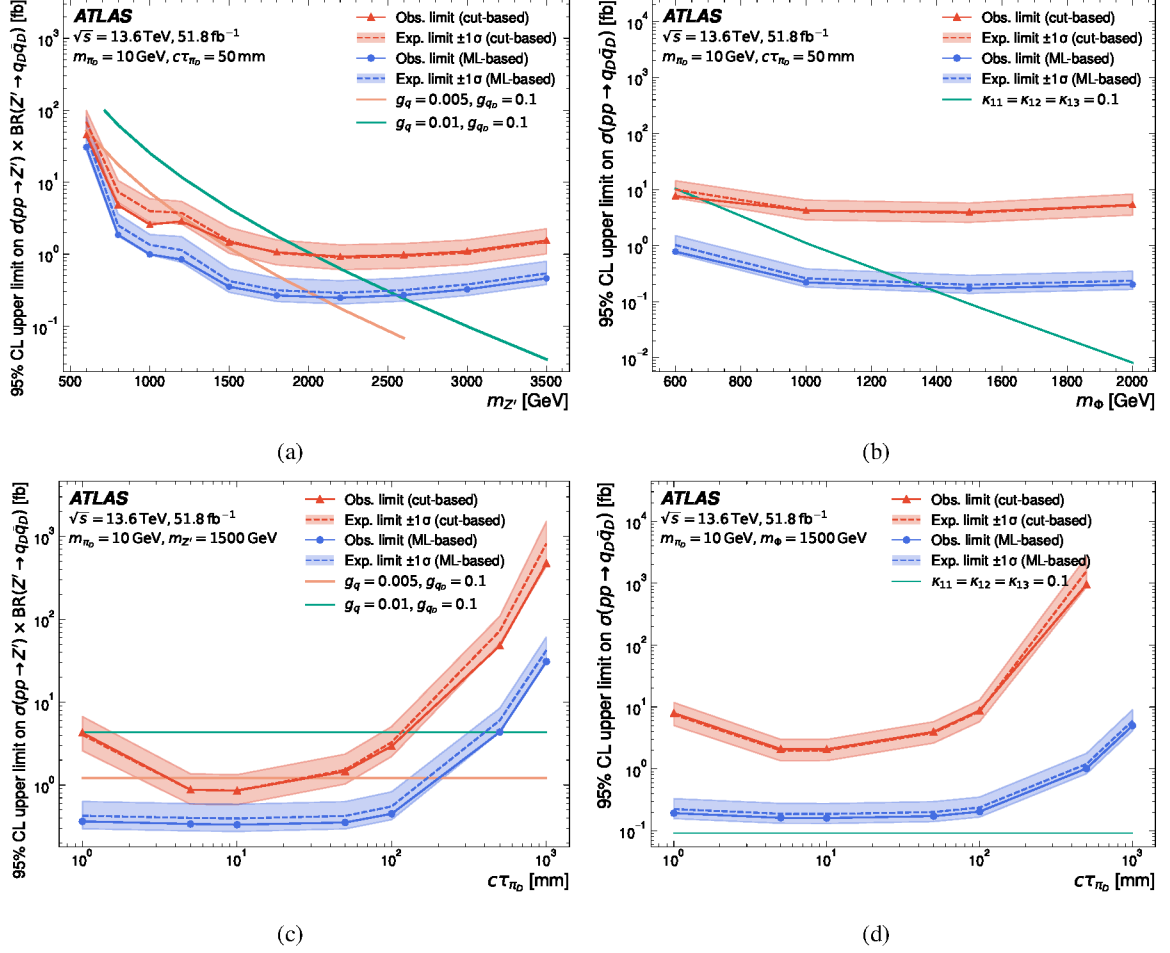
Figure 11: The 95% CL exclusion limits on (a, c) $\sigma(pp \to Z') \times \mathrm{Br}(Z' \to q_D\bar{q}_D)$ and (b, d) $\sigma(pp \to q_D\bar{q}_D)$ for $m_{\pi_D} = 10$ GeV for the cut-based (triangles) and ML-based (circles) strategies. The top row displays the limits as a function of $m_{Z',\Phi}$ for fixed $c\tau_{\pi_D} = 50$ mm, while the bottom row displays the limits as a function of $c\tau_{\pi_D}$ for $m_{Z',\Phi} = 1500$ GeV. Theoretical predictions are shown as solid lines.

Figure 12 shows the observed upper limits as a function of m_{π_D}. Both the cut-based and ML-based strategies exhibit minimal dependence on the dark pion mass, with the exception of dark pion proper decay lengths of 500 mm. In this case, the increased boost of lighter dark pions causes their decay vertices to occur further from the interaction point, often outside the acceptance of the inner detector, leading to a degradation in sensitivity.

9 Conclusion

This paper presents a search for emerging jets using 51.8 fb^{-1} of $\sqrt{s}$ = 13.6 TeV pp collision data collected by the ATLAS experiment at the LHC between 2022 and 2023. Two complementary analysis strategies are employed: one based on selections of high-level jet observables and the other using a custom transformer-based emerging jet tagging algorithm. The analysis is performed separately in the low-m_{jj} and high-m_{jj} regions, each with distinct trigger strategies. No significant excess is observed above the
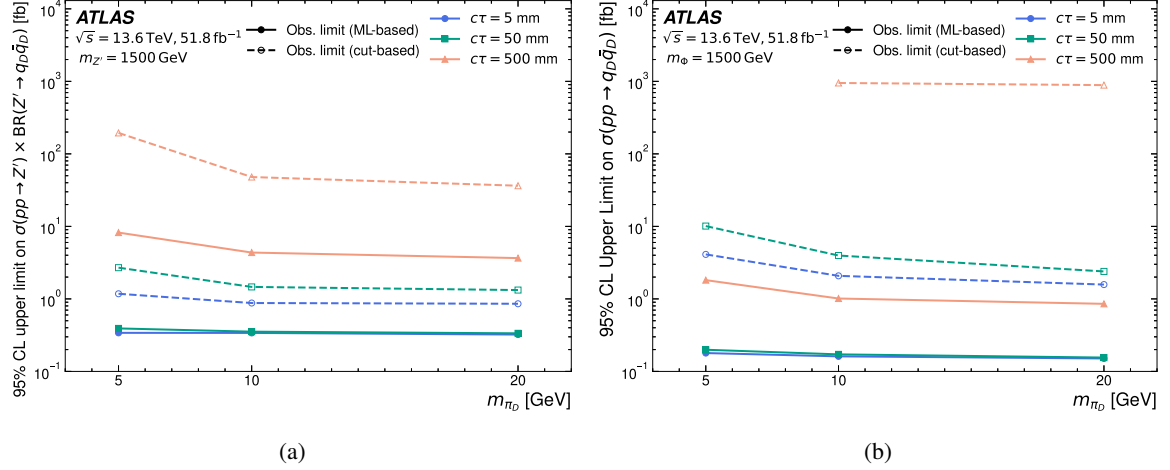
Figure 12: The 95% CL exclusion limits on (a) $\sigma(pp \to Z') \times \mathrm{Br}(Z' \to q_D\bar{q}_D)$ and (b) $\sigma(pp \to q_D\bar{q}_D)$ for $m_{Z',\Phi} = 1500$ GeV for the cut-based (hollow markers and dashed lines) and ML-based (filled markers and solid lines) strategies. The limits are shown for $c\tau_{\pi_D} = 5$ mm (circles), 50 mm (squares) and 500 mm (triangles).

expected background, which is estimated using a fully data-driven approach. Limits are placed at the 95% confidence level on two different mediator scenarios: a vector mediator Z' and a scalar bi-fundamental mediator Φ. Z' masses of up to 2.5 TeV are excluded assuming quark and dark quark coupling values of $g_q = 0.01$ and $g_{q_D} = 0.1$, respectively, and Φ masses up to 1350 GeV are excluding for a quark-dark quark coupling value of 0.1. This search is part of a broader search programme for dark QCD signatures within the ATLAS experiment and offers unique sensitivity to dark mesons with laboratory decay lengths on the order of 100 mm. Notably, it represents the first search for emerging jet production via a resonant s-channel mediator and the first application of a transformer-based algorithm for emerging jet tagging. This analysis establishes new constraints on emerging jet production and represents a significant step forward in the ATLAS dark sector search programme.

Acknowledgements

References

[1] V. C. Rubin, W. K. Ford Jr. and N. Thonnard, *Rotational properties of 21 SC galaxies with a large range of luminosities and radii, from NGC 4605 (R = 4 kpc) to UGC 2885 (R = 122 kpc)*, The Astrophysical Journal **238** (1980) 471.

[2] M. Persic, P. Salucci and F. Stel, *The Universal rotation curve of spiral galaxies — I. The Dark matter connection*, Monthly Notices of the Royal Astronomical Society **281** (1996) 27, arXiv: `astro-ph/9506004`.

[3] D. Clowe et al., *A Direct Empirical Proof of the Existence of Dark Matter*, The Astrophysical Journal **648** (2006) L109, arXiv: `astro-ph/0608407`.

[4] G. Jungman, M. Kamionkowski and K. Griest, *Supersymmetric dark matter*, Phys. Rept. **267** (1996) 195, arXiv: `hep-ph/9506380`.

[5] G. Steigman, B. Dasgupta and J. F. Beacom, *Precise relic WIMP abundance and its impact on searches for dark matter annihilation*, Phys. Rev. D **86** (2012) 023506, arXiv: `1204.3622 [hep-ph]`.

[6] PandaX-II Collaboration, *Dark Matter Results from 54-Ton-Day Exposure of PandaX-II Experiment*, Phys. Rev. Lett. **119** (2017) 181302, arXiv: `1708.06917 [astro-ph.CO]`.

[7] PICO Collaboration, *Dark matter search results from the complete exposure of the PICO-60 C_3F_8 bubble chamber*, Phys. Rev. D **100** (2019) 022001, arXiv: `1902.04031 [astro-ph.CO]`.

[8] DarkSide Collaboration, *DarkSide-50 532-day dark matter search with low-radioactivity argon*, Phys. Rev. D **98** (2018) 102006, arXiv: `1802.07198 [astro-ph.CO]`.

[9] CRESST Collaboration, *First results from the CRESST-III low-mass dark matter program*, Phys. Rev. D **100** (2019) 102002, arXiv: `1904.00498 [astro-ph.CO]`.

[10] DarkSide Collaboration, *Low-Mass Dark Matter Search with the DarkSide-50 Experiment*, Phys. Rev. Lett. **121** (2018) 081307, arXiv: `1802.06994 [astro-ph.HE]`.

[11] LUX Collaboration, *Results from a Search for Dark Matter in the Complete LUX Exposure*, Phys. Rev. Lett. **118** (2017) 021303, arXiv: `1608.07648 [astro-ph.CO]`.

[12] XENON Collaboration, *Search for Coherent Elastic Scattering of Solar ^{8}B Neutrinos in the XENON1T Dark Matter Experiment*, Phys. Rev. Lett. **126** (2021) 091301, arXiv: `2012.02846 [hep-ex]`.

[13] M. Lai (on behalf of DEAP-3600 Collaboration), *Recent results from DEAP-3600*, JINST **18** (2023) C02046, arXiv: `2302.14484 [hep-ex]`.

[14] SuperCDMS Collaboration, *Search for low-mass dark matter with CDMSlite using a profile likelihood fit*, Phys. Rev. D **99** (2019) 062001, arXiv: `1808.09098 [astro-ph.CO]`.

[15] Fermi-LAT Collaboration, *Searching for Dark Matter Annihilation from Milky Way Dwarf Spheroidal Galaxies with Six Years of Fermi Large Area Telescope Data*, Phys. Rev. Lett. **115** (2015) 231301, arXiv: `1503.02641 [astro-ph.HE]`.

[16] H.E.S.S. Collaboration, *Search for Dark Matter Annihilation Signals in the H.E.S.S. Inner Galaxy Survey*, Phys. Rev. Lett. **129** (2022) 111101, arXiv: `2207.10471 [astro-ph.HE]`.

[17] ATLAS Collaboration, *Search for new phenomena in events with an energetic jet and missing transverse momentum in pp collisions at $\sqrt{s} = 13$ TeV with the ATLAS detector*, Phys. Rev. D **103** (2021) 112006, arXiv: `2102.10874 [hep-ex]`.

[18] CMS Collaboration, *Search for new particles in events with energetic jets and large missing transverse momentum in proton–proton collisions at $\sqrt{s} = 13$ TeV*, JHEP **11** (2021) 153, arXiv: `2107.13021 [hep-ex]`.

[19] M. J. Strassler and K. M. Zurek, *Echoes of a hidden valley at hadron colliders*, Phys. Lett. B **651** (2007) 374, arXiv: `hep-ph/0604261`.

[20] M. J. Strassler and K. M. Zurek, *Discovering the Higgs through highly-displaced vertices*, Phys. Lett. B **661** (2008) 263, arXiv: `hep-ph/0605193`.

[21] T. Han, Z. Si, K. M. Zurek and M. J. Strassler, *Phenomenology of hidden valleys at hadron colliders*, JHEP **07** (2008) 008, arXiv: `0712.2041 [hep-ph]`.

[22] Y. Bai and P. Schwaller, *Scale of dark QCD*, Phys. Rev. D **89** (2014) 063522, arXiv: `1306.4676 [hep-ph]`.

[23] H. Beauchesne, E. Bertuzzo and G. Grilli di Cortona, *Dark matter in Hidden Valley models with stable and unstable light dark mesons*, JHEP **04** (2019) 118, arXiv: `1809.10152 [hep-ph]`.

[24] G. Albouy et al., *Theory, phenomenology, and experimental avenues for dark showers: a Snowmass 2021 report*, Eur. Phys. J. C **82** (2022) 1132, arXiv: `2203.09503 [hep-ph]`.

[25] T. Cohen, M. Lisanti and H. K. Lou, *Semivisible Jets: Dark Matter Undercover at the LHC*, Phys. Rev. Lett. **115** (2015) 171804, arXiv: `1503.00009 [hep-ph]`.

[26] P. Schwaller, D. Stolarski and A. Weiler, *Emerging jets*, JHEP **05** (2015) 059, arXiv: `1502.05409 [hep-ph]`.

[27] ATLAS Collaboration, *Search for non-resonant production of semi-visible jets using Run 2 data in ATLAS*, Phys. Lett. B **848** (2024) 138324, arXiv: `2305.18037 [hep-ex]`.

[28] CMS Collaboration, *Search for resonant production of strongly coupled dark matter in proton–proton collisions at 13 TeV*, JHEP **06** (2022) 156, arXiv: `2112.11125 [hep-ex]`.

[29] ATLAS Collaboration, *Search for new physics in final states with semi-visible jets or anomalous signatures using the ATLAS detector*, CERN-EP-2025-101, 2025.

[30] ATLAS Collaboration, *Search for long-lived, weakly interacting particles that decay to displaced hadronic jets in proton–proton collisions at $\sqrt{s} = 8$ TeV with the ATLAS detector*, Phys. Rev. D **92** (2015) 012010, arXiv: `1504.03634 [hep-ex]`.

[31] CMS Collaboration, *Search for new particles decaying to a jet and an emerging jet*, JHEP **02** (2019) 179, arXiv: `1810.10069 [hep-ex]`.

[32] CMS Collaboration, *Search for dark QCD with emerging jets in proton–proton collisions at $\sqrt{s} = 13$ TeV*, JHEP **07** (2024) 142, arXiv: `2403.01556 [hep-ex]`.

[33] A. Carmona, F. Elahi, C. Scherb and P. Schwaller, *Dark showers from sneaky dark matter*, (2025), arXiv: `2411.15073 [hep-ph]`.

29

[34] ATLAS Collaboration, *The ATLAS Experiment at the CERN Large Hadron Collider*, JINST **3** (2008) S08003.

[35] ATLAS Collaboration, *The ATLAS experiment at the CERN Large Hadron Collider: a description of the detector configuration for Run 3*, JINST **19** (2024) P05063, arXiv: 2305.16623 [physics.ins-det].

[36] ATLAS Collaboration, *ATLAS Insertable B-Layer: Technical Design Report*, ATLAS-TDR-19; CERN-LHCC-2010-013, 2010, URL: https://cds.cern.ch/record/1291633, Addendum: ATLAS-TDR-19-ADD-1; CERN-LHCC-2012-009, 2012, URL: https://cds.cern.ch/record/1451888.

[37] B. Abbott et al., *Production and integration of the ATLAS Insertable B-Layer*, JINST **13** (2018) T05008, arXiv: 1803.00844 [physics.ins-det].

[38] G. Avoni et al., *The new LUCID-2 detector for luminosity measurement and monitoring in ATLAS*, JINST **13** (2018) P07017.

[39] ATLAS Collaboration, *The ATLAS trigger system for LHC Run 3 and trigger performance in 2022*, JINST **19** (2024) P06029, arXiv: 2401.06630 [hep-ex].

[40] ATLAS Collaboration, *Software and computing for Run 3 of the ATLAS experiment at the LHC*, Eur. Phys. J. C **85** (2025) 234, arXiv: 2404.06335 [hep-ex].

[41] ATLAS Collaboration, *ATLAS data quality operations and performance for 2015–2018 data-taking*, JINST **15** (2020) P04003, arXiv: 1911.04632 [physics.ins-det].

[42] ATLAS Collaboration, *Emulating the impact of additional proton–proton interactions in the ATLAS simulation by presampling sets of inelastic Monte Carlo events*, Comput. Softw. Big Sci. **6** (2022) 3, arXiv: 2102.09495 [hep-ex].

[43] K. Werner, F.-M. Liu and T. Pierog, *Parton ladder splitting and the rapidity dependence of transverse momentum spectra in deuteron-gold collisions at the BNL Relativistic Heavy Ion Collider*, Phys. Rev. C **74** (2006) 044902, arXiv: hep-ph/0506232 [hep-ph].

[44] C. Bierlich et al., *A comprehensive guide to the physics and usage of PYTHIA 8.3*, SciPost Phys. Codeb. (2022) 8, arXiv: 2203.11601 [hep-ph].

[45] S. Agostinelli et al., *Geant4 – a simulation toolkit*, Nucl. Instrum. Meth. A **506** (2003) 250.

[46] ATLAS Collaboration, *The ATLAS Simulation Infrastructure*, Eur. Phys. J. C **70** (2010) 823, arXiv: 1005.4568 [physics.ins-det].

[47] D. Abercrombie et al., *Dark Matter benchmark models for early LHC Run-2 Searches: Report of the ATLAS/CMS Dark Matter Forum*, Physics of the Dark Universe **27** (2020) 100371, ed. by A. Boveia, C. Doglioni, S. Lowette, S. Malik and S. Mrenna, arXiv: 1507.00966 [hep-ex].

[48] J. Alwall et al., *The automated computation of tree-level and next-to-leading order differential cross sections, and their matching to parton shower simulations*, JHEP **07** (2014) 079, arXiv: 1405.0301 [hep-ph].

[49] M. L. Mangano, M. Moretti, F. Piccinini and M. Treccani, *Matching matrix elements and shower evolution for top-pair production in hadronic collisions*, JHEP **01** (2007) 013, arXiv: hep-ph/0611129.

[50] NNPDF Collaboration, R. D. Ball et al., *Parton distributions with LHC data*,
Nucl. Phys. B **867** (2013) 244, arXiv: 1207.1303 [hep-ph].

[51] ATLAS Collaboration, *ATLAS Pythia 8 tunes to 7 TeV data*, ATL-PHYS-PUB-2014-021, 2014,
URL: https://cds.cern.ch/record/1966419.

[52] L. Carloni and T. Sjöstrand, *Visible effects of invisible hidden valley radiation*,
JHEP **09** (2010) 105, arXiv: 1006.2911 [hep-ph].

[53] L. Carloni, J. Rathsman and T. Sjöstrand, *Discerning secluded sector gauge structures*,
JHEP **04** (2011) 091, arXiv: 1102.3795 [hep-ph].

[54] T. Sjöstrand et al., *An introduction to PYTHIA 8.2*, Comput. Phys. Commun. **191** (2015) 159,
arXiv: 1410.3012 [hep-ph].

[55] S. Frixione, G. Ridolfi and P. Nason,
A positive-weight next-to-leading-order Monte Carlo for heavy flavour hadroproduction,
JHEP **09** (2007) 126, arXiv: 0707.3088 [hep-ph].

[56] P. Nason, *A new method for combining NLO QCD with shower Monte Carlo algorithms*,
JHEP **11** (2004) 040, arXiv: hep-ph/0409146.

[57] S. Frixione, P. Nason and C. Oleari,
Matching NLO QCD computations with parton shower simulations: the POWHEG method,
JHEP **11** (2007) 070, arXiv: 0709.2092 [hep-ph].

[58] S. Alioli, P. Nason, C. Oleari and E. Re, *A general framework for implementing NLO calculations
in shower Monte Carlo programs: the POWHEG BOX*, JHEP **06** (2010) 043,
arXiv: 1002.2581 [hep-ph].

[59] NNPDF Collaboration, R. D. Ball et al., *Parton distributions for the LHC run II*,
JHEP **04** (2015) 040, arXiv: 1410.8849 [hep-ph].

[60] ATLAS Collaboration, *Studies on top-quark Monte Carlo modelling for Top2016*,
ATL-PHYS-PUB-2016-020, 2016, URL: https://cds.cern.ch/record/2216168.

[61] D. J. Lange, *The EvtGen particle decay simulation package*,
Nucl. Instrum. Meth. A **462** (2001) 152.

[62] E. Bothmann et al., *Event generation with Sherpa 2.2*, SciPost Phys. **7** (2019) 034,
arXiv: 1905.09127 [hep-ph].

[63] T. Gleisberg and S. Höche, *Comix, a new matrix element generator*, JHEP **12** (2008) 039,
arXiv: 0808.3674 [hep-ph].

[64] F. Buccioni et al., *OpenLoops 2*, Eur. Phys. J. C **79** (2019) 866, arXiv: 1907.13071 [hep-ph].

[65] F. Cascioli, P. Maierhöfer and S. Pozzorini, *Scattering Amplitudes with Open Loops*,
Phys. Rev. Lett. **108** (2012) 111601, arXiv: 1111.5206 [hep-ph].

[66] A. Denner, S. Dittmaier and L. Hofer,
Collier: A fortran-based complex one-loop library in extended regularizations,
Comput. Phys. Commun. **212** (2017) 220, arXiv: 1604.06792 [hep-ph].

[67] S. Schumann and F. Krauss,
A parton shower algorithm based on Catani–Seymour dipole factorisation, JHEP **03** (2008) 038,
arXiv: 0709.1027 [hep-ph].

[68] S. Höche, F. Krauss, M. Schönherr and F. Siegert,
A critical appraisal of NLO+PS matching methods, JHEP **09** (2012) 049,
arXiv: 1111.1220 [hep-ph].

[69] S. Höche, F. Krauss, M. Schönherr and F. Siegert,
QCD matrix elements + parton showers. The NLO case, JHEP **04** (2013) 027,
arXiv: 1207.5030 [hep-ph].

[70] S. Catani, F. Krauss, B. R. Webber and R. Kuhn, *QCD Matrix Elements + Parton Showers*,
JHEP **11** (2002) 063, arXiv: hep-ph/0109231.

[71] S. Höche, F. Krauss, S. Schumann and F. Siegert, *QCD matrix elements and truncated showers*,
JHEP **05** (2009) 053, arXiv: 0903.1219 [hep-ph].

[72] C. Anastasiou, L. Dixon, K. Melnikov and F. Petriello, *High-precision QCD at hadron colliders:
Electroweak gauge boson rapidity distributions at next-to-next-to leading order*,
Phys. Rev. D **69** (2004) 094008, arXiv: hep-ph/0312266.

[73] R. Frühwirth, *Application of Kalman filtering to track and vertex fitting*,
Nucl. Instrum. Meth. A **262** (1987) 444.

[74] ATLAS Collaboration,
Performance of the reconstruction of large impact parameter tracks in the inner detector of ATLAS,
Eur. Phys. J. C **83** (2023) 1081, arXiv: 2304.12867 [hep-ex].

[75] M. Cacciari, G. P. Salam and G. Soyez, *The anti-k_t jet clustering algorithm*, JHEP **04** (2008) 063,
arXiv: 0802.1189 [hep-ph].

[76] M. Cacciari, G. P. Salam and G. Soyez, *FastJet user manual*, Eur. Phys. J. C **72** (2012) 1896,
arXiv: 1111.6097 [hep-ph].

[77] ATLAS Collaboration,
Jet reconstruction and performance using particle flow with the ATLAS Detector,
Eur. Phys. J. C **77** (2017) 466, arXiv: 1703.10485 [hep-ex].

[78] ATLAS Collaboration,
Topological cell clustering in the ATLAS calorimeters and its performance in LHC Run 1,
Eur. Phys. J. C **77** (2017) 490, arXiv: 1603.02934 [hep-ex].

[79] ATLAS Collaboration, *Jet energy scale and resolution measured in proton–proton collisions at
$\sqrt{s}$ = 13 TeV with the ATLAS detector*, Eur. Phys. J. C **81** (2021) 689,
arXiv: 2007.02645 [hep-ex].

[80] ATLAS Collaboration, *ATLAS flavour-tagging algorithms for the LHC Run 2 pp collision dataset*,
Eur. Phys. J. C **83** (2023) 681, arXiv: 2211.16345 [physics.data-an].

[81] M. Cacciari, G. P. Salam and G. Soyez, *The catchment area of jets*, JHEP **04** (2008) 005,
arXiv: 0802.1188 [hep-ph].

[82] ATLAS Collaboration, *Electron and photon performance measurements with the ATLAS detector
using the 2015–2017 LHC proton–proton collision data*, JINST **14** (2019) P12006,
arXiv: 1908.00005 [hep-ex].

[83] ATLAS Collaboration, *Development of ATLAS Primary Vertex Reconstruction for LHC Run 3*,
ATL-PHYS-PUB-2019-015, 2019, URL: https://cds.cern.ch/record/2670380.

32

[84] ATLAS Collaboration,
The performance of the jet trigger for the ATLAS detector during 2011 data taking,
Eur. Phys. J. C **76** (2016) 526, arXiv: 1606.07759 [hep-ex].

[85] ATLAS Collaboration,
Performance of the upgraded PreProcessor of the ATLAS Level-1 Calorimeter Trigger,
JINST **15** (2020) P11016, arXiv: 2005.04179 [physics.ins-det].

[86] ATLAS Collaboration, *Performance of vertex reconstruction algorithms for detection of new long-lived particle decays within the ATLAS inner detector*, ATL-PHYS-PUB-2019-013, 2019, URL: https://cds.cern.ch/record/2669425.

[87] ATLAS Collaboration, *Search for long-lived, massive particles in events with displaced vertices and multiple jets in pp collisions at $\sqrt{s} = 13\,TeV$ with the ATLAS detector*, JHEP **06** (2023) 200, arXiv: 2301.13866 [hep-ex].

[88] A. J. Larkoski, G. P. Salam and J. Thaler, *Energy correlation functions for jet substructure*,
JHEP **06** (2013) 108, arXiv: 1305.0007 [hep-ph].

[89] ATLAS Collaboration, *Graph Neural Network Jet Flavour Tagging with the ATLAS Detector*,
ATL-PHYS-PUB-2022-027, 2022, URL: https://cds.cern.ch/record/2811135.

[90] Y. Li, D. Tarlow, M. Brockschmidt and R. Zemel, *Gated Graph Sequence Neural Networks*, 2017,
arXiv: 1511.05493 [cs.LG].

[91] A. F. Agarap, *Deep Learning using Rectified Linear Units (ReLU)*, (2019),
arXiv: 1803.08375 [cs.NE].

[92] D. C. Kozen, 'Union-Find', *The Design and Analysis of Algorithms*,
New York, NY: Springer New York, 1992 48, ISBN: 978-1-4612-4400-4.

[93] ATLAS Collaboration, *Study of the material of the ATLAS inner detector for Run 2 of the LHC*,
JINST **12** (2017) P12009, arXiv: 1707.02826 [hep-ex].

[94] ATLAS Collaboration, *Measurement of the Inelastic Proton–Proton Cross Section at $\sqrt{s} = 13\,TeV$ with the ATLAS Detector at the LHC*, Phys. Rev. Lett. **117** (2016) 182002,
arXiv: 1606.02625 [hep-ex].

[95] J. Butterworth et al., *PDF4LHC recommendations for LHC Run II*, J. Phys. G **43** (2016) 023001,
arXiv: 1510.03865 [hep-ph].

[96] S. Mrenna and P. Skands, *Automated parton-shower variations in PYTHIA 8*,
Phys. Rev. D **94** (2016) 074005, arXiv: 1605.08352 [hep-ph].

[97] A. L. Read, *Presentation of search results: the CL_s technique*, J. Phys. G **28** (2002) 2693.

[98] G. Cowan, K. Cranmer, E. Gross and O. Vitells,
Asymptotic formulae for likelihood-based tests of new physics, Eur. Phys. J. C **71** (2011) 1554,
arXiv: 1007.1727 [physics.data-an], Erratum: Eur. Phys. J. C **73** (2013) 2501.

[99] L. Heinrich, M. Feickert and G. Stark, *scikit-hep/pyhf: v0.7.6*,
version 0.7.6, https://github.com/scikit-hep/pyhf/releases/tag/v0.7.6.

[100] L. Heinrich, M. Feickert, G. Stark and K. Cranmer,
pyhf: pure-Python implementation of HistFactory statistical models,
Journal of Open Source Software **6** (2021) 2823.

[101] ATLAS Collaboration, *Search for new resonances in mass distributions of jet pairs using* $139\,fb^{-1}$ *of pp collisions at* $\sqrt{s} = 13\,TeV$ *with the ATLAS detector*, JHEP **03** (2020) 145,
arXiv: 1910.08447 [hep-ex].

[102] ATLAS Collaboration, *Constraints on dark matter models involving an s-channel mediator with the ATLAS detector in pp collisions at* $\sqrt{s} = 13\,TeV$, Eur. Phys. J. C **84** (2024) 1102,
arXiv: 2404.15930 [hep-ex].

[103] ATLAS Collaboration, *ATLAS Computing Acknowledgements*, ATL-SOFT-PUB-2025-001, 2025,
URL: https://cds.cern.ch/record/2922210.

The ATLAS Collaboration

G. Aad [104], E. Aakvaag [17], B. Abbott [123], S. Abdelhameed [119a], K. Abeling [55], N.J. Abicht [49], S.H. Abidi [30], M. Aboelela [45], A. Aboulhorma [36e], H. Abramowicz [157], Y. Abulaiti [120], B.S. Acharya [69a,69b,m], A. Ackermann [63a], C. Adam Bourdarios [4], L. Adamczyk [86a], S.V. Addepalli [149], M.J. Addison [103], J. Adelman [118], A. Adiguzel [22c], T. Adye [137], A.A. Affolder [139], Y. Afik [40], M.N. Agaras [13], A. Aggarwal [102], C. Agheorghiesei [28c], F. Ahmadov [39,ad], S. Ahuja [97], X. Ai [143b], G. Aielli [76a,76b], A. Aikot [169], M. Ait Tamlihat [36e], B. Aitbenchikh [36a], M. Akbiyik [102], T.P.A. Åkesson [100], A.V. Akimov [151], D. Akiyama [174], N.N. Akolkar [25], S. Aktas [22a], G.L. Alberghi [24b], J. Albert [171], U. Alberti [20], P. Albicocco [53], G.L. Albouy [60], S. Alderweireldt [52], Z.L. Alegria [124], M. Aleksa [37], I.N. Aleksandrov [39], C. Alexa [28b], T. Alexopoulos [10], F. Alfonsi [24b], M. Algren [56], M. Alhroob [173], B. Ali [135], H.M.J. Ali [93,w], S. Ali [32], S.W. Alibocus [94], M. Aliev [34c], G. Alimonti [71a], W. Alkakhi [55], C. Allaire [66], B.M.M. Allbrooke [152], J.S. Allen [103], J.F. Allen [52], P.P. Allport [21], A. Aloisio [72a,72b], F. Alonso [92], C. Alpigiani [142], Z.M.K. Alsolami [93], A. Alvarez Fernandez [102], M. Alves Cardoso [56], M.G. Alviggi [72a,72b], M. Aly [103], Y. Amaral Coutinho [83b], A. Ambler [106], C. Amelung[37], M. Amerl [103], C.G. Ames [111], T. Amezza [130], D. Amidei [108], B. Amini [54], K. Amirie [161], A. Amirkhanov [39], S.P. Amor Dos Santos [133a], K.R. Amos [169], D. Amperiadou [158], S. An[84], C. Anastopoulos [145], T. Andeen [11], J.K. Anders [94], A.C. Anderson [59], A. Andreazza [71a,71b], S. Angelidakis [9], A. Angerami [42], A.V. Anisenkov [39], A. Annovi [74a], C. Antel [37], E. Antipov [151], M. Antonelli [53], F. Anulli [75a], M. Aoki [84], T. Aoki [159], M.A. Aparo [152], L. Aperio Bella [48], M. Apicella[31], C. Appelt [157], A. Apyan [27], M. Arampatzi [10], S.J. Arbiol Val [87], C. Arcangeletti [53], A.T.H. Arce [51], J-F. Arguin [110], S. Argyropoulos [158], J.-H. Arling [48], O. Arnaez [4], H. Arnold [151], G. Artoni [75a,75b], H. Asada [113], K. Asai [121], S. Asatryan [179], N.A. Asbah [37], R.A. Ashby Pickering [173], A.M. Aslam [97], K. Assamagan [30], R. Astalos [29a], K.S.V. Astrand [100], S. Atashi [165], R.J. Atkin [34a], H. Atmani[36f], P.A. Atmasiddha [131], K. Augsten [135], A.D. Auriol [41], V.A. Austrup [103], G. Avolio [37], K. Axiotis [56], A. Azzam [13], D. Babal [29b], H. Bachacou [138], K. Bachas [158,q], A. Bachiu [35], E. Bachmann [50], M.J. Backes [63a], A. Badea [40], T.M. Baer [108], P. Bagnaia [75a,75b], M. Bahmani [19], D. Bahner [54], K. Bai [126], J.T. Baines [137], L. Baines [96], O.K. Baker [178], E. Bakos [16], D. Bakshi Gupta [8], L.E. Balabram Filho [83b], V. Balakrishnan [123], R. Balasubramanian [4], E.M. Baldin [38], P. Balek [86a], E. Ballabene [24b,24a], F. Balli [138], L.M. Baltes [63a], W.K. Balunas [33], J. Balz [102], I. Bamwidhi [119b], E. Banas [87], M. Bandieramonte [132], A. Bandyopadhyay [25], S. Bansal [25], L. Barak [157], M. Barakat [48], E.L. Barberio [107], D. Barberis [18b], M. Barbero [104], M.Z. Barel [117], T. Barillari [112], M-S. Barisits [37], T. Barklow [149], P. Baron [136], D.A. Baron Moreno [103], A. Baroncelli [62], A.J. Barr [129], J.D. Barr [98], F. Barreiro [101], J. Barreiro Guimarães da Costa [14], M.G. Barros Teixeira [133a], S. Barsov [38], F. Bartels [63a], R. Bartoldus [149], A.E. Barton [93], P. Bartos [29a], A. Basan [102], M. Baselga [49], S. Bashiri[87], A. Bassalat [66,b], M.J. Basso [162a], S. Bataju [45], R. Bate [170], R.L. Bates [59], S. Batlamous[101], M. Battaglia [139], D. Battulga [19], M. Bauce [75a,75b], M. Bauer [79], P. Bauer [25], L.T. Bayer [48], L.T. Bazzano Hurrell [31], J.B. Beacham [112], T. Beau [130], J.Y. Beaucamp [92], P.H. Beauchemin [164], P. Bechtle [25], H.P. Beck [20,p], K. Becker [173], A.J. Beddall [82], V.A. Bednyakov [39], C.P. Bee [151], L.J. Beemster [16], M. Begalli [83d], M. Begel [30], J.K. Behr [48], J.F. Beirer [37], F. Beisiegel [25], M. Belfkir [119b], G. Bella [157], L. Bellagamba [24b], A. Bellerive [35], C.D. Bellgraph [68], P. Bellos [21], K. Beloborodov [38], D. Benchekroun [36a], F. Bendebba [36a], Y. Benhammou [157],

K.C. Benkendorfer [61], L. Beresford [48], M. Beretta [53], E. Bergeaas Kuutmann [167], N. Berger [4], B. Bergmann [135], J. Beringer [18a], G. Bernardi [5], C. Bernius [149], F.U. Bernlochner [25], F. Bernon [37], A. Berrocal Guardia [13], T. Berry [97], P. Berta [136], A. Berthold [50], A. Berti [133a], R. Bertrand [104], S. Bethke [112], A. Betti [75a,75b], A.J. Bevan [96], L. Bezio [56], N.K. Bhalla [54], S. Bharthuar [112], S. Bhatta [151], P. Bhattarai [149], Z.M. Bhatti [120], K.D. Bhide [54], V.S. Bhopatkar [124], R.M. Bianchi [132], G. Bianco [24b,24a], O. Biebel [111], M. Biglietti [77a], C.S. Billingsley [45], Y. Bimgdi [36f], M. Bindi [55], A. Bingham [177], A. Bingul [22b], C. Bini [75a,75b], G.A. Bird [33], M. Birman [175], M. Biros [136], S. Biryukov [152], T. Bisanz [49], E. Bisceglie [24b,24a], J.P. Biswal [137], D. Biswas [147], I. Bloch [48], A. Blue [59], U. Blumenschein [96], J. Blumenthal [102], V.S. Bobrovnikov [39], L. Boccardo [57b,57a], M. Boehler [54], B. Boehm [172], D. Bogavac [13], A.G. Bogdanchikov [38], L.S. Boggia [130], V. Boisvert [97], P. Bokan [37], T. Bold [86a], M. Bomben [5], M. Bona [96], M. Boonekamp [138], A.G. Borbély [59], I.S. Bordulev [38], G. Borissov [93], D. Bortoletto [129], D. Boscherini [24b], M. Bosman [13], K. Bouaouda [36a], N. Bouchhar [169], L. Boudet [4], J. Boudreau [132], E.V. Bouhova-Thacker [93], D. Boumediene [41], R. Bouquet [57b,57a], A. Boveia [122], J. Boyd [37], D. Boye [30], I.R. Boyko [39], L. Bozianu [56], J. Bracinik [21], N. Brahimi [4], G. Brandt [177], O. Brandt [33], B. Brau [105], J.E. Brau [126], R. Brener [175], L. Brenner [117], R. Brenner [167], S. Bressler [175], G. Brianti [78a,78b], D. Britton [59], D. Britzger [112], I. Brock [25], R. Brock [109], G. Brooijmans [42], A.J. Brooks[68], E.M. Brooks [162b], E. Brost [30], L.M. Brown [171,162a], L.E. Bruce [61], T.L. Bruckler [129], P.A. Bruckman de Renstrom [87], B. Brüers [48], A. Bruni [24b], G. Bruni [24b], D. Brunner [47a,47b], M. Bruschi [24b], N. Bruscino [75a,75b], T. Buanes [17], Q. Buat [142], D. Buchin [112], A.G. Buckley [59], O. Bulekov [82], B.A. Bullard [149], S. Burdin [94], C.D. Burgard [49], A.M. Burger [91], B. Burghgrave [8], O. Burlayenko [54], J. Burleson [168], J.C. Burzynski [148], E.L. Busch [42], V. Büscher [102], P.J. Bussey [59], J.M. Butler [26], C.M. Buttar [59], J.M. Butterworth [98], W. Buttinger [137], C.J. Buxo Vazquez [109], A.R. Buzykaev [39], S. Cabrera Urbán [169], L. Cadamuro [66], H. Cai [132], Y. Cai [24b,114c,24a], Y. Cai [114a], V.M.M. Cairo [37], O. Cakir [3a], N. Calace [37], P. Calafiura [18a], G. Calderini [130], P. Calfayan [35], L. Calic [100], G. Callea [59], L.P. Caloba[83b], D. Calvet [41], S. Calvet [41], R. Camacho Toro [130], S. Camarda [37], D. Camarero Munoz [27], P. Camarri [76a,76b], C. Camincher [171], M. Campanelli [98], A. Camplani [43], V. Canale [72a,72b], A.C. Canbay [3a], E. Canonero [97], J. Cantero [169], Y. Cao [168], F. Capocasa [27], M. Capua [44b,44a], A. Carbone [71a,71b], R. Cardarelli [76a], J.C.J. Cardenas [8], M.P. Cardiff [27], G. Carducci [44b,44a], T. Carli [37], G. Carlino [72a], J.I. Carlotto [13], B.T. Carlson [132,r], E.M. Carlson [171], J. Carmignani [94], L. Carminati [71a,71b], A. Carnelli [4], M. Carnesale [37], S. Caron [116], E. Carquin [140g], I.B. Carr [107], S. Carrá [73a,73b], G. Carratta [24b,24a], A.M. Carroll [126], M.P. Casado [13,h], P. Casolaro [72a,72b], M. Caspar [48], F.L. Castillo [4], L. Castillo Garcia [13], V. Castillo Gimenez [169], N.F. Castro [133a,133e], A. Catinaccio [37], J.R. Catmore [128], T. Cavaliere [4], V. Cavaliere [30], L.J. Caviedes Betancourt [23b], E. Celebi [82], S. Cella [37], V. Cepaitis [56], K. Cerny [125], A.S. Cerqueira [83a], A. Cerri [74a,74b,ak], L. Cerrito [76a,76b], F. Cerutti [18a], B. Cervato [71a,71b], A. Cervelli [24b], G. Cesarini [53], S.A. Cetin [82], P.M. Chabrillat [130], R. Chakkappai [66], S. Chakraborty [173], J. Chan [18a], W.Y. Chan [159], J.D. Chapman [33], E. Chapon [138], B. Chargeishvili [155b], D.G. Charlton [21], C. Chauhan [136], Y. Che [114a], S. Chekanov [6], S.V. Chekulaev [162a], G.A. Chelkov [39,a], B. Chen [157], B. Chen [171], H. Chen [114a], H. Chen [30], J. Chen [144a], J. Chen [148], M. Chen [129], S. Chen [89], S.J. Chen [114a], X. Chen [144a], X. Chen [15,ag], Z. Chen [62], C.L. Cheng [176], H.C. Cheng [64a], S. Cheong [149], A. Cheplakov [39], E. Cherepanova [117], R. Cherkaoui El Moursli [36e], E. Cheu [7], K. Cheung [65], L. Chevalier [138], V. Chiarella [53], G. Chiarelli [74a], G. Chiodini [70a], A.S. Chisholm [21], A. Chitan [28b], M. Chitishvili [169], M.V. Chizhov [39,s], K. Choi [11], Y. Chou [142], H. Choudhary [148], E.Y.S. Chow [116], K.L. Chu [175], M.C. Chu [64a], X. Chu [14,114c], Z. Chubinidze [53], J. Chudoba [134],

J.J. Chwastowski [87], D. Cieri [112], K.M. Ciesla [86a], V. Cindro [95], A. Ciocio [18a], F. Cirotto [72a,72b], Z.H. Citron [175], M. Citterio [71a], D.A. Ciubotaru [28b], A. Clark [56], P.J. Clark [52], N. Clarke Hall [98], C. Clarry [161], S.E. Clawson [48], C. Clement [47a,47b], Y. Coadou [104], M. Cobal [69a,69c], A. Coccaro [57b], R.F. Coelho Barrue [133a], R. Coelho Lopes De Sa [105], S. Coelli [71a], L.S. Colangeli [161], B. Cole [42], P. Collado Soto [101], J. Collot [60], R. Coluccia [70a,70b], P. Conde Muiño [133a,133g], M.P. Connell [34c], S.H. Connell [34c], E.I. Conroy [129], F. Conventi [72a,ai], A.M. Cooper-Sarkar [129], L. Corazzina [75a,75b], F.A. Corchia [24b,24a], A. Cordeiro Oudot Choi [142], L.D. Corpe [41], M. Corradi [75a,75b], F. Corriveau [106,ab], A. Cortes-Gonzalez [159], M.J. Costa [169], F. Costanza [4], D. Costanzo [145], B.M. Cote [122], J. Couthures [4], G. Cowan [97], K. Cranmer [176], L. Cremer [49], D. Cremonini [24b,24a], S. Crépé-Renaudin [60], F. Crescioli [130], T. Cresta [73a,73b], M. Cristinziani [147], M. Cristoforetti [78a,78b], V. Croft [117], J.E. Crosby [124], G. Crosetti [44b,44a], A. Cueto [101], H. Cui [98], Z. Cui [7], B.M. Cunnett [152], W.R. Cunningham [59], F. Curcio [169], J.R. Curran [52], M.J. Da Cunha Sargedas De Sousa [57b,57a], J.V. Da Fonseca Pinto [83b], C. Da Via [103], W. Dabrowski [86a], T. Dado [37], S. Dahbi [154], T. Dai [108], D. Dal Santo [20], C. Dallapiccola [105], M. Dam [43], G. D'amen [30], V. D'Amico [111], J. Damp [102], J.R. Dandoy [35], M. D'andrea [57b,57a], D. Dannheim [37], G. D'anniballe [74a,74b], M. Danninger [148], V. Dao [151], G. Darbo [57b], S.J. Das [30], F. Dattola [48], S. D'Auria [71a,71b], A. D'Avanzo [72a,72b], T. Davidek [136], J. Davidson [173], I. Dawson [96], K. De [8], C. De Almeida Rossi [161], R. De Asmundis [72a], N. De Biase [48], S. De Castro [24b,24a], N. De Groot [116], P. de Jong [117], H. De la Torre [118], A. De Maria [114a], A. De Salvo [75a], U. De Sanctis [76a,76b], F. De Santis [70a,70b], A. De Santo [152], J.B. De Vivie De Regie [60], J. Debevc [95], D.V. Dedovich [39], J. Degens [94], A.M. Deiana [45], J. Del Peso [101], L. Delagrange [130], F. Deliot [138], C.M. Delitzsch [49], M. Della Pietra [72a,72b], D. Della Volpe [56], A. Dell'Acqua [37], L. Dell'Asta [71a,71b], M. Delmastro [4], C.C. Delogu [102], P.A. Delsart [60], S. Demers [178], M. Demichev [39], S.P. Denisov [38], H. Denizli [22a,l], L. D'Eramo [41], D. Derendarz [87], F. Derue [130], P. Dervan [94], A.M. Desai [1], K. Desch [25], F.A. Di Bello [57b,57a], A. Di Ciaccio [76a,76b], L. Di Ciaccio [4], A. Di Domenico [75a,75b], C. Di Donato [72a,72b], A. Di Girolamo [37], G. Di Gregorio [37], A. Di Luca [78a,78b], B. Di Micco [77a,77b], R. Di Nardo [77a,77b], K.F. Di Petrillo [40], M. Diamantopoulou [35], F.A. Dias [117], M.A. Diaz [140a,140b], A.R. Didenko [39], M. Didenko [169], S.D. Diefenbacher [18a], E.B. Diehl [108], S. Díez Cornell [48], C. Diez Pardos [147], C. Dimitriadi [150], A. Dimitrievska [21], A. Dimri [151], Y. Ding [62], J. Dingfelder [25], T. Dingley [129], I-M. Dinu [28b], S.J. Dittmeier [63b], F. Dittus [37], M. Divisek [136], B. Dixit [94], F. Djama [104], T. Djobava [155b], C. Doglioni [103,100], A. Dohnalova [29a], Z. Dolezal [136], K. Domijan [86a], K.M. Dona [40], M. Donadelli [83d], B. Dong [109], J. Donini [41], A. D'Onofrio [72a,72b], M. D'Onofrio [94], J. Dopke [137], A. Doria [72a], N. Dos Santos Fernandes [133a], I.A. Dos Santos Luz [83e], P. Dougan [103], M.T. Dova [92], A.T. Doyle [59], M.P. Drescher [55], E. Dreyer [175], I. Drivas-koulouris [10], M. Drnevich [120], D. Du [62], T.A. du Pree [117], Z. Duan [114a], M. Dubau [4], F. Dubinin [39], M. Dubovsky [29a], E. Duchovni [175], G. Duckeck [111], P.K. Duckett [98], O.A. Ducu [28b], D. Duda [52], A. Dudarev [37], E.R. Duden [27], M. D'uffizi [103], L. Duflot [66], M. Dührssen [37], I. Duminica [28g], A.E. Dumitriu [28b], M. Dunford [63a], K. Dunne [47a,47b], A. Duperrin [104], H. Duran Yildiz [3a], A. Durglishvili [155b], D. Duvnjak [35], G.I. Dyckes [18a], M. Dyndal [86a], B.S. Dziedzic [37], Z.O. Earnshaw [152], G.H. Eberwein [129], B. Eckerova [29a], S. Eggebrecht [55], E. Egidio Purcino De Souza [83e], G. Eigen [17], K. Einsweiler [18a], T. Ekelof [167], P.A. Ekman [100], S. El Farkh [36b], Y. El Ghazali [62], H. El Jarrari [37], A. El Moussaouy [36a], M. Ellert [167], F. Ellinghaus [177], T.A. Elliot [97], N. Ellis [37], J. Elmsheuser [30], M. Elsawy [119a], M. Elsing [37], D. Emeliyanov [137], Y. Enari [84], I. Ene [18a], S. Epari [110], D. Ernani Martins Neto [87], F. Ernst [37], M. Errenst [177], M. Escalier [66], C. Escobar [169], E. Etzion [157], G. Evans [133a,133b], H. Evans [68],

37

L.S. Evans [97], A. Ezhilov [38], S. Ezzarqtouni [36a], F. Fabbri [24b,24a], L. Fabbri [24b,24a], G. Facini [98], V. Fadeyev [139], R.M. Fakhrutdinov [38], D. Fakoudis [102], S. Falciano [75a], L.F. Falda Ulhoa Coelho [133a], F. Fallavollita [112], G. Falsetti [44b,44a], J. Faltova [136], C. Fan [168], K.Y. Fan [64b], Y. Fan [14], Y. Fang [14,114c], M. Fanti [71a,71b], M. Faraj [69a,69b], Z. Farazpay [99], A. Farbin [8], A. Farilla [77a], K. Farman [154], T. Farooque [109], J.N. Farr [178], S.M. Farrington [137,52], F. Fassi [36e], D. Fassouliotis [9], L. Fayard [66], P. Federic [136], P. Federicova [134], O.L. Fedin [38,a], M. Feickert [176], L. Feligioni [104], D.E. Fellers [18a], C. Feng [143a], Y. Feng [14], Z. Feng [117], M.J. Fenton [165], L. Ferencz [48], B. Fernandez Barbadillo [93], P. Fernandez Martinez [67], M.J.V. Fernoux [104], J. Ferrando [93], A. Ferrari [167], P. Ferrari [117,116], R. Ferrari [73a], D. Ferrere [56], C. Ferretti [108], M.P. Fewell [1], D. Fiacco [75a,75b], F. Fiedler [102], P. Fiedler [135], S. Filimonov [39], M.S. Filip [28b,t], A. Filipčič [95], E.K. Filmer [162a], F. Filthaut [116], M.C.N. Fiolhais [133a,133c,c], L. Fiorini [169], W.C. Fisher [109], T. Fitschen [103], P.M. Fitzhugh [138], I. Fleck [147], P. Fleischmann [108], T. Flick [177], M. Flores [34d,af], L.R. Flores Castillo [64a], L. Flores Sanz De Acedo [37], F.M. Follega [78a,78b], N. Fomin [33], J.H. Foo [161], A. Formica [138], A.C. Forti [103], E. Fortin [37], A.W. Fortman [18a], L. Foster [18a], L. Fountas [9,i], D. Fournier [66], H. Fox [93], P. Francavilla [74a,74b], S. Francescato [61], S. Franchellucci [56], M. Franchini [24b,24a], S. Franchino [63a], D. Francis [37], L. Franco [116], V. Franco Lima [37], L. Franconi [48], M. Franklin [61], G. Frattari [27], Y.Y. Frid [157], J. Friend [59], N. Fritzsche [37], A. Froch [56], D. Froidevaux [37], J.A. Frost [129], Y. Fu [109], S. Fuenzalida Garrido [140g], M. Fujimoto [104], K.Y. Fung [64a], E. Furtado De Simas Filho [83e], M. Furukawa [159], J. Fuster [169], A. Gaa [55], A. Gabrielli [24b,24a], A. Gabrielli [161], P. Gadow [37], G. Gagliardi [57b,57a], L.G. Gagnon [18a], S. Gaid [88b], S. Galantzan [157], J. Gallagher [1], E.J. Gallas [129], A.L. Gallen [167], B.J. Gallop [137], K.K. Gan [122], S. Ganguly [159], Y. Gao [52], A. Garabaglu [142], F.M. Garay Walls [140a,140b], C. García [169], A. Garcia Alonso [117], A.G. Garcia Caffaro [178], J.E. García Navarro [169], M.A. Garcia Ruiz [23b], M. Garcia-Sciveres [18a], G.L. Gardner [131], R.W. Gardner [40], N. Garelli [164], R.B. Garg [149], J.M. Gargan [52], C.A. Garner [161], C.M. Garvey [34a], V.K. Gassmann [164], G. Gaudio [73a], V. Gautam [13], P. Gauzzi [75a,75b], J. Gavranovic [95], I.L. Gavrilenko [133a], A. Gavrilyuk [38], C. Gay [170], G. Gaycken [126], E.N. Gazis [10], A. Gekow [122], C. Gemme [57b], M.H. Genest [60], A.D. Gentry [115], S. George [97], T. Geralis [46], A.A. Gerwin [123], P. Gessinger-Befurt [37], M.E. Geyik [177], M. Ghani [173], K. Ghorbanian [96], A. Ghosal [147], A. Ghosh [165], A. Ghosh [7], B. Giacobbe [24b], S. Giagu [75a,75b], T. Giani [117], A. Giannini [62], S.M. Gibson [97], M. Gignac [139], D.T. Gil [86b], A.K. Gilbert [86a], B.J. Gilbert [42], D. Gillberg [35], G. Gilles [117], D.M. Gingrich [2,ah], M.P. Giordani [69a,69c], P.F. Giraud [138], G. Giugliarelli [69a,69c], D. Giugni [71a], F. Giuli [76a,76b], I. Gkialas [9,i], L.K. Gladilin [38], C. Glasman [101], M. Glazewska [20], R.M. Gleason [165], G. Glemža [48], M. Glisic [126], I. Gnesi [44b], Y. Go [30], M. Goblirsch-Kolb [37], B. Gocke [49], D. Godin [110], B. Gokturk [22a], S. Goldfarb [107], T. Golling [56], M.G.D. Gololo [34c], D. Golubkov [38], J.P. Gombas [109], A. Gomes [133a,133b], G. Gomes Da Silva [147], A.J. Gomez Delegido [37], R. Gonçalo [133a], L. Gonella [21], A. Gongadze [155c], F. Gonnella [21], J.L. Gonski [149], R.Y. González Andana [52], S. González de la Hoz [169], M.V. Gonzalez Rodrigues [48], R. Gonzalez Suarez [167], S. Gonzalez-Sevilla [56], L. Goossens [37], B. Gorini [37], E. Gorini [70a,70b], A. Gorišek [95], T.C. Gosart [131], A.T. Goshaw [51], M.I. Gostkin [39], S. Goswami [124], C.A. Gottardo [37], S.A. Gotz [111], M. Gouighri [36b], A.G. Goussiou [142], N. Govender [34c], R.P. Grabarczyk [129], I. Grabowska-Bold [86a], K. Graham [35], E. Gramstad [128], S. Grancagnolo [70a,70b], C.M. Grant [1], P.M. Gravila [28f], F.G. Gravili [70a,70b], H.M. Gray [18a], M. Greco [112], M.J. Green [1], C. Grefe [25], A.S. Grefsrud [17], I.M. Gregor [48], K.T. Greif [165], P. Grenier [149], S.G. Grewe [112], A.A. Grillo [139], K. Grimm [32], S. Grinstein [13,x], J.-F. Grivaz [66], E. Gross [175], J. Grosse-Knetter [55], L. Guan [108], G. Guerrieri [37], R. Guevara [128], R. Gugel [102],

J.A.M. Guhit [108], A. Guida [19], E. Guilloton [173], S. Guindon [37], F. Guo [14,114c], J. Guo [144a], L. Guo [48], L. Guo [114b,v], Y. Guo [108], A. Gupta [49], R. Gupta [132], S. Gupta [27], S. Gurbuz [25], S.S. Gurdasani [48], G. Gustavino [75a,75b], P. Gutierrez [123], L.F. Gutierrez Zagazeta [131], M. Gutsche [50], C. Gutschow [98], C. Gwenlan [129], C.B. Gwilliam [94], E.S. Haaland [128], A. Haas [120], M. Habedank [59], C. Haber [18a], H.K. Hadavand [8], A. Haddad [41], A. Hadef [50], A.I. Hagan [93], J.J. Hahn [147], E.H. Haines [98], M. Haleem [172], J. Haley [124], R.P. Hall [148], G.D. Hallewell [104], K. Hamano [171], H. Hamdaoui [167], M. Hamer [25], S.E.D. Hammoud [66], E.J. Hampshire [97], J. Han [143a], L. Han [114a], L. Han [62], S. Han [14], K. Hanagaki [84], M. Hance [139], D.A. Hangal [42], H. Hanif [148], M.D. Hank [131], J.B. Hansen [43], P.H. Hansen [43], D. Harada [56], T. Harenberg [177], S. Harkusha [179], M.L. Harris [105], Y.T. Harris [25], J. Harrison [13], N.M. Harrison [122], P.F. Harrison[173], M.L.E. Hart [98], N.M. Hartman [112], N.M. Hartmann [111], R.Z. Hasan [97,137], Y. Hasegawa [146], F. Haslbeck [129], S. Hassan [17], R. Hauser [109], M. Haviernik [136], C.M. Hawkes [21], R.J. Hawkings [37], Y. Hayashi [159], D. Hayden [109], C. Hayes [108], R.L. Hayes [117], C.P. Hays [129], J.M. Hays [96], H.S. Hayward [94], M. He [14,114c], Y. He [48], Y. He [98], N.B. Heatley [96], V. Hedberg [100], C. Heidegger [54], K.K. Heidegger [54], J. Heilman [35], S. Heim [48], T. Heim [18a], J.G. Heinlein [131], J.J. Heinrich [126], L. Heinrich [112], J. Hejbal [134], M. Helbig [50], A. Held [176], S. Hellesund [17], C.M. Helling [170], S. Hellman [47a,47b], A.M. Henriques Correia[37], H. Herde [100], Y. Hernández Jiménez [151], L.M. Herrmann [25], T. Herrmann [50], G. Herten [54], R. Hertenberger [111], L. Hervas [37], M.E. Hesping [102], N.P. Hessey [162a], J. Hessler [112], M. Hidaoui [36b], N. Hidic [136], E. Hill [161], T.S. Hillersoy [17], S.J. Hillier [21], J.R. Hinds [109], F. Hinterkeuser [25], M. Hirose [127], S. Hirose [163], D. Hirschbuehl [177], T.G. Hitchings [103], B. Hiti [95], J. Hobbs [151], R. Hobincu [28e], N. Hod [175], A.M. Hodges [168], M.C. Hodgkinson [145], B.H. Hodkinson [129], A. Hoecker [37], D.D. Hofer [108], J. Hofer [169], M. Holzbock [37], L.B.A.H. Hommels [33], V. Homsak [129], B.P. Honan [103], J.J. Hong [68], T.M. Hong [132], B.H. Hooberman [168], W.H. Hopkins [6], M.C. Hoppesch [168], Y. Horii [113], M.E. Horstmann [112], S. Hou [154], M.R. Housenga [168], J. Howarth [59], J. Hoya [6], M. Hrabovsky [125], T. Hryn'ova [4], P.J. Hsu [65], S.-C. Hsu [142], T. Hsu [66], M. Hu [18a], Q. Hu [62], S. Huang [33], X. Huang [14,114c], Y. Huang [136], Y. Huang [114b], Y. Huang [102], Y. Huang [14], Z. Huang [66], Z. Hubacek [135], M. Huebner [25], F. Huegging [25], T.B. Huffman [129], M. Hufnagel Maranha De Faria [83a], C.A. Hugli [48], M. Huhtinen [37], S.K. Huiberts [17], R. Hulsken [106], C.E. Hultquist [18a], D.L. Humphreys [105], N. Huseynov [12], J. Huston [109], J. Huth [61], R. Hyneman [7], G. Iacobucci [56], G. Iakovidis [30], L. Iconomidou-Fayard [66], J.P. Iddon [37], P. Iengo [72a,72b], R. Iguchi [159], Y. Iiyama [159], T. Iizawa [159], Y. Ikegami [84], D. Iliadis [158], N. Ilic [161], H. Imam [36a], G. Inacio Goncalves [83d], S.A. Infante Cabanas [140c], T. Ingebretsen Carlson [47a,47b], J.M. Inglis [96], G. Introzzi [73a,73b], M. Iodice [77a], V. Ippolito [75a,75b], R.K. Irwin [94], M. Ishino [159], W. Islam [176], C. Issever [19], S. Istin [22a,am], K. Itabashi [84], H. Ito [174], R. Iuppa [78a,78b], A. Ivina [175], V. Izzo [72a], P. Jacka [135], P. Jackson [1], P. Jain [48], K. Jakobs [54], T. Jakoubek [175], J. Jamieson [59], W. Jang [159], S. Jankovych [136], M. Javurkova [105], P. Jawahar [103], L. Jeanty [126], J. Jejelava [155a,ae], P. Jenni [54,f], C.E. Jessiman [35], C. Jia [143a], H. Jia [170], J. Jia [151], X. Jia [112,114c], Z. Jia [114a], C. Jiang [52], Q. Jiang [64b], S. Jiggins [48], M. Jimenez Ortega [169], J. Jimenez Pena [13], S. Jin [114a], A. Jinaru [28b], O. Jinnouchi [141], P. Johansson [145], K.A. Johns [7], J.W. Johnson [139], F.A. Jolly [48], D.M. Jones [152], E. Jones [48], K.S. Jones[8], P. Jones [33], R.W.L. Jones [93], T.J. Jones [94], H.L. Joos [55], R. Joshi [122], J. Jovicevic [16], X. Ju [18a], J.J. Junggeburth [37], T. Junkermann [63a], A. Juste Rozas [13,x], M.K. Juzek [87], S. Kabana [140f], A. Kaczmarska [87], S.A. Kadir[149], M. Kado [112], H. Kagan [122], M. Kagan [149], A. Kahn [131], C. Kahra [102], T. Kaji [159], E. Kajomovitz [156], N. Kakati [175], N. Kakoty [13], I. Kalaitzidou [54], S. Kandel [8], N.J. Kang [139], D. Kar [34h], E. Karentzos [25],

39

O. Karkout [117], S.N. Karpov [39], Z.M. Karpova [39], V. Kartvelishvili [93], A.N. Karyukhin [38], E. Kasimi [158], J. Katzy [48], S. Kaur [35], K. Kawade [146], M.P. Kawale [123], C. Kawamoto [89], T. Kawamoto [62], E.F. Kay [37], F.I. Kaya [164], S. Kazakos [109], V.F. Kazanin [38], J.M. Keaveney [34a], R. Keeler [171], G.V. Kehris [61], J.S. Keller [35], J.M. Kelly [171], J.J. Kempster [152], O. Kepka [134], J. Kerr [162b], B.P. Kerridge [137], B.P. Kerševan [95], L. Keszeghova [29a], R.A. Khan [132], A. Khanov [124], A.G. Kharlamov [38], T. Kharlamova [38], E.E. Khoda [142], M. Kholodenko [133a], T.J. Khoo [19], G. Khoriauli [172], Y. Khoulaki [36a], J. Khubua [155b,*], Y.A.R. Khwaira [130], B. Kibirige[34h], D. Kim [6], D.W. Kim [47a,47b], Y.K. Kim [40], N. Kimura [98], M.K. Kingston [55], A. Kirchhoff [55], C. Kirfel [25], F. Kirfel [25], J. Kirk [137], A.E. Kiryunin [112], S. Kita [163], O. Kivernyk [25], M. Klassen [164], C. Klein [35], L. Klein [172], M.H. Klein [45], S.B. Klein [56], U. Klein [94], A. Klimentov [30], T. Klioutchnikova [37], P. Kluit [117], S. Kluth [112], E. Kneringer [79], T.M. Knight [161], A. Knue [49], M. Kobel [50], D. Kobylianskii [175], S.F. Koch [129], M. Kocian [149], P. Kodyš [136], D.M. Koeck [126], T. Koffas [35], O. Kolay [50], I. Koletsou [4], T. Komarek [87], K. Köneke [55], A.X.Y. Kong [1], T. Kono [121], N. Konstantinidis [98], P. Kontaxakis [56], B. Konya [100], R. Kopeliansky [42], S. Koperny [86a], K. Korcyl [87], K. Kordas [158,d], A. Korn [98], S. Korn [55], I. Korolkov [13], N. Korotkova [38], B. Kortman [117], O. Kortner [112], S. Kortner [112], W.H. Kostecka [118], M. Kostov [29a], V.V. Kostyukhin [147], A. Kotsokechagia [37], A. Kotwal [51], A. Koulouris [37], A. Kourkoumeli-Charalampidi [73a,73b], C. Kourkoumelis [9], E. Kourlitis [112], O. Kovanda [126], R. Kowalewski [171], W. Kozanecki [126], A.S. Kozhin [38], V.A. Kramarenko [38], G. Kramberger [95], P. Kramer [25], M.W. Krasny [130], A. Krasznahorkay [105], A.C. Kraus [118], J.W. Kraus [177], J.A. Kremer [48], N.B. Krengel [147], T. Kresse [50], L. Kretschmann [177], J. Kretzschmar [94], P. Krieger [161], K. Krizka [21], K. Kroeninger [49], H. Kroha [112], J. Kroll [134], J. Kroll [131], K.S. Krowpman [109], U. Kruchonak [39], H. Krüger [25], N. Krumnack[81], M.C. Kruse [51], O. Kuchinskaia [39], S. Kuday [3a], S. Kuehn [37], R. Kuesters [54], T. Kuhl [48], V. Kukhtin [39], Y. Kulchitsky [39], S. Kuleshov [140d,140b], J. Kull [1], E.V. Kumar [111], M. Kumar [34h], N. Kumari [48], P. Kumari [162b], A. Kupco [134], T. Kupfer[49], A. Kupich [38], O. Kuprash [54], H. Kurashige [85], L.L. Kurchaninov [162a], O. Kurdysh [4], Y.A. Kurochkin [38], A. Kurova [38], M. Kuze [141], A.K. Kvam [105], J. Kvita [125], N.G. Kyriacou [108], C. Lacasta [169], F. Lacava [75a,75b], H. Lacker [19], D. Lacour [130], N.N. Lad [98], E. Ladygin [39], A. Lafarge [41], B. Laforge [130], T. Lagouri [178], F.Z. Lahbabi [36a], S. Lai [55], W.S. Lai [98], J.E. Lambert [171], S. Lammers [68], W. Lampl [7], C. Lampoudis [158,d], G. Lamprinoudis [102], A.N. Lancaster [118], E. Lançon [30], U. Landgraf [54], M.P.J. Landon [96], V.S. Lang [54], O.K.B. Langrekken [128], A.J. Lankford [165], F. Lanni [37], K. Lantzsch [25], A. Lanza [73a], M. Lanzac Berrocal [169], J.F. Laporte [138], T. Lari [71a], D. Larsen [17], L. Larson [11], F. Lasagni Manghi [24b], M. Lassnig [37], S.D. Lawlor [145], R. Lazaridou[173], M. Lazzaroni [71a,71b], H.D.M. Le [109], E.M. Le Boulicaut [178], L.T. Le Pottier [18a], B. Leban [24b,24a], F. Ledroit-Guillon [60], T.F. Lee [162b], L.L. Leeuw [34c], M. Lefebvre [171], C. Leggett [18a], G. Lehmann Miotto [37], M. Leigh [56], W.A. Leight [105], W. Leinonen [116], A. Leisos [158,u], M.A.L. Leite [83c], C.E. Leitgeb [19], R. Leitner [136], K.J.C. Leney [45], T. Lenz [25], S. Leone [74a], C. Leonidopoulos [52], A. Leopold [150], J.H. Lepage Bourbonnais [35], R. Les [109], C.G. Lester [33], M. Levchenko [38], J. Levêque [4], L.J. Levinson [175], G. Levrini [24b,24a], M.P. Lewicki [87], C. Lewis [142], D.J. Lewis [4], L. Lewitt [145], A. Li [30], B. Li [143a], C. Li[108], C-Q. Li [112], H. Li [143a], H. Li [103], H. Li [15], H. Li[62], H. Li [143a], J. Li [144a], K. Li [14], L. Li [144a], R. Li [178], S. Li [14,114c], S. Li [144b,144a], T. Li [5], X. Li [106], Z. Li [159], Z. Li [14,114c], Z. Li [62], S. Liang [14,114c], Z. Liang [14], M. Liberatore [138], B. Liberti [76a], K. Lie [64c], J. Lieber Marin [83e], H. Lien [68], H. Lin [108], S.F. Lin [151], L. Linden [111], R.E. Lindley [7], J.H. Lindon [37], J. Ling [61], E. Lipeles [131], A. Lipniacka [17], A. Lister [170], J.D. Little [68], B. Liu [14], B.X. Liu [114b], D. Liu [144b,144a], D. Liu [139], E.H.L. Liu [21], J.K.K. Liu [120], K. Liu [144b], K. Liu [144b,144a], M. Liu [62], M.Y. Liu [62],

40

P. Liu [14], Q. Liu [144b,142,144a], X. Liu [62], X. Liu [143a], Y. Liu [114b,114c], Y.L. Liu [143a],
Y.W. Liu [62], Z. Liu [66,k], S.L. Lloyd [96], E.M. Lobodzinska [48], P. Loch [7], E. Lodhi [161],
K. Lohwasser [145], E. Loiacono [48], J.D. Lomas [21], J.D. Long [42], I. Longarini [165], R. Longo [168],
A. Lopez Solis [13], N.A. Lopez-canelas [7], N. Lorenzo Martinez [4], A.M. Lory [111], M. Losada [119a],
G. Löschcke Centeno [152], X. Lou [47a,47b], X. Lou [14,114c], A. Lounis [66], P.A. Love [93], M. Lu [66],
S. Lu [131], Y.J. Lu [154], H.J. Lubatti [142], C. Luci [75a,75b], F.L. Lucio Alves [114a], F. Luehring [68],
B.S. Lunday [131], O. Lundberg [150], J. Lunde [37], N.A. Luongo [6], M.S. Lutz [37], A.B. Lux [26],
D. Lynn [30], R. Lysak [134], V. Lysenko [135], E. Lytken [100], V. Lyubushkin [39], T. Lyubushkina [39],
M.M. Lyukova [151], M.Firdaus M. Soberi [52], H. Ma [30], K. Ma [62], L.L. Ma [143a], W. Ma [62],
Y. Ma [124], J.C. MacDonald [102], P.C. Machado De Abreu Farias [83e], R. Madar [41], T. Madula [98],
J. Maeda [85], T. Maeno [30], P.T. Mafa [34c,j], H. Maguire [145], M. Maheshwari [33], V. Maiboroda [66],
A. Maio [133a,133b,133d], K. Maj [86a], O. Majersky [48], S. Majewski [126], R. Makhmanazarov [38],
N. Makovec [66], V. Maksimovic [16], B. Malaescu [130], J. Malamant [128], Pa. Malecki [87],
V.P. Maleev [38], F. Malek [60,o], M. Mali [95], D. Malito [97], U. Mallik [80,*], A. Maloizel [5],
S. Maltezos [10], A. Malvezzi Lopes [83d], S. Malyukov [39], J. Mamuzic [95], G. Mancini [53],
M.N. Mancini [27], G. Manco [73a,73b], J.P. Mandalia [96], S.S. Mandarry [152], I. Mandić [95],
L. Manhaes de Andrade Filho [83a], I.M. Maniatis [175], J. Manjarres Ramos [91], D.C. Mankad [175],
A. Mann [111], T. Manoussos [37], M.N. Mantinan [40], S. Manzoni [37], L. Mao [144a], X. Mapekula [34c],
A. Marantis [158], R.R. Marcelo Gregorio [96], G. Marchiori [5], C. Marcon [71a], E. Maricic [138],
M. Marinescu [48], S. Marium [48], M. Marjanovic [123], A. Markhoos [54], M. Markovitch [66],
M.K. Maroun [105], G.T. Marsden [103], E.J. Marshall [93], Z. Marshall [18a], S. Marti-Garcia [169],
J. Martin [98], T.A. Martin [137], V.J. Martin [52], B. Martin dit Latour [17], L. Martinelli [75a,75b],
M. Martinez [13,x], P. Martinez Agullo [169], V.I. Martinez Outschoorn [105], P. Martinez Suarez [37],
S. Martin-Haugh [137], G. Martinovicova [136], V.S. Martoiu [28b], A.C. Martyniuk [98], A. Marzin [37],
D. Mascione [78a,78b], L. Masetti [102], J. Masik [103], A.L. Maslennikov [39], S.L. Mason [42],
P. Massarotti [72a,72b], P. Mastrandrea [74a,74b], A. Mastroberardino [44b,44a], T. Masubuchi [127],
T.T. Mathew [126], J. Matousek [136], D.M. Mattern [49], J. Maurer [28b], T. Maurin [59], A.J. Maury [66],
B. Maček [95], C. Mavungu Tsava [104], D.A. Maximov [38], A.E. May [103], E. Mayer [41],
R. Mazini [34h], I. Maznas [118], S.M. Mazza [139], E. Mazzeo [37], J.P. Mc Gowan [171],
S.P. Mc Kee [108], C.A. Mc Lean [6], C.C. McCracken [170], E.F. McDonald [107], A.E. McDougall [117],
L.F. Mcelhinney [93], J.A. Mcfayden [152], R.P. McGovern [131], R.P. Mckenzie [34h],
T.C. Mclachlan [48], D.J. Mclaughlin [98], S.J. McMahon [137], C.M. Mcpartland [94],
R.A. McPherson [171,ab], S. Mehlhase [111], A. Mehta [94], D. Melini [169], B.R. Mellado Garcia [34h],
A.H. Melo [55], F. Meloni [48], A.M. Mendes Jacques Da Costa [103], L. Meng [93], S. Menke [112],
M. Mentink [37], E. Meoni [44b,44a], G. Mercado [118], S. Merianos [158], C. Merlassino [69a,69c],
C. Meroni [71a,71b], J. Metcalfe [6], A.S. Mete [6], E. Meuser [102], C. Meyer [68], J-P. Meyer [138],
Y. Miao [114a], R.P. Middleton [137], M. Mihovilovic [66], L. Mijović [52], G. Mikenberg [175],
M. Mikestikova [134], M. Mikuž [95], H. Mildner [102], A. Milic [37], D.W. Miller [40], E.H. Miller [149],
A. Milov [175], D.A. Milstead [47a,47b], T. Min [114a], A.A. Minaenko [38], I.A. Minashvili [155b],
A.I. Mincer [120], B. Mindur [86a], M. Mineev [39], Y. Mino [89], L.M. Mir [13], M. Miralles Lopez [59],
M. Mironova [18a], M.C. Missio [116], A. Mitra [173], V.A. Mitsou [169], Y. Mitsumori [113], O. Miu [161],
P.S. Miyagawa [96], T. Mkrtchyan [63a], M. Mlinarevic [98], T. Mlinarevic [98], M. Mlynarikova [136],
S. Mobius [20], M.H. Mohamed Farook [115], S. Mohapatra [42], S. Mohiuddin [124],
G. Mokgatitswane [34h], L. Moleri [175], U. Molinatti [129], L.G. Mollier [20], B. Mondal [147],
S. Mondal [135], K. Mönig [48], E. Monnier [104], L. Monsonis Romero [169], J. Montejo Berlingen [13],
A. Montella [47a,47b], M. Montella [122], F. Montereali [77a,77b], F. Monticelli [92], S. Monzani [69a,69c],
A. Morancho Tarda [43], N. Morange [66], A.L. Moreira De Carvalho [48], M. Moreno Llácer [169],

41

C. Moreno Martinez [56], J.M. Moreno Perez[23b], P. Morettini [57b], S. Morgenstern [37], M. Morii [61], M. Morinaga [159], M. Moritsu [90], F. Morodei [75a,75b], P. Moschovakos [37], B. Moser [54], M. Mosidze [155b], T. Moskalets [45], P. Moskvitina [116], J. Moss [32], P. Moszkowicz [86a], A. Moussa [36d], Y. Moyal [175], H. Moyano Gomez [13], E.J.W. Moyse [105], T.G. Mroz [87], O. Mtintsilana [34h], S. Muanza [104], M. Mucha[25], J. Mueller [132], R. Müller [37], G.A. Mullier [167], A.J. Mullin[33], J.J. Mullin[51], A.C. Mullins[45], A.E. Mulski [61], D.P. Mungo [161], D. Munoz Perez [169], F.J. Munoz Sanchez [103], W.J. Murray [173,137], M. Muškinja [95], C. Mwewa [48], A.G. Myagkov [38,a], A.J. Myers [8], G. Myers [108], M. Myska [135], B.P. Nachman [18a], K. Nagai [129], K. Nagano [84], R. Nagasaka[159], J.L. Nagle [30,aj], E. Nagy [104], A.M. Nairz [37], Y. Nakahama [84], K. Nakamura [84], K. Nakkalil [5], A. Nandi [63b], H. Nanjo [127], E.A. Narayanan [45], Y. Narukawa [159], I. Naryshkin [38], L. Nasella [71a,71b], S. Nasri [119b], C. Nass [25], G. Navarro [23a], J. Navarro-Gonzalez [169], A. Nayaz [19], P.Y. Nechaeva [38], S. Nechaeva [24b,24a], F. Nechansky [134], L. Nedic [129], T.J. Neep [21], A. Negri [73a,73b], M. Negrini [24b], C. Nellist [117], C. Nelson [106], K. Nelson [108], S. Nemecek [134], M. Nessi [37,g], M.S. Neubauer [168], J. Newell [94], P.R. Newman [21], Y.W.Y. Ng [168], B. Ngair [119a], H.D.N. Nguyen [110], J.D. Nichols [123], R.B. Nickerson [129], R. Nicolaidou [138], J. Nielsen [139], M. Niemeyer [55], J. Niermann [37], N. Nikiforou [37], V. Nikolaenko [38,a], I. Nikolic-Audit [130], P. Nilsson [30], I. Ninca [48], G. Ninio [157], A. Nisati [75a], R. Nisius [112], N. Nitika [69a,69c], J-E. Nitschke [50], E.K. Nkadimeng [34b], T. Nobe [159], D. Noll [18a], T. Nommensen [153], M.B. Norfolk [145], B.J. Norman [35], M. Noury [36a], J. Novak [95], T. Novak [95], R. Novotny [135], L. Nozka [125], K. Ntekas [165], N.M.J. Nunes De Moura Junior [83b], J. Ocariz [130], A. Ochi [85], I. Ochoa [133a], S. Oerdek [48,y], J.T. Offermann [40], A. Ogrodnik [136], A. Oh [103], C.C. Ohm [150], H. Oide [84], M.L. Ojeda [37], Y. Okumura [159], L.F. Oleiro Seabra [133a], I. Oleksiyuk [56], G. Oliveira Correa [13], D. Oliveira Damazio [30], J.L. Oliver [165], R. Omar [68], Ö.O. Öncel [54], A.P. O'Neill [20], A. Onofre [133a,133e,e], P.U.E. Onyisi [11], M.J. Oreglia [40], D. Orestano [77a,77b], R. Orlandini [77a,77b], R.S. Orr [161], L.M. Osojnak [131], Y. Osumi [113], G. Otero y Garzon [31], H. Otono [90], M. Ouchrif [36d], F. Ould-Saada [128], T. Ovsiannikova [142], M. Owen [59], R.E. Owen [137], V.E. Ozcan [22a], F. Ozturk [87], N. Ozturk [8], S. Ozturk [82], H.A. Pacey [129], K. Pachal [162a], A. Pacheco Pages [13], C. Padilla Aranda [13], G. Padovano [75a,75b], S. Pagan Griso [18a], G. Palacino [68], A. Palazzo [70a,70b], J. Pampel [25], J. Pan [178], T. Pan [64a], D.K. Panchal [11], C.E. Pandini [60], J.G. Panduro Vazquez [137], H.D. Pandya [1], H. Pang [138], P. Pani [48], G. Panizzo [69a,69c], L. Panwar [130], L. Paolozzi [56], S. Parajuli [168], A. Paramonov [6], C. Paraskevopoulos [53], D. Paredes Hernandez [64b], A. Pareti [73a,73b], K.R. Park [42], T.H. Park [112], F. Parodi [57b,57a], J.A. Parsons [42], U. Parzefall [54], B. Pascual Dias [41], L. Pascual Dominguez [101], E. Pasqualucci [75a], S. Passaggio [57b], F. Pastore [97], P. Patel [87], U.M. Patel [51], J.R. Pater [103], T. Pauly [37], F. Pauwels [136], C.I. Pazos [164], M. Pedersen [128], R. Pedro [133a], S.V. Peleganchuk [38], O. Penc [134], E.A. Pender [52], S. Peng [15], G.D. Penn [178], K.E. Penski [111], M. Penzin [38], B.S. Peralva [83d], A.P. Pereira Peixoto [142], L. Pereira Sanchez [149], D.V. Perepelitsa [30,aj], G. Perera [105], E. Perez Codina [37], M. Perganti [10], H. Pernegger [37], S. Perrella [75a,75b], K. Peters [48], R.F.Y. Peters [103], B.A. Petersen [37], T.C. Petersen [43], E. Petit [104], V. Petousis [135], A.R. Petri [71a,71b], C. Petridou [158,d], T. Petru [136], A. Petrukhin [147], M. Pettee [18a], A. Petukhov [82], K. Petukhova [37], R. Pezoa [140g], L. Pezzotti [24b,24a], G. Pezzullo [178], L. Pfaffenbichler [37], A.J. Pfleger [79], T.M. Pham [176], T. Pham [107], P.W. Phillips [137], G. Piacquadio [151], E. Pianori [18a], F. Piazza [126], R. Piegaia [31], D. Pietreanu [28b], A.D. Pilkington [103], M. Pinamonti [69a,69c], J.L. Pinfold [2], B.C. Pinheiro Pereira [133a], J. Pinol Bel [13], A.E. Pinto Pinoargote [130], L. Pintucci [69a,69c], K.M. Piper [152], A. Pirttikoski [56], D.A. Pizzi [35], L. Pizzimento [64b], A. Plebani [33], M.-A. Pleier [30], V. Pleskot [136], E. Plotnikova[39], G. Poddar [96], R. Poettgen [100], L. Poggioli [130], S. Polacek [136], G. Polesello [73a], A. Poley [148], A. Polini [24b], C.S. Pollard [173],

Z.B. Pollock [122], E. Pompa Pacchi [123], N.I. Pond [98], D. Ponomarenko [68], L. Pontecorvo [37], S. Popa [28a], G.A. Popeneciu [28d], A. Poreba [37], D.M. Portillo Quintero [162a], S. Pospisil [135], M.A. Postill [145], P. Postolache [28c], K. Potamianos [173], P.A. Potepa [86a], I.N. Potrap [39], C.J. Potter [33], H. Potti [153], J. Poveda [169], M.E. Pozo Astigarraga [37], R. Pozzi [37], A. Prades Ibanez [76a,76b], S.R. Pradhan [145], J. Pretel [171], D. Price [103], M. Primavera [70a], L. Primomo [69a,69c], M.A. Principe Martin [101], R. Privara [125], T. Procter [86b], M.L. Proffitt [142], N. Proklova [131], K. Prokofiev [64c], G. Proto [112], J. Proudfoot [6], M. Przybycien [86a], W.W. Przygoda [86b], A. Psallidas [46], J.E. Puddefoot [145], D. Pudzha [53], H.I. Purnell [1], D. Pyatiizbyantseva [116], J. Qian [108], R. Qian [109], D. Qichen [129], Y. Qin [13], T. Qiu [52], A. Quadt [55], M. Queitsch-Maitland [103], G. Quetant [56], R.P. Quinn [170], G. Rabanal Bolanos [61], D. Rafanoharana [112], F. Raffaeli [76a,76b], F. Ragusa [71a,71b], J.L. Rainbolt [40], S. Rajagopalan [30], E. Ramakoti [39], L. Rambelli [57b,57a], I.A. Ramirez-Berend [35], K. Ran [48,114c], D.S. Rankin [131], N.P. Rapheeha [34h], H. Rasheed [28b], D.F. Rassloff [63a], A. Rastogi [18a], S. Rave [102], S. Ravera [57b,57a], B. Ravina [37], I. Ravinovich [175], M. Raymond [37], A.L. Read [128], N.P. Readioff [145], D.M. Rebuzzi [73a,73b], A.S. Reed [59], K. Reeves [27], J.A. Reidelsturz [177], D. Reikher [126], A. Rej [49], C. Rembser [37], H. Ren [62], M. Renda [28b], F. Renner [48], A.G. Rennie [59], A.L. Rescia [57b,57a], S. Resconi [71a], M. Ressegotti [57b,57a], S. Rettie [37], W.F. Rettie [35], M.M. Revering [33], E. Reynolds [18a], O.L. Rezanova [39], P. Reznicek [136], H. Riani [36d], N. Ribaric [51], B. Ricci [69a,69c], E. Ricci [78a,78b], R. Richter [112], S. Richter [47a,47b], E. Richter-Was [86b], M. Ridel [130], S. Ridouani [36d], P. Rieck [120], P. Riedler [37], E.M. Riefel [47a,47b], J.O. Rieger [117], M. Rijssenbeek [151], M. Rimoldi [37], L. Rinaldi [24b,24a], P. Rincke [167,55], G. Ripellino [167], I. Riu [13], J.C. Rivera Vergara [171], F. Rizatdinova [124], E. Rizvi [96], B.R. Roberts [18a], S.S. Roberts [139], D. Robinson [33], M. Robles Manzano [102], A. Robson [59], A. Rocchi [76a,76b], C. Roda [74a,74b], S. Rodriguez Bosca [37], Y. Rodriguez Garcia [23a], A.M. Rodríguez Vera [118], S. Roe [37], J.T. Roemer [37], O. Røhne [128], R.A. Rojas [37], C.P.A. Roland [130], A. Romaniouk [79], E. Romano [73a,73b], M. Romano [24b], A.C. Romero Hernandez [168], N. Rompotis [94], L. Roos [130], S. Rosati [75a], B.J. Rosser [40], E. Rossi [129], E. Rossi [72a,72b], L.P. Rossi [61], L. Rossini [54], R. Rosten [122], M. Rotaru [28b], B. Rottler [54], D. Rousseau [66], D. Rousso [48], S. Roy-Garand [161], A. Rozanov [104], Z.M.A. Rozario [59], Y. Rozen [156], A. Rubio Jimenez [169], V.H. Ruelas Rivera [19], T.A. Ruggeri [1], A. Ruggiero [129], A. Ruiz-Martinez [169], A. Rummler [37], Z. Rurikova [54], N.A. Rusakovich [39], S. Ruscelli [49], H.L. Russell [171], G. Russo [75a,75b], J.P. Rutherfoord [7], S. Rutherford Colmenares [33], M. Rybar [136], P. Rybczynski [86a], A. Ryzhov [45], J.A. Sabater Iglesias [56], H.F-W. Sadrozinski [139], F. Safai Tehrani [75a], S. Saha [1], M. Sahinsoy [82], B. Sahoo [175], A. Saibel [169], B.T. Saifuddin [123], M. Saimpert [138], G.T. Saito [83c], M. Saito [159], T. Saito [159], A. Sala [71a,71b], A. Salnikov [149], J. Salt [169], A. Salvador Salas [157], F. Salvatore [152], A. Salzburger [37], D. Sammel [54], E. Sampson [93], D. Sampsonidis [158,d], D. Sampsonidou [126], J. Sánchez [169], V. Sanchez Sebastian [169], H. Sandaker [128], C.O. Sander [48], J.A. Sandesara [176], M. Sandhoff [177], C. Sandoval [23b], L. Sanfilippo [63a], D.P.C. Sankey [137], T. Sano [89], A. Sansoni [53], M. Santana Queiroz [18b], L. Santi [37], C. Santoni [41], H. Santos [133a,133b], A. Santra [175], E. Sanzani [24b,24a], K.A. Saoucha [88b], J.G. Saraiva [133a,133d], J. Sardain [7], O. Sasaki [84], K. Sato [163], C. Sauer [37], E. Sauvan [4], P. Savard [161,ah], R. Sawada [159], C. Sawyer [137], L. Sawyer [99], C. Sbarra [24b], A. Sbrizzi [24b,24a], T. Scanlon [98], J. Schaarschmidt [142], U. Schäfer [102], A.C. Schaffer [66,45], D. Schaile [111], R.D. Schamberger [151], C. Scharf [19], M.M. Schefer [20], V.A. Schegelsky [38], D. Scheirich [136], M. Schernau [140f], C. Scheulen [56], C. Schiavi [57b,57a], M. Schioppa [44b,44a], B. Schlag [149], S. Schlenker [37], J. Schmeing [177], E. Schmidt [112], M.A. Schmidt [177], K. Schmieden [102], C. Schmitt [102], N. Schmitt [102],

43

S. Schmitt [48], N.A. Schneider [111], L. Schoeffel [138], A. Schoening [63b], P.G. Scholer [35], E. Schopf [147], M. Schott [25], S. Schramm [56], T. Schroer [56], H-C. Schultz-Coulon [63a], M. Schumacher [54], B.A. Schumm [139], Ph. Schune [138], H.R. Schwartz [7], A. Schwartzman [149], T.A. Schwarz [108], Ph. Schwemling [138], R. Schwienhorst [109], F.G. Sciacca [20], A. Sciandra [30], G. Sciolla [27], F. Scuri [74a], C.D. Sebastiani [37], K. Sedlaczek [118], S.C. Seidel [115], A. Seiden [139], B.D. Seidlitz [42], C. Seitz [48], J.M. Seixas [83b], G. Sekhniaidze [72a], L. Selem [60], N. Semprini-Cesari [24b,24a], A. Semushin [179], D. Sengupta [56], V. Senthilkumar [169], L. Serin [66], M. Sessa [72a,72b], H. Severini [123], F. Sforza [57b,57a], A. Sfyrla [56], Q. Sha [14], E. Shabalina [55], H. Shaddix [118], A.H. Shah [33], R. Shaheen [150], J.D. Shahinian [131], M. Shamim [37], L.Y. Shan [14], M. Shapiro [18a], A. Sharma [37], A.S. Sharma [170], P. Sharma [30], P.B. Shatalov [38], K. Shaw [152], S.M. Shaw [103], Q. Shen [144a], D.J. Sheppard [148], P. Sherwood [98], L. Shi [98], X. Shi [14], S. Shimizu [84], C.O. Shimmin [178], I.P.J. Shipsey [129,*], S. Shirabe [90], M. Shiyakova [39,z], M.J. Shochet [40], D.R. Shope [128], B. Shrestha [123], S. Shrestha [122,al], I. Shreyber [39], M.J. Shroff [171], P. Sicho [134], A.M. Sickles [168], E. Sideras Haddad [34h,166], A.C. Sidley [117], A. Sidoti [24b], F. Siegert [50], Dj. Sijacki [16], F. Sili [92], J.M. Silva [52], I. Silva Ferreira [83b], M.V. Silva Oliveira [30], S.B. Silverstein [47a], S. Simion [66], R. Simoniello [37], E.L. Simpson [103], H. Simpson [152], L.R. Simpson [6], S. Simsek [82], S. Sindhu [55], P. Sinervo [161], S.N. Singh [27], S. Singh [30], S. Sinha [48], S. Sinha [103], M. Sioli [24b,24a], K. Sioulas [9], I. Siral [37], E. Sitnikova [48], J. Sjölin [47a,47b], A. Skaf [55], E. Skorda [21], P. Skubic [123], M. Slawinska [87], I. Slazyk [17], I. Sliusar [128], V. Smakhtin [175], B.H. Smart [137], S.Yu. Smirnov [140b], Y. Smirnov [82], L.N. Smirnova [38,a], O. Smirnova [100], A.C. Smith [42], D.R. Smith [165], J.L. Smith [103], M.B. Smith [35], R. Smith [149], H. Smitmanns [102], M. Smizanska [93], K. Smolek [135], P. Smolyanskiy [135], A.A. Snesarev [39], H.L. Snoek [117], S. Snyder [30], R. Sobie [171,ab], A. Soffer [157], C.A. Solans Sanchez [37], E.Yu. Soldatov [39], U. Soldevila [169], A.A. Solodkov [34h], S. Solomon [27], A. Soloshenko [39], K. Solovieva [54], O.V. Solovyanov [41], P. Sommer [50], A. Sonay [13], A. Sopczak [135], A.L. Sopio [52], F. Sopkova [29b], J.D. Sorenson [115], I.R. Sotarriva Alvarez [141], V. Sothilingam [63a], O.J. Soto Sandoval [140c,140b], S. Sottocornola [68], R. Soualah [88a], Z. Soumaimi [36e], D. South [48], N. Soybelman [175], S. Spagnolo [70a,70b], M. Spalla [112], D. Sperlich [54], B. Spisso [72a,72b], D.P. Spiteri [59], L. Splendori [104], M. Spousta [136], E.J. Staats [35], R. Stamen [63a], E. Stanecka [87], W. Stanek-Maslouska [48], M.V. Stange [50], B. Stanislaus [18a], M.M. Stanitzki [48], B. Stapf [48], E.A. Starchenko [38], G.H. Stark [139], J. Stark [91], P. Staroba [134], P. Starovoitov [88b], R. Staszewski [87], C. Stauch [111], G. Stavropoulos [46], A. Stefl [37], A. Stein [102], P. Steinberg [30], B. Stelzer [148,162a], H.J. Stelzer [132], O. Stelzer-Chilton [162a], H. Stenzel [58], T.J. Stevenson [152], G.A. Stewart [37], J.R. Stewart [124], G. Stoicea [28b], M. Stolarski [133a], S. Stonjek [112], A. Straessner [50], J. Strandberg [150], S. Strandberg [47a,47b], M. Stratmann [177], M. Strauss [123], T. Strebler [104], P. Strizenec [29b], R. Ströhmer [172], D.M. Strom [126], R. Stroynowski [45], A. Strubig [47a,47b], S.A. Stucci [30], B. Stugu [17], J. Stupak [123], N.A. Styles [48], D. Su [149], S. Su [62], X. Su [62], D. Suchy [29a], K. Sugizaki [131], V.V. Sulin [38], D.M.S. Sultan [129], L. Sultanaliyeva [38], S. Sultansoy [3b], S. Sun [176], W. Sun [14], O. Sunneborn Gudnadottir [167], N. Sur [100], M.R. Sutton [152], M. Svatos [134], P.N. Swallow [33], M. Swiatlowski [162a], T. Swirski [172], A. Swoboda [37], I. Sykora [29a], M. Sykora [136], T. Sykora [136], D. Ta [102], K. Tackmann [48,y], A. Taffard [165], R. Tafirout [162a], Y. Takubo [84], M. Talby [104], A.A. Talyshev [38], K.C. Tam [64b], N.M. Tamir [157], A. Tanaka [159], J. Tanaka [159], R. Tanaka [66], M. Tanasini [151], Z. Tao [170], S. Tapia Araya [140g], S. Tapprogge [102], A. Tarek Abouelfadl Mohamed [109], S. Tarem [156], K. Tariq [14], G. Tarna [37], G.F. Tartarelli [71a], M.J. Tartarin [91], P. Tas [136], M. Tasevsky [134], E. Tassi [44b,44a], A.C. Tate [168], Y. Tayalati [36e,aa], G.N. Taylor [107], W. Taylor [162b], A.S. Tegetmeier [91], P. Teixeira-Dias [97], J.J. Teoh [161], K. Terashi [159],

J. Terron[101], S. Terzo[13], M. Testa[53], R.J. Teuscher[161,ab], A. Thaler[79], O. Theiner[56],
T. Theveneaux-Pelzer[104], D.W. Thomas[97], J.P. Thomas[21], E.A. Thompson[18a], P.D. Thompson[21],
E. Thomson[131], R.E. Thornberry[45], C. Tian[62], Y. Tian[56], V. Tikhomirov[82],
Yu.A. Tikhonov[39], S. Timoshenko[38], D. Timoshyn[136], E.X.L. Ting[1], P. Tipton[178],
A. Tishelman-Charny[30], K. Todome[141], S. Todorova-Nova[136], L. Toffolin[69a,69c], M. Togawa[84],
J. Tojo[90], S. Tokár[29a], O. Toldaiev[68], G. Tolkachev[104], M. Tomoto[84], L. Tompkins[149,n],
E. Torrence[126], H. Torres[91], E. Torró Pastor[169], M. Toscani[31], C. Tosciri[40], M. Tost[11],
D.R. Tovey[145], T. Trefzger[172], P.M. Tricarico[13], A. Tricoli[30], I.M. Trigger[162a],
S. Trincaz-Duvoid[130], D.A. Trischuk[27], A. Tropina[39], L. Truong[34c], M. Trzebinski[87],
A. Trzupek[87], F. Tsai[151], M. Tsai[108], A. Tsiamis[158], P.V. Tsiareshka[39], S. Tsigaridas[162a],
A. Tsirigotis[158,u], V. Tsiskaridze[155a], E.G. Tskhadadze[155a], M. Tsopoulou[158], Y. Tsujikawa[89],
I.I. Tsukerman[38], V. Tsulaia[18a], S. Tsuno[84], K. Tsuri[121], D. Tsybychev[151], Y. Tu[64b],
A. Tudorache[28b], V. Tudorache[28b], S.B. Tuncay[129], S. Turchikhin[57b,57a], I. Turk Cakir[3a],
R. Turra[71a], T. Turtuvshin[39,ac], P.M. Tuts[42], S. Tzamarias[158,d], E. Tzovara[102], Y. Uematsu[84],
F. Ukegawa[163], P.A. Ulloa Poblete[140c,140b], E.N. Umaka[30], G. Unal[37], A. Undrus[30],
G. Unel[165], J. Urban[29b], P. Urrejola[140a], G. Usai[8], R. Ushioda[160], M. Usman[110],
F. Ustuner[52], Z. Uysal[82], V. Vacek[135], B. Vachon[106], T. Vafeiadis[37], A. Vaitkus[98],
C. Valderanis[111], E. Valdes Santurio[47a,47b], M. Valente[37], S. Valentinetti[24b,24a], A. Valero[169],
E. Valiente Moreno[169], A. Vallier[91], J.A. Valls Ferrer[169], D.R. Van Arneman[117],
A. Van Der Graaf[49], H.Z. Van Der Schyf[34h], P. Van Gemmeren[6], M. Van Rijnbach[37],
S. Van Stroud[98], I. Van Vulpen[117], P. Vana[136], M. Vanadia[76a,76b], U.M. Vande Voorde[150],
W. Vandelli[37], E.R. Vandewall[124], D. Vannicola[157], L. Vannoli[53], R. Vari[75a], M. Varma[178],
E.W. Varnes[7], C. Varni[118], D. Varouchas[66], L. Varriale[169], K.E. Varvell[153], M.E. Vasile[28b],
L. Vaslin[84], M.D. Vassilev[149], A. Vasyukov[39], L.M. Vaughan[124], R. Vavricka[136],
T. Vazquez Schroeder[13], J. Veatch[32], V. Vecchio[103], M.J. Veen[105], I. Veliscek[30],
I. Velkovska[95], L.M. Veloce[161], F. Veloso[133a,133c], S. Veneziano[75a], A. Ventura[70a,70b],
A. Verbytskyi[112], M. Verducci[74a,74b], C. Vergis[96], M. Verissimo De Araujo[83b],
W. Verkerke[117], J.C. Vermeulen[117], C. Vernieri[149], M. Vessella[165], M.C. Vetterli[148,ah],
A. Vgenopoulos[102], N. Viaux Maira[140g], T. Vickey[145], O.E. Vickey Boeriu[145],
G.H.A. Viehhauser[129], L. Vigani[63b], M. Vigl[112], M. Villa[24b,24a], M. Villaplana Perez[169],
E.M. Villhauer[40], E. Vilucchi[53], M. Vincent[169], M.G. Vincter[35], A. Visibile[117], C. Vittori[37],
I. Vivarelli[24b,24a], E. Voevodina[112], F. Vogel[111], J.C. Voigt[50], P. Vokac[135], Yu. Volkotrub[86b],
L. Vomberg[25], E. Von Toerne[25], B. Vormwald[37], K. Vorobev[51], M. Vos[169], K. Voss[147],
M. Vozak[37], L. Vozdecky[123], N. Vranjes[16], M. Vranjes Milosavljevic[16], M. Vreeswijk[117],
N.K. Vu[144b,144a], R. Vuillermet[37], O. Vujinovic[102], I. Vukotic[40], I.K. Vyas[35], J.F. Wack[33],
S. Wada[163], C. Wagner[149], J.M. Wagner[18a], W. Wagner[177], S. Wahdan[177], H. Wahlberg[92],
C.H. Waits[123], J. Walder[137], R. Walker[111], K. Walkingshaw Pass[59], W. Walkowiak[147],
A. Wall[131], E.J. Wallin[100], T. Wamorkar[18a], K. Wandall-Christensen[169], A. Wang[62],
A.Z. Wang[139], C. Wang[102], C. Wang[11], H. Wang[18a], J. Wang[64c], P. Wang[103], P. Wang[98],
R. Wang[61], R. Wang[6], S.M. Wang[154], S. Wang[14], T. Wang[116], T. Wang[62], W.T. Wang[80],
W. Wang[14], X. Wang[168], X. Wang[144a], X. Wang[48], Y. Wang[114a], Y. Wang[62], Z. Wang[108],
Z. Wang[144b], Z. Wang[108], C. Wanotayaroj[84], A. Warburton[106], A.L. Warnerbring[147],
S. Waterhouse[97], A.T. Watson[21], H. Watson[52], M.F. Watson[21], E. Watton[59], G. Watts[142],
B.M. Waugh[98], J.M. Webb[54], C. Weber[30], H.A. Weber[19], M.S. Weber[20], S.M. Weber[63a],
C. Wei[62], Y. Wei[54], A.R. Weidberg[129], E.J. Weik[120], J. Weingarten[49], C. Weiser[54],
C.J. Wells[48], T. Wenaus[30], T. Wengler[37], N.S. Wenke[112], N. Wermes[25], M. Wessels[63a],
A.M. Wharton[93], A.S. White[61], A. White[8], M.J. White[1], D. Whiteson[165],

L. Wickremasinghe [127], W. Wiedenmann [176], M. Wielers [137], R. Wierda [150], C. Wiglesworth [43], H.G. Wilkens [37], J.J.H. Wilkinson [33], D.M. Williams [42], H.H. Williams[131], S. Williams [33], S. Willocq [105], B.J. Wilson [103], D.J. Wilson [103], P.J. Windischhofer [40], F.I. Winkel [31], F. Winklmeier [126], B.T. Winter [54], M. Wittgen[149], M. Wobisch [99], T. Wojtkowski[60], Z. Wolffs [117], J. Wollrath[37], M.W. Wolter [87], H. Wolters [133a,133c], M.C. Wong[139], E.L. Woodward [42], S.D. Worm [48], B.K. Wosiek [87], K.W. Woźniak [87], S. Wozniewski [55], K. Wraight [59], C. Wu [161], C. Wu [21], J. Wu [159], M. Wu [114b], M. Wu [116], S.L. Wu [176], S. Wu [14], X. Wu [62], Y. Wu [62], Z. Wu [4], J. Wuerzinger [112], T.R. Wyatt [103], B.M. Wynne [52], S. Xella [43], L. Xia [114a], M. Xia [15], M. Xie [62], A. Xiong [126], J. Xiong [18a], D. Xu [14], H. Xu [62], L. Xu [62], R. Xu [131], T. Xu [108], Y. Xu [142], Z. Xu [52], R. Xue [132], B. Yabsley [153], S. Yacoob [34a], Y. Yamaguchi [84], E. Yamashita [159], H. Yamauchi [163], T. Yamazaki [18a], Y. Yamazaki [85], S. Yan [59], Z. Yan [105], H.J. Yang [144a,144b], H.T. Yang [62], S. Yang [62], T. Yang [64c], X. Yang [37], X. Yang [14], Y. Yang [159], Y. Yang[62], W-M. Yao [18a], C.L. Yardley [152], J. Ye [14], S. Ye [30], X. Ye [62], Y. Yeh [98], I. Yeletskikh [39], B. Yeo [18b], M.R. Yexley [98], T.P. Yildirim [129], K. Yorita [174], C.J.S. Young [37], C. Young [149], N.D. Young[126], Y. Yu [62], J. Yuan [14,114c], M. Yuan [108], R. Yuan [144b,144a], L. Yue [98], M. Zaazoua [62], B. Zabinski [87], I. Zahir [36a], A. Zaio[57b,57a], Z.K. Zak [87], T. Zakareishvili [169], S. Zambito [56], J.A. Zamora Saa [140d], J. Zang [159], R. Zanzottera [71a,71b], O. Zaplatilek [135], C. Zeitnitz [177], H. Zeng [14], J.C. Zeng [168], D.T. Zenger Jr [27], O. Zenin [38], T. Ženiš [29a], S. Zenz [96], D. Zerwas [66], M. Zhai [14,114c], D.F. Zhang [145], G. Zhang [14], J. Zhang [143a], J. Zhang [6], K. Zhang [14,114c], L. Zhang [62], L. Zhang [114a], P. Zhang [14,114c], R. Zhang [114a], S. Zhang [91], T. Zhang [159], Y. Zhang [142], Y. Zhang [98], Y. Zhang [62], Y. Zhang [114a], Z. Zhang [143a], Z. Zhang [66], H. Zhao [142], T. Zhao [143a], Y. Zhao [35], Z. Zhao [62], Z. Zhao [62], A. Zhemchugov [39], J. Zheng [114a], K. Zheng [168], X. Zheng [62], Z. Zheng [149], D. Zhong [168], B. Zhou [108], H. Zhou [7], N. Zhou [144a], Y. Zhou [15], Y. Zhou [114a], Y. Zhou[7], C.G. Zhu [143a], J. Zhu [108], X. Zhu[144b], Y. Zhu [144a], Y. Zhu [62], X. Zhuang [14], K. Zhukov [68], N.I. Zimine [39], J. Zinsser [63b], M. Ziolkowski [147], L. Živković [16], A. Zoccoli [24b,24a], K. Zoch [61], A. Zografos [37], T.G. Zorbas [145], O. Zormpa [46], L. Zwalinski [37].

[1] Department of Physics, University of Adelaide, Adelaide; Australia.
[2] Department of Physics, University of Alberta, Edmonton AB; Canada.
[3] [a] Department of Physics, Ankara University, Ankara; [b] Division of Physics, TOBB University of Economics and Technology, Ankara; Türkiye.
[4] LAPP, Université Savoie Mont Blanc, CNRS/IN2P3, Annecy; France.
[5] APC, Université Paris Cité, CNRS/IN2P3, Paris; France.
[6] High Energy Physics Division, Argonne National Laboratory, Argonne IL; United States of America.
[7] Department of Physics, University of Arizona, Tucson AZ; United States of America.
[8] Department of Physics, University of Texas at Arlington, Arlington TX; United States of America.
[9] Physics Department, National and Kapodistrian University of Athens, Athens; Greece.
[10] Physics Department, National Technical University of Athens, Zografou; Greece.
[11] Department of Physics, University of Texas at Austin, Austin TX; United States of America.
[12] Institute of Physics, Azerbaijan Academy of Sciences, Baku; Azerbaijan.
[13] Institut de Física d'Altes Energies (IFAE), Barcelona Institute of Science and Technology, Barcelona; Spain.
[14] Institute of High Energy Physics, Chinese Academy of Sciences, Beijing; China.
[15] Physics Department, Tsinghua University, Beijing; China.
[16] Institute of Physics, University of Belgrade, Belgrade; Serbia.
[17] Department for Physics and Technology, University of Bergen, Bergen; Norway.

[18][(a)]Physics Division, Lawrence Berkeley National Laboratory, Berkeley CA;[(b)]University of California, Berkeley CA; United States of America.

[19]Institut für Physik, Humboldt Universität zu Berlin, Berlin; Germany.

[20]Albert Einstein Center for Fundamental Physics and Laboratory for High Energy Physics, University of Bern, Bern; Switzerland.

[21]School of Physics and Astronomy, University of Birmingham, Birmingham; United Kingdom.

[22][(a)]Department of Physics, Bogazici University, Istanbul;[(b)]Department of Physics Engineering, Gaziantep University, Gaziantep;[(c)]Department of Physics, Istanbul University, Istanbul; Türkiye.

[23][(a)]Facultad de Ciencias y Centro de Investigaciónes, Universidad Antonio Nariño, Bogotá;[(b)]Departamento de Física, Universidad Nacional de Colombia, Bogotá; Colombia.

[24][(a)]Dipartimento di Fisica e Astronomia A. Righi, Università di Bologna, Bologna;[(b)]INFN Sezione di Bologna; Italy.

[25]Physikalisches Institut, Universität Bonn, Bonn; Germany.

[26]Department of Physics, Boston University, Boston MA; United States of America.

[27]Department of Physics, Brandeis University, Waltham MA; United States of America.

[28][(a)]Transilvania University of Brasov, Brasov;[(b)]Horia Hulubei National Institute of Physics and Nuclear Engineering, Bucharest;[(c)]Department of Physics, Alexandru Ioan Cuza University of Iasi, Iasi;[(d)]National Institute for Research and Development of Isotopic and Molecular Technologies, Physics Department, Cluj-Napoca;[(e)]National University of Science and Technology Politechnica, Bucharest;[(f)]West University in Timisoara, Timisoara;[(g)]Faculty of Physics, University of Bucharest, Bucharest; Romania.

[29][(a)]Faculty of Mathematics, Physics and Informatics, Comenius University, Bratislava;[(b)]Department of Subnuclear Physics, Institute of Experimental Physics of the Slovak Academy of Sciences, Kosice; Slovak Republic.

[30]Physics Department, Brookhaven National Laboratory, Upton NY; United States of America.

[31]Universidad de Buenos Aires, Facultad de Ciencias Exactas y Naturales, Departamento de Física, y CONICET, Instituto de Física de Buenos Aires (IFIBA), Buenos Aires; Argentina.

[32]California State University, CA; United States of America.

[33]Cavendish Laboratory, University of Cambridge, Cambridge; United Kingdom.

[34][(a)]Department of Physics, University of Cape Town, Cape Town;[(b)]iThemba Labs, Western Cape;[(c)]Department of Mechanical Engineering Science, University of Johannesburg, Johannesburg;[(d)]National Institute of Physics, University of the Philippines Diliman (Philippines);[(e)]Department of Physics, Stellenbosch University, Matieland;[(f)]University of South Africa, Department of Physics, Pretoria;[(g)]University of Zululand, KwaDlangezwa;[(h)]School of Physics, University of the Witwatersrand, Johannesburg; South Africa.

[35]Department of Physics, Carleton University, Ottawa ON; Canada.

[36][(a)]Faculté des Sciences Ain Chock, Université Hassan II de Casablanca;[(b)]Faculté des Sciences, Université Ibn-Tofail, Kénitra;[(c)]Faculté des Sciences Semlalia, Université Cadi Ayyad, LPHEA-Marrakech;[(d)]LPMR, Faculté des Sciences, Université Mohamed Premier, Oujda;[(e)]Faculté des sciences, Université Mohammed V, Rabat;[(f)]Institute of Applied Physics, Mohammed VI Polytechnic University, Ben Guerir; Morocco.

[37]CERN, Geneva; Switzerland.

[38]Affiliated with an institute formerly covered by a cooperation agreement with CERN.

[39]Affiliated with an international laboratory covered by a cooperation agreement with CERN.

[40]Enrico Fermi Institute, University of Chicago, Chicago IL; United States of America.

[41]LPC, Université Clermont Auvergne, CNRS/IN2P3, Clermont-Ferrand; France.

[42]Nevis Laboratory, Columbia University, Irvington NY; United States of America.

[43]Niels Bohr Institute, University of Copenhagen, Copenhagen; Denmark.

[44](a)Dipartimento di Fisica, Università della Calabria, Rende;(b)INFN Gruppo Collegato di Cosenza, Laboratori Nazionali di Frascati; Italy.

[45]Physics Department, Southern Methodist University, Dallas TX; United States of America.

[46]National Centre for Scientific Research "Demokritos", Agia Paraskevi; Greece.

[47](a)Department of Physics, Stockholm University;(b)Oskar Klein Centre, Stockholm; Sweden.

[48]Deutsches Elektronen-Synchrotron DESY, Hamburg and Zeuthen; Germany.

[49]Fakultät Physik , Technische Universität Dortmund, Dortmund; Germany.

[50]Institut für Kern- und Teilchenphysik, Technische Universität Dresden, Dresden; Germany.

[51]Department of Physics, Duke University, Durham NC; United States of America.

[52]SUPA - School of Physics and Astronomy, University of Edinburgh, Edinburgh; United Kingdom.

[53]INFN e Laboratori Nazionali di Frascati, Frascati; Italy.

[54]Physikalisches Institut, Albert-Ludwigs-Universität Freiburg, Freiburg; Germany.

[55]II. Physikalisches Institut, Georg-August-Universität Göttingen, Göttingen; Germany.

[56]Département de Physique Nucléaire et Corpusculaire, Université de Genève, Genève; Switzerland.

[57](a)Dipartimento di Fisica, Università di Genova, Genova;(b)INFN Sezione di Genova; Italy.

[58]II. Physikalisches Institut, Justus-Liebig-Universität Giessen, Giessen; Germany.

[59]SUPA - School of Physics and Astronomy, University of Glasgow, Glasgow; United Kingdom.

[60]LPSC, Université Grenoble Alpes, CNRS/IN2P3, Grenoble INP, Grenoble; France.

[61]Laboratory for Particle Physics and Cosmology, Harvard University, Cambridge MA; United States of America.

[62]Department of Modern Physics and State Key Laboratory of Particle Detection and Electronics, University of Science and Technology of China, Hefei; China.

[63](a)Kirchhoff-Institut für Physik, Ruprecht-Karls-Universität Heidelberg, Heidelberg;(b)Physikalisches Institut, Ruprecht-Karls-Universität Heidelberg, Heidelberg; Germany.

[64](a)Department of Physics, Chinese University of Hong Kong, Shatin, N.T., Hong Kong;(b)Department of Physics, University of Hong Kong, Hong Kong;(c)Department of Physics and Institute for Advanced Study, Hong Kong University of Science and Technology, Clear Water Bay, Kowloon, Hong Kong; China.

[65]Department of Physics, National Tsing Hua University, Hsinchu; Taiwan.

[66]IJCLab, Université Paris-Saclay, CNRS/IN2P3, 91405, Orsay; France.

[67]Centro Nacional de Microelectrónica (IMB-CNM-CSIC), Barcelona; Spain.

[68]Department of Physics, Indiana University, Bloomington IN; United States of America.

[69](a)INFN Gruppo Collegato di Udine, Sezione di Trieste, Udine;(b)ICTP, Trieste;(c)Dipartimento Politecnico di Ingegneria e Architettura, Università di Udine, Udine; Italy.

[70](a)INFN Sezione di Lecce;(b)Dipartimento di Matematica e Fisica, Università del Salento, Lecce; Italy.

[71](a)INFN Sezione di Milano;(b)Dipartimento di Fisica, Università di Milano, Milano; Italy.

[72](a)INFN Sezione di Napoli;(b)Dipartimento di Fisica, Università di Napoli, Napoli; Italy.

[73](a)INFN Sezione di Pavia;(b)Dipartimento di Fisica, Università di Pavia, Pavia; Italy.

[74](a)INFN Sezione di Pisa;(b)Dipartimento di Fisica E. Fermi, Università di Pisa, Pisa; Italy.

[75](a)INFN Sezione di Roma;(b)Dipartimento di Fisica, Sapienza Università di Roma, Roma; Italy.

[76](a)INFN Sezione di Roma Tor Vergata;(b)Dipartimento di Fisica, Università di Roma Tor Vergata, Roma; Italy.

[77](a)INFN Sezione di Roma Tre;(b)Dipartimento di Matematica e Fisica, Università Roma Tre, Roma; Italy.

[78](a)INFN-TIFPA;(b)Università degli Studi di Trento, Trento; Italy.

[79]Universität Innsbruck, Department of Astro and Particle Physics, Innsbruck; Austria.

[80]University of Iowa, Iowa City IA; United States of America.

[81]Department of Physics and Astronomy, Iowa State University, Ames IA; United States of America.

[82]Istinye University, Sariyer, Istanbul; Türkiye.

[83](a)Departamento de Engenharia Elétrica, Universidade Federal de Juiz de Fora (UFJF), Juiz de Fora;(b)Universidade Federal do Rio De Janeiro COPPE/EE/IF, Rio de Janeiro;(c)Instituto de Física, Universidade de São Paulo, São Paulo;(d)Rio de Janeiro State University, Rio de Janeiro;(e)Federal University of Bahia, Bahia; Brazil.

[84]KEK, High Energy Accelerator Research Organization, Tsukuba; Japan.

[85]Graduate School of Science, Kobe University, Kobe; Japan.

[86](a)AGH University of Krakow, Faculty of Physics and Applied Computer Science, Krakow;(b)Marian Smoluchowski Institute of Physics, Jagiellonian University, Krakow; Poland.

[87]Institute of Nuclear Physics Polish Academy of Sciences, Krakow; Poland.

[88](a)Khalifa University of Science and Technology, Abu Dhabi;(b)University of Sharjah, Sharjah; United Arab Emirates.

[89]Faculty of Science, Kyoto University, Kyoto; Japan.

[90]Research Center for Advanced Particle Physics and Department of Physics, Kyushu University, Fukuoka ; Japan.

[91]L2IT, Université de Toulouse, CNRS/IN2P3, UPS, Toulouse; France.

[92]Instituto de Física La Plata, Universidad Nacional de La Plata and CONICET, La Plata; Argentina.

[93]Physics Department, Lancaster University, Lancaster; United Kingdom.

[94]Oliver Lodge Laboratory, University of Liverpool, Liverpool; United Kingdom.

[95]Department of Experimental Particle Physics, Jožef Stefan Institute and Department of Physics, University of Ljubljana, Ljubljana; Slovenia.

[96]Department of Physics and Astronomy, Queen Mary University of London, London; United Kingdom.

[97]Department of Physics, Royal Holloway University of London, Egham; United Kingdom.

[98]Department of Physics and Astronomy, University College London, London; United Kingdom.

[99]Louisiana Tech University, Ruston LA; United States of America.

[100]Fysiska institutionen, Lunds universitet, Lund; Sweden.

[101]Departamento de Física Teorica C-15 and CIAFF, Universidad Autónoma de Madrid, Madrid; Spain.

[102]Institut für Physik, Universität Mainz, Mainz; Germany.

[103]School of Physics and Astronomy, University of Manchester, Manchester; United Kingdom.

[104]CPPM, Aix-Marseille Université, CNRS/IN2P3, Marseille; France.

[105]Department of Physics, University of Massachusetts, Amherst MA; United States of America.

[106]Department of Physics, McGill University, Montreal QC; Canada.

[107]School of Physics, University of Melbourne, Victoria; Australia.

[108]Department of Physics, University of Michigan, Ann Arbor MI; United States of America.

[109]Department of Physics and Astronomy, Michigan State University, East Lansing MI; United States of America.

[110]Group of Particle Physics, University of Montreal, Montreal QC; Canada.

[111]Fakultät für Physik, Ludwig-Maximilians-Universität München, München; Germany.

[112]Max-Planck-Institut für Physik (Werner-Heisenberg-Institut), München; Germany.

[113]Graduate School of Science and Kobayashi-Maskawa Institute, Nagoya University, Nagoya; Japan.

[114](a)Department of Physics, Nanjing University, Nanjing;(b)School of Science, Shenzhen Campus of Sun Yat-sen University;(c)University of Chinese Academy of Science (UCAS), Beijing; China.

[115]Department of Physics and Astronomy, University of New Mexico, Albuquerque NM; United States of America.

[116]Institute for Mathematics, Astrophysics and Particle Physics, Radboud University/Nikhef, Nijmegen; Netherlands.

[117]Nikhef National Institute for Subatomic Physics and University of Amsterdam, Amsterdam;

Netherlands.

[118]Department of Physics, Northern Illinois University, DeKalb IL; United States of America.

[119][a]New York University Abu Dhabi, Abu Dhabi;[b]United Arab Emirates University, Al Ain; United Arab Emirates.

[120]Department of Physics, New York University, New York NY; United States of America.

[121]Ochanomizu University, Otsuka, Bunkyo-ku, Tokyo; Japan.

[122]Ohio State University, Columbus OH; United States of America.

[123]Homer L. Dodge Department of Physics and Astronomy, University of Oklahoma, Norman OK; United States of America.

[124]Department of Physics, Oklahoma State University, Stillwater OK; United States of America.

[125]Palacký University, Joint Laboratory of Optics, Olomouc; Czech Republic.

[126]Institute for Fundamental Science, University of Oregon, Eugene, OR; United States of America.

[127]Graduate School of Science, University of Osaka, Osaka; Japan.

[128]Department of Physics, University of Oslo, Oslo; Norway.

[129]Department of Physics, Oxford University, Oxford; United Kingdom.

[130]LPNHE, Sorbonne Université, Université Paris Cité, CNRS/IN2P3, Paris; France.

[131]Department of Physics, University of Pennsylvania, Philadelphia PA; United States of America.

[132]Department of Physics and Astronomy, University of Pittsburgh, Pittsburgh PA; United States of America.

[133][a]Laboratório de Instrumentação e Física Experimental de Partículas - LIP, Lisboa;[b]Departamento de Física, Faculdade de Ciências, Universidade de Lisboa, Lisboa;[c]Departamento de Física, Universidade de Coimbra, Coimbra;[d]Centro de Física Nuclear da Universidade de Lisboa, Lisboa;[e]Departamento de Física, Escola de Ciências, Universidade do Minho, Braga;[f]Departamento de Física Teórica y del Cosmos, Universidad de Granada, Granada (Spain);[g]Departamento de Física, Instituto Superior Técnico, Universidade de Lisboa, Lisboa; Portugal.

[134]Institute of Physics of the Czech Academy of Sciences, Prague; Czech Republic.

[135]Czech Technical University in Prague, Prague; Czech Republic.

[136]Charles University, Faculty of Mathematics and Physics, Prague; Czech Republic.

[137]Particle Physics Department, Rutherford Appleton Laboratory, Didcot; United Kingdom.

[138]IRFU, CEA, Université Paris-Saclay, Gif-sur-Yvette; France.

[139]Santa Cruz Institute for Particle Physics, University of California Santa Cruz, Santa Cruz CA; United States of America.

[140][a]Departamento de Física, Pontificia Universidad Católica de Chile, Santiago;[b]Millennium Institute for Subatomic physics at high energy frontier (SAPHIR), Santiago;[c]Instituto de Investigación Multidisciplinario en Ciencia y Tecnología, y Departamento de Física, Universidad de La Serena;[d]Universidad Andres Bello, Department of Physics, Santiago;[e]Universidad San Sebastian, Recoleta;[f]Instituto de Alta Investigación, Universidad de Tarapacá, Arica;[g]Departamento de Física, Universidad Técnica Federico Santa María, Valparaíso; Chile.

[141]Department of Physics, Institute of Science, Tokyo; Japan.

[142]Department of Physics, University of Washington, Seattle WA; United States of America.

[143][a]Institute of Frontier and Interdisciplinary Science and Key Laboratory of Particle Physics and Particle Irradiation (MOE), Shandong University, Qingdao;[b]School of Physics, Zhengzhou University; China.

[144][a]State Key Laboratory of Dark Matter Physics, School of Physics and Astronomy, Shanghai Jiao Tong University, Key Laboratory for Particle Astrophysics and Cosmology (MOE), SKLPPC, Shanghai;[b]State Key Laboratory of Dark Matter Physics, Tsung-Dao Lee Institute, Shanghai Jiao Tong University, Shanghai; China.

[145]Department of Physics and Astronomy, University of Sheffield, Sheffield; United Kingdom.

[146]Department of Physics, Shinshu University, Nagano; Japan.

[147]Department Physik, Universität Siegen, Siegen; Germany.

[148]Department of Physics, Simon Fraser University, Burnaby BC; Canada.

[149]SLAC National Accelerator Laboratory, Stanford CA; United States of America.

[150]Department of Physics, Royal Institute of Technology, Stockholm; Sweden.

[151]Departments of Physics and Astronomy, Stony Brook University, Stony Brook NY; United States of America.

[152]Department of Physics and Astronomy, University of Sussex, Brighton; United Kingdom.

[153]School of Physics, University of Sydney, Sydney; Australia.

[154]Institute of Physics, Academia Sinica, Taipei; Taiwan.

[155][a]E. Andronikashvili Institute of Physics, Iv. Javakhishvili Tbilisi State University, Tbilisi;[b]High Energy Physics Institute, Tbilisi State University, Tbilisi;[c]University of Georgia, Tbilisi; Georgia.

[156]Department of Physics, Technion, Israel Institute of Technology, Haifa; Israel.

[157]Raymond and Beverly Sackler School of Physics and Astronomy, Tel Aviv University, Tel Aviv; Israel.

[158]Department of Physics, Aristotle University of Thessaloniki, Thessaloniki; Greece.

[159]International Center for Elementary Particle Physics and Department of Physics, University of Tokyo, Tokyo; Japan.

[160]Graduate School of Science and Technology, Tokyo Metropolitan University, Tokyo; Japan.

[161]Department of Physics, University of Toronto, Toronto ON; Canada.

[162][a]TRIUMF, Vancouver BC;[b]Department of Physics and Astronomy, York University, Toronto ON; Canada.

[163]Division of Physics and Tomonaga Center for the History of the Universe, Faculty of Pure and Applied Sciences, University of Tsukuba, Tsukuba; Japan.

[164]Department of Physics and Astronomy, Tufts University, Medford MA; United States of America.

[165]Department of Physics and Astronomy, University of California Irvine, Irvine CA; United States of America.

[166]University of West Attica, Athens; Greece.

[167]Department of Physics and Astronomy, University of Uppsala, Uppsala; Sweden.

[168]Department of Physics, University of Illinois, Urbana IL; United States of America.

[169]Instituto de Física Corpuscular (IFIC), Centro Mixto Universidad de Valencia - CSIC, Valencia; Spain.

[170]Department of Physics, University of British Columbia, Vancouver BC; Canada.

[171]Department of Physics and Astronomy, University of Victoria, Victoria BC; Canada.

[172]Fakultät für Physik und Astronomie, Julius-Maximilians-Universität Würzburg, Würzburg; Germany.

[173]Department of Physics, University of Warwick, Coventry; United Kingdom.

[174]Waseda University, Tokyo; Japan.

[175]Department of Particle Physics and Astrophysics, Weizmann Institute of Science, Rehovot; Israel.

[176]Department of Physics, University of Wisconsin, Madison WI; United States of America.

[177]Fakultät für Mathematik und Naturwissenschaften, Fachgruppe Physik, Bergische Universität Wuppertal, Wuppertal; Germany.

[178]Department of Physics, Yale University, New Haven CT; United States of America.

[179]Yerevan Physics Institute, Yerevan; Armenia.

[a] Also at Affiliated with an institute formerly covered by a cooperation agreement with CERN.

[b] Also at An-Najah National University, Nablus; Palestine.

[c] Also at Borough of Manhattan Community College, City University of New York, New York NY; United States of America.

[d] Also at Center for Interdisciplinary Research and Innovation (CIRI-AUTH), Thessaloniki; Greece.

[e] Also at Centre of Physics of the Universities of Minho and Porto (CF-UM-UP); Portugal.

[f] Also at CERN, Geneva; Switzerland.

[g] Also at Département de Physique Nucléaire et Corpusculaire, Université de Genève, Genève; Switzerland.

[h] Also at Departament de Fisica de la Universitat Autonoma de Barcelona, Barcelona; Spain.

[i] Also at Department of Financial and Management Engineering, University of the Aegean, Chios; Greece.

[j] Also at Department of Mathematical Sciences, University of South Africa, Johannesburg; South Africa.

[k] Also at Department of Modern Physics and State Key Laboratory of Particle Detection and Electronics, University of Science and Technology of China, Hefei; China.

[l] Also at Department of Physics, Bolu Abant Izzet Baysal University, Bolu; Türkiye.

[m] Also at Department of Physics, King's College London, London; United Kingdom.

[n] Also at Department of Physics, Stanford University, Stanford CA; United States of America.

[o] Also at Department of Physics, Stellenbosch University; South Africa.

[p] Also at Department of Physics, University of Fribourg, Fribourg; Switzerland.

[q] Also at Department of Physics, University of Thessaly; Greece.

[r] Also at Department of Physics, Westmont College, Santa Barbara; United States of America.

[s] Also at Faculty of Physics, Sofia University, 'St. Kliment Ohridski', Sofia; Bulgaria.

[t] Also at Faculty of Physics, University of Bucharest ; Romania.

[u] Also at Hellenic Open University, Patras; Greece.

[v] Also at Henan University; China.

[w] Also at Imam Mohammad Ibn Saud Islamic University; Saudi Arabia.

[x] Also at Institucio Catalana de Recerca i Estudis Avancats, ICREA, Barcelona; Spain.

[y] Also at Institut für Experimentalphysik, Universität Hamburg, Hamburg; Germany.

[z] Also at Institute for Nuclear Research and Nuclear Energy (INRNE) of the Bulgarian Academy of Sciences, Sofia; Bulgaria.

[aa] Also at Institute of Applied Physics, Mohammed VI Polytechnic University, Ben Guerir; Morocco.

[ab] Also at Institute of Particle Physics (IPP); Canada.

[ac] Also at Institute of Physics and Technology, Mongolian Academy of Sciences, Ulaanbaatar; Mongolia.

[ad] Also at Institute of Physics, Azerbaijan Academy of Sciences, Baku; Azerbaijan.

[ae] Also at Institute of Theoretical Physics, Ilia State University, Tbilisi; Georgia.

[af] Also at National Institute of Physics, University of the Philippines Diliman (Philippines); Philippines.

[ag] Also at The Collaborative Innovation Center of Quantum Matter (CICQM), Beijing; China.

[ah] Also at TRIUMF, Vancouver BC; Canada.

[ai] Also at Università di Napoli Parthenope, Napoli; Italy.

[aj] Also at University of Colorado Boulder, Department of Physics, Colorado; United States of America.

[ak] Also at University of Sienna; Italy.

[al] Also at Washington College, Chestertown, MD; United States of America.

[am] Also at Yeditepe University, Physics Department, Istanbul; Türkiye.

[*] Deceased